To the Graduate Council:

I am submitting herewith a thesis written by Jayendra H. Bheda entitled "The Effect of Process and Polymer Variables on Light Transmission Properties of Polypropylene Tubular Blown Films." I have examined the final copy of this thesis for form and content and recommend that it be accepted in partial fulfillment of the requirements for the degree of Master of Science, with a major in Polymer Engineering.

J. E. Spruiell

J. E. Spruiell, Major Professor

We have read this thesis
and recommend its acceptance:

J. F. Fellers

Edward S. Clark

Accepted for the Council:

Lou Winkel

The Graduate School

4

THE EFFECT OF PROCESS AND POLYMER VARIABLES ON LIGHT TRANSMISSION PROPERTIES OF POLYPROPYLENE TUBULAR BLOWN FILMS

A Thesis

Presented for the

Master of Science

Degree

The University of Tennessee, Knoxville

Jayendra H. Bheda

March 1984

To

Hansa and Poonam

ACKNOWLEDGEMENTS

There are many people who in some or other way assisted in the completion of this thesis and the research work preceding it. While it is not possible to mention everyone involved, there are several persons who deserve special mention for their efforts.

I am indebted to my adviser Dr. J. E. Spruiell for his guidance and patience throughout this work.

Appreciation is also extended to Dr. Chambus of Chemistry department for his valuable help and suggestions.

The capable assistance of the personnel of the Machine Shop and Electronic Shop is gratefully acknowledged.

The series of polypropylene samples were kindly supplied by The Gulf Chemical Company. Financial assistance provided by Chemical and Metallurgical Engineering department is acknowledged.

I further wish to acknowledge the many students and the faculty members who made my stay at the University an enjoyable and stimulating experience.

Without the continuous support of my family this work would not have been possible. To my wife Hansa and my daughter Poonam, I express my greatest love and appreciation.

ABSTRACT

The direct light transmission factors of polypropylene (PP) tubular blown films are measured as a function of film preparation conditions such as blow-up ratio (BUR), draw down ratio (DDR), cooling rates (frost line height, FLH) and polymer variables such as molecular weight, molecular weight distribution (MWD) and nucleating agent additive.

The contribution of light scattering from the film surface is investigated by separating the overall direct light transmission factor in to components due to transmission through the bulk phase and through the surface phase of films. It was found that overall direct transmission factor is controlled by the surface phase transmission factor. The bulk phase of film was further investigated by small angle light scattering which confirmed the spherulitic morphology for PP blown films. The size of spherulites is correlated to bulk phase transmission factors.

The surface phase transmission factor is separated in to inside and outside surface phase transmission factors. Light transmission through inside surface was found to be higher than that from outside surface. Profiles of surface irregularities of the films were obtained using a mechanical surface profiler with a diamond stylus and were characterized statistically. The standard variation of

height deviation of the surface irregularities correlate well with the surface phase transmission factors.

Overall light transmission factors were higher for films prepared at high BUR/DDR and low FLH. Films made from high molecular weight resin with narrow MWD and nucleating agent additive exibit highest values of light transmission factors. However, narrow MWD resins showed increased bubble instabilities.

TABLE OF CONTENTS

CHAPTER PAGE

CHAPTER PAGE

LIST OF TABLES

TABLE PAGE

LIST OF FIGURES

FIGURE PAGE

FIGURE PAGE

CHAPTER 1

INTRODUCTION

Tubular blown film extrusion is one of the most important of polymer processing operations for the production of thermoplastic films. This process is commonly used for polymer film manufacturing because of its better economics and the satisfactory mechanical properties of the films produced.

Polyethylenes are the most widely used materials for the tubular blown film process and so there have been a number of studies entirely limited to these materials (4,13,21,22,35,36,37,38,44,49,50,59,60,61,73). Most of the fundamental studies have dealt with structure development (4,13,21,22,49,50,59,60,61) or film stability (35,36,37,38,44,73) and their relation to specific processing conditions. Only a small amount of published information is available on isotactic polypropylene (32,73,91) which is the subject of the present research. A considerable number of the prior studies have been carried out in the Polymer Engineering laboratories at the University of Tennessee.

Clarity/haze of the film is one of the most important requirements of commercial films for packaging applications. A few authors have reported investigations of light transmission by polymer films and factors that affect film

clarity (4,14,42,94). Again most of these investigations have dealt with polyethylenes, including one study carried out in our laboratories at the University of Tennessee (4). There is little information on factors affecting film clarity for polypropylene tubular blown films.

The purpose of this thesis is to acquire a fundamental understanding of the relation of optical properties of polypropylene blown film to polymer and processing variables. The measurement of direct light transmission factors of the so-called surface phase and the bulk phase of the films is used to establish which source of the light scattering is predominant. Further, for the surface phase scattering we shall attempt to understand which source of roughening is important- "extrusion haze" or "crystallization haze."

CHAPTER 2

BACKGROUND REVIEW AND LITERATURE SURVEY

A. POLYPROPYLENE(PP) STRUCTURE AND PROPERTIES

Crystal Structure and Morphology

Polymerization of propylene produces two different forms of PP: an essentially amorphous rubbery and soluble fraction and a highly crystalline hard and insoluble fraction. Crystallographic examinations of the crystalline fraction showed that it exibited a high level of stereoregularity along the polymer chains. Depending on the nature of stereospecific polymerization conditions, the stereoregular polypropylene can be either isotactic or syndiotactic. The isotactic form is of greatest commercial interest because of its excellent thermoplastic properties. In the usual commercial production, the above mentioned amorphous fraction can be classified as essentially atactic PP with a density of 0.86-0.89 g/cc, representing a by-product of the stereospecific polymerization process; the crystalline fraction represents isotactic PP with m.p. about 170^{o}C, density about 0.91 g/cc. The term "isotactic" identifies the particular spatial position of the propylene methyl group, being on the same side of the main chain carbon backbone. The discovery of stereospecific polymerization represents a turning point in polymer

chemistry; up to that time it had not been possible to exercise any steric control on polymerization processes.

X-ray methods are most important tools in elucidating structural characteristics of crystalline polymers. The crystal structure of isotactic PP was classified by Natta and Corradini (76). From X-ray fiber patterns a monoclinic unit cell containing four chains and twelve monomer units was derived which had a calculated density of 0.936 g/cc and the following unit cell parameters:

$$a = 6.65\ \text{Å},\ b = 20.96\ \text{Å},\ c = 6.50\ \text{Å},\ \beta = 99°26'$$

From the identity period in the c-axis, it was concluded that the chains have a three fold helical conformation (3_1 helix) as shown in Figure 1.

Besides the ordinary monoclinic form of isotactic PP another polymorphic form is the hexagonal one with unit cell parameters:

$$a = 12.74\ \text{Å},\ c = 6.35\ \text{Å}$$

which occurs under certain conditions of spherulite formation (43,48). The hexagonal form is characterized by the three fold helical conformation of polymer chains. By rapid quenching of molten PP, a so-called 'smectic' or quenched form of isotactic PP can be obtained (29). This form is believed to be closely related to the hexagonal form

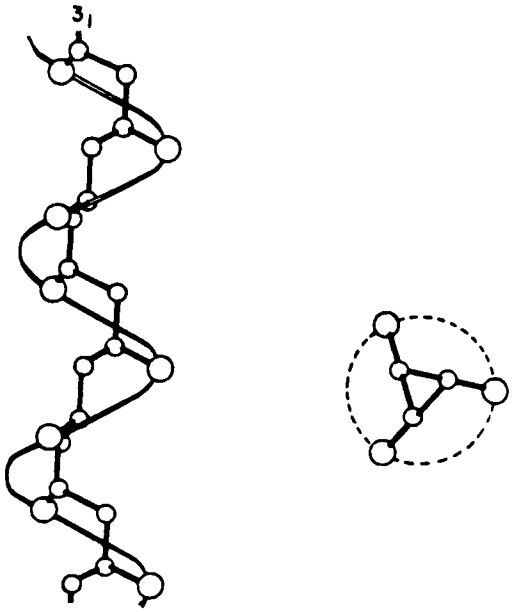

Figure 1. 3_1 Helix of Isotactic Polypropylene

with, however, a lesser degree of lateral order and consisting mainly of hexagonal crystallites.

The normal morphology of polymers which are crystallized from the melt in the absence of stress is growth of spherulites. Spherulites are a birefringent assemblage of crystals emnating from a heterogeneous nucleus and spreading out in a spherical fashion until they impinge on each other and fill practically the entire volume of the bulk crystallized polymer (74). When observed in a polarizing microscope between crossed polaroids, spherulites display a dark maltese cross (Figure 2A). Under certain conditions the crystallization of isotactic PP may produce at least two different spherulitic habits simultaneously : monoclinic and hexagonal (Figure 2B).

Quiescent Crystallization Kinetics

The most common experimental techniques to follow the crystallization process are dilatometric and microscopic methods (26). The results of isothermal crystallization studies on isotactic PP obey the general Avarami equation :

$$\gamma = 1 - \exp(-kt^n) \qquad (1)$$

Where γ is the crystallized volume fraction, k is a rate constant, t is the crystallization time and n is called the Avrami exponent.

Under quiescent conditions nucleation in PP was found to be heterogeneous. The exponent n assumes a value of 3,

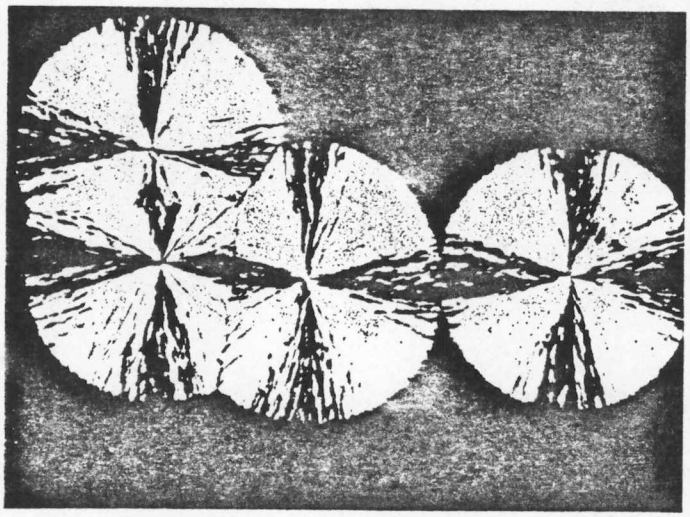

A. Spherulites of It. PP (50)

Source: Keller, A., Makromol. Chem., 34, 1(1959).

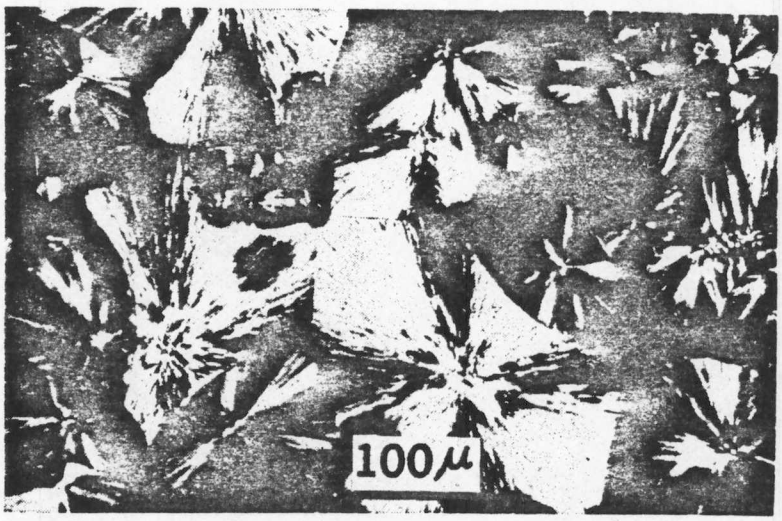

B. Bright - Hexagonal; Dark - Monoclinic (68)

Source: Mejer, J., Kunstst., 54, 578(1964).

Figure 2. Polypropylene Spherulites

indicating spherical growth and heterogeneous athermal nucleation. An important observation is that increasing melt temperatures and melt times reduce the nucleus concentration significantly. Since the linear growth rate of a given nucleus is essentially independent of these variations, the overall crystallization rate is reduced. The addition of small quantities of nucleating agents (aluminium/ sodium benzoate) increases the nucleii concentration and accelerates the overall rate of crystallization (also leading to finer and more numerous spherulites). These effects of nucleation have important practical consequences in terms of better processing characteristics, improved strength and optical properties for crystallization modified polymer (54).

Flow Induced Crystallization

Polyolefin melts crystallize normally in the supercooled state forming a spherulitic morphology. Other morphologies can be obtained when the melt is deformed or subjected to high pressures. Studies of the kinetics of the flow induced crystallization process are helpful in better understanding the morphologies obtained subsequent to polymer processing and in the development of processing methods for producing stronger polymer articles.

Specifically, Gogos and Tan (30) pointed out that "extended chain" crystals were observed in HDPE under very

high crystallization pressure and constant temperature. The so called shish-kebab morphology was reported by Keller and Machin (52). They pointed out that crystallizing PE films at constant elongation produced evidence for their proposed two-stage mechanism of shish-kebab formation; the first stage is the formation of extended chain nucleii and is followed by the second, which consists of the growth of twisted or parallel lamellar crystals. The shish-kebab morphology can also be obtained by flow-induced crystallization of dilute solutions of PE. Haas and Maxwell (34) studied the stress-induced crystallization of supercooled PE melts and followed the crystallization process with polarized light microscopy, agreeing with the viewpoint of Keller on the mechanism of crystallization. In case of PP fibers, Dees and spruiell (20) sought to measure the effect flow has on physical properties and to determine how on-line spinning conditions affect morphological structure. They measured tension in the fiber and fiber temperature, diameter, and X-ray diffraction patterns as a function of distance from the spinneret for a running monofilament. Anderson and Carr (3) pointed out that PP, when melt spun into fibers can exibit unusual "elastic-like" properties. Specifically, these fibers show an ability to recover large fractions of apparently plastic strain when relaxed from total strain levels of 50%. It has been hypothesized that this apparent elasticity is due to

deflection of lamellar platelet morphology in the flow-induced crystallized material which results in the formation of voids between the parallel platelets. A proposed model (15) for elasticity involves shearing of lamellae parallel to fiber axis between the points where they are connected by tie molecules. Again this mechanism results in void formation. Nadella, Henson, Spruiell and White (75) studied the on-line crystallization kinetics in melt spinning of PP. They found increased rate of crystallization with increased take-up velocity or tension, other variables being equal.

Rheological Properties

One of the important rheological parameters which is related to melt viscosity and which is commonly used in practice is so called melt-index (MI). It serves as a crude measure of molecular weight and processibility, but it ignores the non-Newtonian nature of flow and does not account for the differences in molecular weight distribution (MWD).

Recently Minoshima, White and Spruiell (71,72) have studied the influence of MWD on the rheological properties of PP melts. They carried out experimental study of shear and elongational flow properties of a series of PP melts of varying MWD. They reported that broadening of MWD increases the non-Newtonian character of the shear viscosity function

and increases the principal normal stress difference at fixed shear stress. They developed correlations for these properties in terms of molecular structure. Elongational flow studies indicate that for the broader MWD samples failure by neck development occurs and the elongational viscosity appears to decrease with increasing elongation rate. For narrower MWD samples, the elongational viscosity is an increasing function of elongation rate.

An estimate of the elastic properties of the melt may be obtained from the elastic recovery or extrudate swell (53) which depends on capillary dimensions, flow rate, molecular weight and molecular weight distribution (33). The extrudate swelling effect decreases with narrowing MWD; this observation is of practical importance for fiber formation in melt spinning.

B. PLASTIC FILMS AND PRODUCTION PROCESSES

General

The term "Plastic Films" encompasses an everincreasing number of self-supporting, transparent films, each tailored to specific marketing requirements. Packaging is the biggest market for various films. Films also find applications in architecture, agriculture and electrical insulation.

Polyethylene film is by far the most popular extruded film. Other materials of interest are polystyrene (oriented films), nylon, polyester, polypropylene and PVC, the later

being rapidly growing in use. Polypropylene assumes a special position because of its stereoregular structure, being the first member of synthetic stereoregular polymers to achieve industrial importance. Other members of this family are polymers of higher α-olefins namely butene-1 and 4-methyl pentene-1 which have also entered the film market.

Plastic films are produced by extrusion of polymer incorporating either cast chill roll or tubular blown technique.

Tubular Blown Film Process

As schematically shown in Figure 3, in the tubular blown film process, a thin film is produced by means of the extrusion of a polymer melt through an annular die. The molten polymer tube exiting from the die is drawn upward by a take-up device. At the bottom of the die, air is introduced blowing the tube to form a bubble. An air ring which is located around the die is also used to cool the hot bubble rapidly and solidifying it at some distance above the die exit. The blown and solidified bubble is then flattened as it passes through a pair of rolls called nip rolls. The nip rolls, driven by a variable speed motor, provide the axial tension needed to pull the film upwards, and to form an airtight seal, so that a constant air pressure is maintained in the blown bubble. The pressure inside the bubble is controlled by the air supply to the bottom of the die.

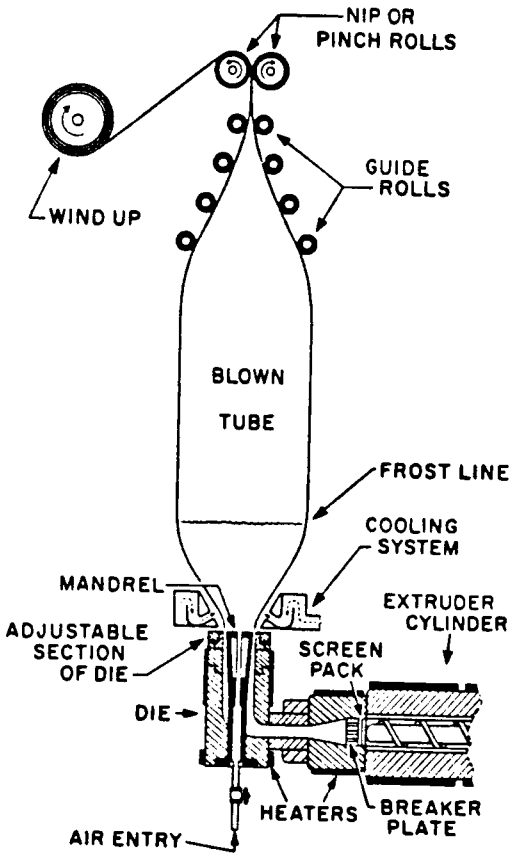

Figure 3. Tubular Blown Film Extrusion Process

The tubular blown film process is most commonly used for branched LDPE and less frequently for linear HDPE and isotactic PP. The not very effective cooling of bubble results in poor optical properties (haze, low gloss and clarity imperfections) and the linear operating speeds are comparatively lower. A great variety of dies are being used: side entry types as well as bottom entry types for air. The most rapid cooling of the formed tube may be effected by additional cooling from an internal mandrel. The Shell Company (32) claimed that an internal mandrel cooling or water quench with downward bubble formation leads to glass clear PP films (Figure 4). Extrusion temperatures range between 215-230°C.

Important variables of the blown film process can easily be defined mathematically for complete understanding. (I) Blow-up ratio (BUR) : It is expressed as ratio of constant bubble diameter to die diameter or

$$BUR = \frac{2 \times \text{Blown Film Width}}{\pi \times \text{Die Diameter}} \qquad (2)$$

(II) Draw-down ratio (DDR) : It is expressed as the ratio of linear speed (V_L) of film at the take-up rolls to the linear speed of melt at the die (Vo) or

$$DDR = \frac{V_L}{V_O} \qquad (3)$$

(III) Frost line height (FLH) : It is the distance of film from constant bubble diameter to the die. Constant bubble

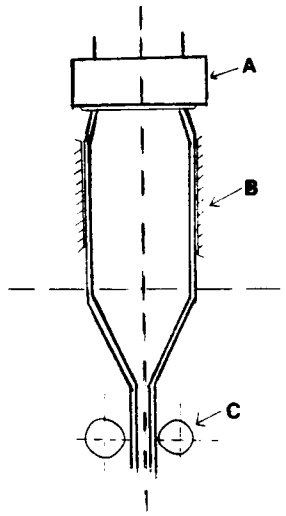

The cooling ring system:
A: die; B: cooling ring C: nip rolls

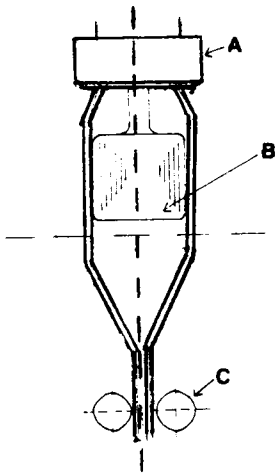

The cooling mandrel system:
A: die; B: cooling mandrel:
C: nip rolls

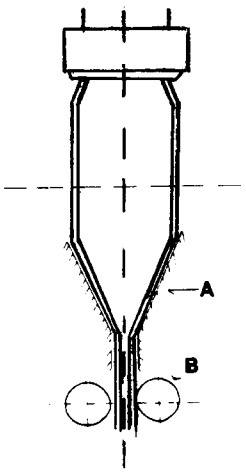

The TQ system: A: film of water; B: nip rolls

Figure 4. Shell Company's Cooling System for Tubular Blown Film Process for PP

Source: Grange, P. W., Editor, Polym. Age, 1, 265 (1970).

diameter occurs at solidification of bubble and also the film frequently appears to change from clear melt to hazy solid.

Chill Roll Cast Film Process

The major contender for the tubular blown film process is the cast film process in which the plastic material is extruded through a slit opening downward over a chill roll and taken to a turret winder through a few rolls (Figure 5).

The chill roll process is considered a practical method for the production of PP films (110). It is also claimed that it allows a better gauge control, produces film with better optical properties and permits greater speeds of extrusion as compared to the blown film process. Extrusion temperatures range between 245-300°C. The chill roll is cooled with water to a temperature of 15°C. The film exiting the chill roll is either unoriented or has a low degree of orientation. These films are particularly suited for uniaxial or biaxial orientation; that is, oriented longitudinally as well as transversely (114). The longitudinal (uniaxial) orientation is effected by passing the partly cooled film through a set of pull rolls into an oven at 120-150°C and thereafter over another faster running set of pull rolls, thus drawing the film and orienting it (typical draw ratios range between 5 to 8). The transverse orientation is performed on a tenter frame which may be

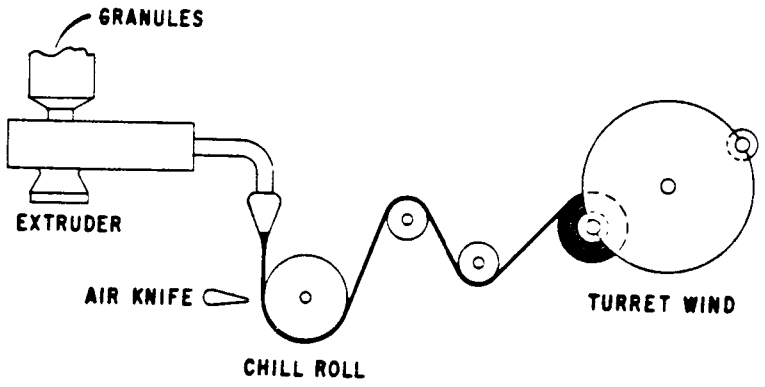

Figure 5. Cast Chill Roll Film Process

mounted in an oven to control the temperature at which orientation occurs. Orientation increases film strength in the direction of orientation, improves clarity, increases impact strength (particularly at low temperatures) and increases stiffness.

In the case of the tubular blown film process longitudinal orientation is effected by draw from the pinch rolls (take-up device) and transverse orientation by blow-up. Thus film with balanced properties in both directions could be achieved directly without incorporating costlier equipment as in the case of the chill roll process.

C. STUDIES OF TUBULAR BLOWN FILM PROCESS

Kinematics, Dynamics and Bubble Instabilities in Tubular Blown Film Process

Kinematics and force balances applicable to tubular blown film extrusion have been developed in a series of papers by Pearson and Petrie (77,78,79) and Han and Park (35,36,37). Recently Kanai and White (44) also studied in detail kinematics, bubble shape, heat transfer profiles and bubble instabilities for LDPE, HDPE and LLDPE. Various kinematic cases have been cited in terms of velocity gradients.

Polymers when melted and extruded through a die, can sometimes give rise to non-uniform extrudate diameters, otherwise known as melt flow instability. In the literature

one type of unstable flow phenomenon is commonly referred to as "melt fracture" (38,104,108). Another type of melt flow instability, which is less studied than melt fracture, is the phenomenon of "draw resonance" which distinguishes itself from the melt fracture in that it occurs only when the extrudate is stretched above a certain critical value. Han et al (38) have pointed out the differences in the causes of the two phenomena. In fiber spinning these have been studied in detail by Kase and Matsuo (46), Matsumoto and Bogue (64) and Minoshima, White and Spruiell (71). Minoshima et al (72) pointed out that there are two types of disturbances, machine noise and vibrations cause spurious "forced oscillations" whereas the true draw resonance phenomenon is a form of "natural oscillations". From studies on a melt spinline involving measurement of elongational viscosity-elongation rate curves for PP, they concluded that narrowing the MWD decreases diameter fluctuations due to forced oscillations and the drawdown required to obtain draw resonance is increased.

According to Han et al (37) two distinct types of flow instabilities have been observed in the blown film process depending on whether a bubble was stretched uniaxially or biaxially. In uniaxial stretching (BUR = 1.0), draw resonance was observed while in the biaxial stretching the phenomenon of surface wave type instability was observed.

This type of instability is very sensitive to a disturbance in processing variables such as the mass flow rate, air pressure, temperature and take-up speed. Kanai and White (44) and Minoshima (73) have recently studied bubble instability phenomenon for a series of polyethylenes. They discuss the differing bubble stabilities of LDPE, LLDPE and HDPE in terms of elongational flow behaviour and they show operating space for various PEs in terms of blow-up ratio, draw down ratio and frost line height.

Structure Development in Tubular Blown Films

Film structural studies of PE related to blown film processing conditions have been carried out by several workers. Homes and Palmer (40) concluded that the a axis of the unit cell lies along the machine direction (MD) and the c axis, the polymer chain direction, tends to orient perpendicular to the MD. Keller (49,50,51) proposed an alternative interpretation, termed row orientation, in which b axis takes up a preferred orientation perpendicular to the MD and the a and c axes are randomly distributed with cylindrical symmetry about the b axis. Lindenmeyer and Lustig (56) constructed pole figures for HDPE and LDPE blown films and concluded that at low blow-up ratios, the crystalline orientations of both HDPE and LDPE films are approximately the same, but at high blow-up ratios the LDPE films showed orientation similar to that proposed by Keller

(49). Desper (21) and Desper and Stein (22) carried out pole figure measurements for LDPE blown films with various cooling rates and calculated the crystalline orientation functions defined by Wilchinsky (111). They reported equal degrees of a and c axes orientation parallel to the MD at low cooling rates, and increasing a axis orientation as the cooling rate increases, coupled with a shift in the c axis from parallel to perpendicular orientation.

More recently Madams and Preedy (59,60,61) have presented orientation of HDPE blown films in a series of papers. They have described two types of crystalline orientations. One is the a and c axes inclined at an angle to the plane of film, which was developed by Keller and Machin (52). The other type is the c axis distributed substantially along the MD and a and b axes rotated around the c axis which is found in cold drawn PE (66,67). For some HDPE film samples under very low stresses, there was almost pure a axis orientation, and under very high draw-down, there was substantial c axis orientation, both with respect to the MD. They concluded that high draw-down and low extrusion temperatures are the most effective factors in promoting high stress induced crystallization.

Choi, White and Spruiell investigated the orientation in blown films of polystyrene(PS) (12) and HDPE (13) as a function of processing conditions. They found that the

orientation was determined by the stresses at the point of solidification. The results were interpreted in terms of White-Spruiell biaxial orientation factors (109) which are given by the expressions

$$f^B_{1j} = 2\overline{\cos^2\phi_{j1}} + \overline{\cos^2\phi_{j2}} - 1 \quad (4)$$

$$f^B_{2j} = 2\overline{\cos^2\phi_{j2}} + \overline{\cos^2\phi_{j1}} - 1 \quad (5)$$

for the case of crystalline polymers, where j represents the a, b and c crystallographic axes, 1 and 2 represent the reference directions (e.g. MD and TD respectively), ϕ is the angle between the crystallographic axes and the reference directions. They found that the HDPE films showed higher levels of crystalline orientations from WAXS than would be expected from the Rheo-Optical law (57,58). This is due to oriented nucleation and growth of crystals. However, for PS films, the orientation in the film was exactly that predicted by the Rheo-Optical law. They reported that in uniaxial HDPE films, a row structure, first described by Keller, was favored and a biaxially oriented sample exibited morphology appearing to be equivalent to two or more superimposed row structures.

Shimomura, Spruiell and White (91) studied orientation development in the PP blown films. They used WAXS and birefringence measurements on films prepared under conditions of known blow-up ratio, draw-down ratio, MD

tension and bubble air pressure. They constructed pole figures and orientation factor biaxial triangle to represent the variation of orientation with processing parameters and concluded that the behavior was similar to that for HDPE found previously by Choi et al (13). At high draw-down ratios the b axis was essentially perpendicular and the c axis tended to align parallel to the MD. As the blow-up ratio increases at given draw-down, there was a tendency for the b axis to become increasingly concentrated in the normal direction i.e. perpendicular to the surface of the film and produces a shift of chain alignment toward the TD.

D. OPTICAL PROPERTIES OF POLYMER FILMS AND THEIR MEASUREMENT

Two principal groups of optical properties can be distinguished : those which depend on molecular property averages and those which depend on local deviations from these averages (that is degree of inhomogeneity of the medium). Refraction, absorption and diffraction phenomena belong to the first group, whereas scattering effects belong to the second group (23). The characteristic optical properties for finished polymer film products such as haze, transmittance, gloss etc are considered to be scattering effects caused by variation in refractive index or differences in the orientation of anisotropic volume

elements within the polymer films and on its surfaces. For example polystyrene film, known as a typical amorphous polymer, has a very low haze value (0.1 to 3%) and very high transmittance value (87 to 92%), because of its homogeneous internal structure and its rather smooth surface. On the other hand polyethylene film, known as a typical semicrystalline polymer, has higher haze value (10 to 50% for HDPE, 5 to 7% for LDPE) and lower transmittance values (0 to 40% for HDPE, 35 to 57% for LDPE), because of its inhomogeneous internal structure and uneven surface (63).

The magnitudes characterizing the scattering properties of solid polymers have been discussed and reviewed by Ross and Birley (88). They define the magnitudes of transparency or clarity, haze and gloss in terms of flux scattered. When a quasi-monochromatic and parallel beam of light of flux ϕ, is normally incident upon a slab of an inhomogeneous material, immersed in a homogeneous medium having a refractive index equal to the average refractive index of inhomogeneous material, a part of the radiation $\Delta\phi_a$ will be absorbed, a certain amount $\Delta\phi_{sc}$ will be scattered and the remaining ϕ_{undev} will be transmitted without deviation through the inhomogeneous medium. Thus :

$$\phi = \phi_{undev} + \Delta\phi_a + \Delta\phi_{sc} \qquad (6)$$

For the vast majority of solid polymers, scattering is the predominant mechanism of attenuation in the visible range of

the electromagnetic spectrum and absorption of light is comparatively very small. Thus :

$$\Delta\phi_a << \Delta\phi_{sc} \tag{7}$$

so equation (6) becomes

$$\phi = \phi_{undev} + \Delta\phi_{sc} \tag{8}$$

The direct transmission factor (T) characterises the attenuation of incident flux throughout a sample in the original direction. T being a dimensionless number, it is usually expressed as a fraction or percentage. Thus :

$$T = \frac{\phi_{undev}}{\phi} \tag{9}$$

equations (8) and (9) give

$$T = 1 - \frac{\Delta\phi_{sc}}{\phi} \tag{10}$$

The direct transmission factor (T) is often utilised in the plastic film industry as a criterion of film clarity (2,5,81). The clarity is a measure of the capacity of the inhomogeneous material for allowing details in the object to be resolved in the image it forms. It usually depends on the distance between the object and inhomogeneous optical system. Equation (10) suggests that the direct transmission factor can be looked upon as a measure of the light

scattering of the plastic films. Several methods for determining clarity have been described (11,14, 107,112). Clampitt et al (14) describe the direct transmission factor as specular transmittance (T) and an instrument to measure T, called Scattermaster (Figure 6) for cast chill rolled PE film, in which light from a mercury discharge lamp is filtered through a 546 μm filter, collimated and is made to pass through a 0.001 inch slit. This slit of light strikes the sample at normal incidence, passes through a second slit, and falls on the detector. When the detector is exactly alligned with the light beam, it will recieve that light which has passed through the sample undeviated from its original path, but will not recieve that light which the sample has reflected, absorbed or scattered. They considered film to consist of an air-side surface phase, a chill roll surface phase and a bulk component phase. They present the technique which allows the total light attenuated by the film to be devided into the attenuation caused by the individual phases. Thus the total light transmitted by the film is the product of transmission values of each phase (55) as shown below

$$T = T_{s1} \cdot T_{s2} \cdot T_b \qquad (11)$$

where T_{s1}, T_{s2}, and T are the transmittances of air side surface phase, chill roll side surface phase and bulk film

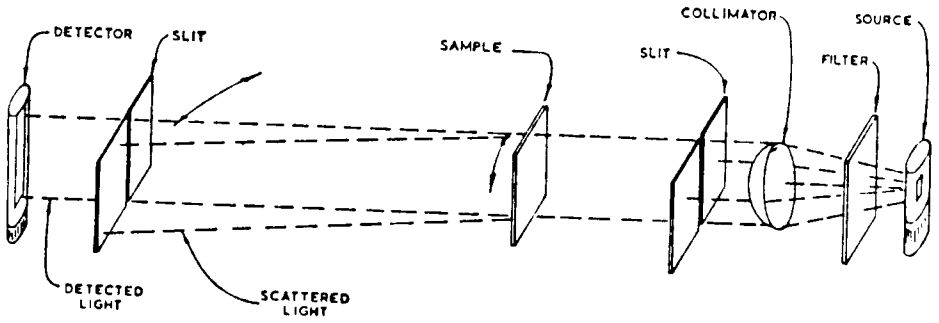

Figure 6. Schematic Diagram of "Scattermaster"

Source: Clampitt, B. H. and D. E. German, Analytical Chemistry, 41, 1306(1969).

phase, respectively. The light attenuation in bulk phase obeys Lambert's law (62)

$$Tb = \exp(-Kt) \tag{12}$$

where K is the apparent absorption coefficient with dimension of inverse of thickness and t is the bulk phase thickness (assumed to be equal to thickness of the sample film). They describe two methods depending on film systems which block readily or which do not block to arrive at transmittance of individual phases. In the former systems they used films of different thicknesses and used a plot of log(Io/I) versus film thickness t which should be linear according to following equation :

$$\log\left(\frac{Io}{I}\right) = \log\left(\frac{1}{T}\right) = K't - \log(Ts_1 \cdot Ts_2) \tag{13}$$

For the later case they used approach of Stein (46) using a liquid of refractive index same as that of the film to eliminate the surface phase scattering.

Haze : As described by Ross and Birley, the total amount of scattered light $\Delta\phi_{sc}$ can be thought of as consisting of two component parts, the forward scattered part $\Delta\phi^{f}_{sc}$ and the backward scattered part $\Delta\phi^{b}_{sc}$ (Figure 7) according to the following equation :

$$\Delta\phi_{sc} = \Delta\phi^{f}_{sc} + \Delta\phi^{b}_{sc} \tag{14}$$

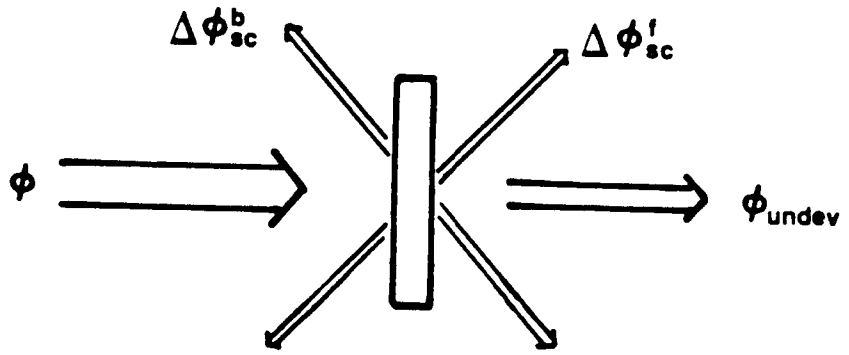

Figure 7. Components of Scattered Light

The total transmitted light flux ϕ through the inhomogeneous medium is given by

$$\phi = \phi_{undev} + \Delta\phi^{f}_{sc} \tag{15}$$

and the forward scattered fraction X^{f}_{sc} is given by

$$X^{f}_{sc} = \frac{\Delta\phi^{f}_{sc}}{\phi} \tag{16}$$

The loss in constrst due to forward scattering is expressed by the forward scattered fraction Xsc and is regarded as 'haze'.

In a similar way, one could define a 'backward scattered fraction' X^{b}_{sc} characterizing the loss in constrast due to backward scattering. The combined effect of forward and backward scattering occurs when objects are viewed through scattering media, from the side on which the radiation is incident and is sometimes called "milkiness." Haze is sometimes defined as the percentage of transmitted light scattered by the film more than 2.5° from the normal incident beam and is measured according to an ASTM procedure (5). A schematic diagram of an instrument for measurement of haze is shown in Figure 8.

Gloss is a property of the surface of a material. Its magnitude depends on the refractive index of the material, the smoothness of the surface and angle of incidence of

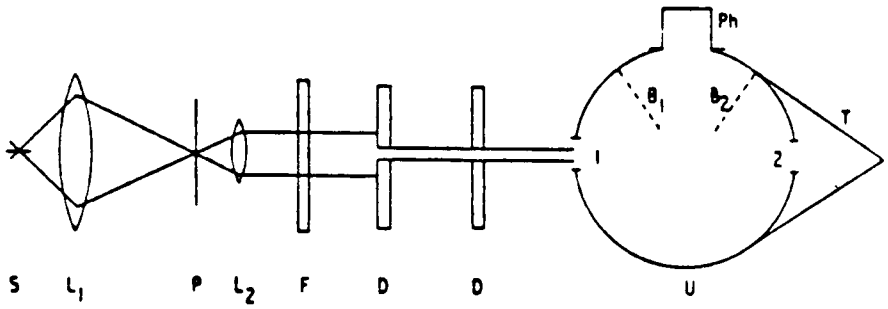

S, light sorce; L_1, condenser system; P, pinhole (secondary light source); L_2, collimator (anastigmat lens); F, monochromatic filter; D, diaphragms for adjusting the beam diameter; U, integrating (Ulbricht) sphere, with a minimum diameter of 250 mm; T, light trap; Ph, photodetector; B_1, baffle used in total transmission factor measurement; B_2, baffle used in total reflection measurement; 1 and 2, apertures diametrically opposite in the integrating sphere.

Figure 8. Schematic Diagram of Commercial Hazemeter

Source: Ross, G. and A. W. Birley, J. Phys., Part D, 6, 795(1973).

light falling on the surface. Sometimes it is defined as 45° specular surface gloss which is measured as the proportion of light reflected from the film at an angle of 45° according to ASTM (6). Mathematically, the gloss is indicated as the ratio of flux, Φ_r^{Wr}, scattered within an arbitrary solid angle Wr around the geometrical direction to the incident flux

$$G = \frac{\phi_r^{wr}}{\phi} \tag{17}$$

The usual procedure for assessing the scattering from the medium and from the surface individually consists of determining their combined contribution and then, using an immersion method, of measuring the effect due only to the medium. A schematic diagram of the instrument for measuring gloss is as shown in Figure 9.

E. LIGHT SCATTERING FROM POLYMER FILMS

Internal Structure of Polymers

Light scattering from the internal structure of polymers was first considered by Debye and Bueche (19) and Goldstein and Michalik (31). Stein and his coworkers (47,97,102) have studied the scattering of light from crystalline polymers experimentally and theoretically. Considering a spherulite as an anisotropic sphere, theoretical equations of intensity scattered by a single spherulite have been presented by Stein and Rhodes (98). The

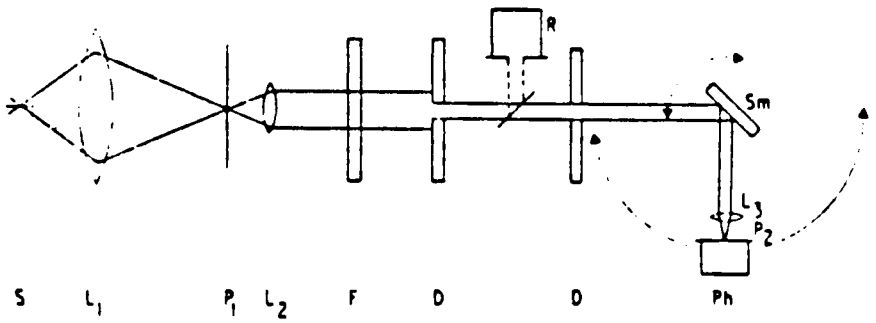

S, light source (mercury arc lamp); L_1, condenser system; P_1, pinhole (secondary light source); $L_2$and L_3, identical anastigmat lenses, for collimating (L_2); F, monochromatic filter; D, diaphragms to adjust the size of the beam; Sm, sample (usually immersed in a liquid having the same refractive index as the sample); Ph, photodetector (photomultiplier or photocell); R, monitor photodetector system.

Figure 9. Schematic Diagram of Commercial Glossmeter

Source: Ross, G. and A. W. Birley, J. Phys., Part D, 6, 795(1973).

scattered intensity depends on volume of spherulite, tangential and radial polarizabilities, radial and azimuthal scattering angles and a shape factor (U). From the Hv-SALS pattern polar angle θmax can be arrived at, for which U has a value of 4.09. This allows us to obtain the size of spherulites in terms of spherulite radius Ro according to the equation :

$$U_{max} = 4.09 = \frac{4\pi Ro}{\lambda} \sin\left(\frac{\Theta_{max}}{2}\right) \qquad (18)$$

where λ is the wavelength of light in the medium. Stein and his coworkers (95,98,99,100,101) have also studied the small angle light scattering from polyethylene films using polarized light. Small angle photographic light scattering patterns from isotropic PE films have been shown to depend on the size of the spherulites and the difference between its radial and tangential polarizabilities. It was concluded that fluctations in orientation are the dominant cause of light scattering in crystalline polyethylene. In most of these investigations, scattering from polymer surfaces have been reduced to negligibly low levels by coating the polymer with a fluid of refractive index equal to that of the polymer or by crystallizing the polymer between smooth microscope slides.

Light Scattering from Oriented Films

In the study of light scattering from oriented polymer films, it was found that the absolute scattering power of an oriented sample is considerably less than that for an unoriented sample. This would be a result of a decrease in both orientation and density fluctuations (96,102) for oriented samples. Studies have been reported (92,93,106) describing procedures for preparing PE films of high optical clarity involving crystallization under conditions leading to orientation. Particularly Wang and Chen (106) indicated that the smaller crystallites may account for the transparency of film in visible light. However, Stein et al (100) asserted from obeservations of SALS patterns of quenched, rolled HDPE film that the transparency of films is not primarily related to crystallite size but rather to the type of morphology and size of superstructures much bigger than the crystallites themselves. Hawkins and Richards (39) as early as 1949 reported a study in aggreement with the Stein et al (100) explanation. They also thought that in the partially crystalline state the light scattering is not a direct consequence of the presence of crystallites but is mainly due to the presence of more or less oriented aggregates of crystallites, of dimensions greater than the wavelength of visible light. They studied light transmission and the formation and decay of spherulites in PE with

temperature change. They reported that lack of transparency is due primarily to internal reflection at boundaries between spherulites where there is a change of refractive index. Some scattering of light may occur within the spherulites themselves. The transparency of the sample will hence depend on the average size of spherulites i.e. the number of spherulite boundaries through which light has to pass and also on perfection of orientation in spherulites. Also for samples of the same degree of crystallinity, transparency tends to increase with molecular weight. This may be due to a tendency for the high molecular weight samples to give larger spherulites. Samuels (89) has studied spherulite structure in cast chill rolled PP films using SALS. The average spherulite size determined from the Hv-SALS pattern was correlated with cast roll temperature during film processing (Figure 10). Similarly, the Hv-SALS pattern was used on a processing line to indicate when increased film thickness prevents efficient quench (Figure 11).

Light Scattering from Rough Surfaces

The light incident on a rough film surface is partially reflected and partially refracted. Refracted light may emerge after internal reflections. The light so emerging and the light directly reflected from the outer surface both contribute to the total scattering by the film. In spite of

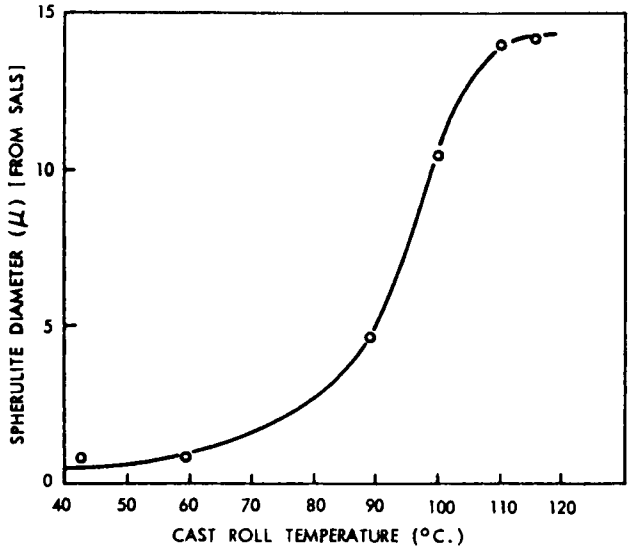

Figure 10. Effect of Cast Roll Temperature on Spherulite Size (Speed and Melt Temperature constant)

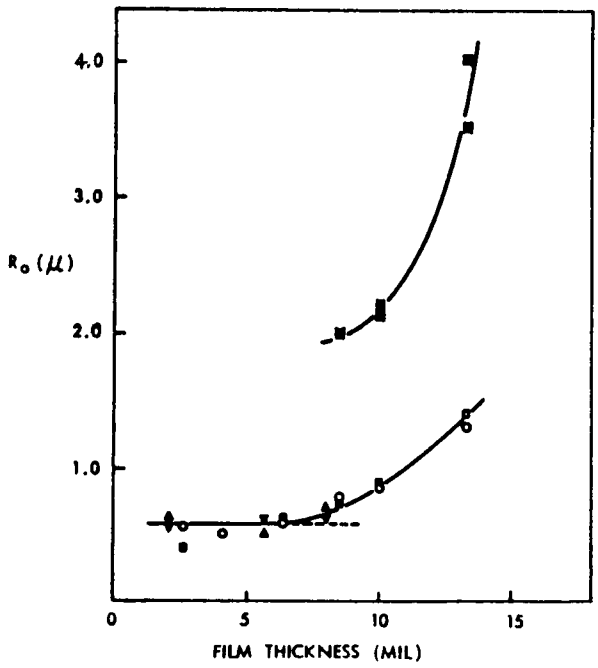

(Δ) cast at 110°C; (▽) preheated at 110°C; (□, ⊠) cast at 135°C; (○, ■) preheated at 135°C.

Figure 11. Effect of Film Thickness and Casting Temperature on Spherulite Dimensions in Cast and Preheated Films

Source: Samuels, R. J., J. Polym. Sci., Part A-2, 9, 2165(1971).

the fact that the haze of thin blown PE film is mainly caused by scattering from rough film surface (27,28,42,69,94) there have been only a few studies done about polymer film surface roughness and scattering behaviour (41,42,94).

In optics,however, surface roughness is a most important problem, since the light scattered from rough surfaces of optical components lowers performance of the optical system itself. The problem of scattering from rough surfaces has been placed on a firm theoretical and experimental basis in a review by Elson, Bennett and Bennett (25).

There are several kinds of surface irregularities which may cause surface scattering :

(I) irregularities such as scratches, digs or particulates which are large relative to the wavelength of the incident light.

(II) isolated irregularities which are comparable to or smaller than the wavelength of incident light.

(III) irregularities which are small in one or more dimensions relative to the wavelength of light but which are so closely spaced that they cannot be treated as independent scattering centers. The effect of each center is correlated with that of its neighbors; scattering from such ensembles is often called "microirregularity scattering."

In the case of blown films, irregularities commonly termed as "extrudate distortion", "melt fracture" etc involve gross distortion of extrudates, or surface roughness known as "shark-skin" as well as scratches and die streaks belong to category (I). Those irregularities such as "grain" or morphological boundaries (spherulites in case of PP) in extruded blown films belong to category (II), and those irregularities arising from rheological behavior of polymer belong to category (III). The appropriate theoretical treatment of scattering depends on which of the above categories the scattering elements fall into. If the dimensions of the irregularities are large compared with the wavelength of light, the reflectance of the surface is determined entirely by geometrical optics and is a function of the inclinations of facets. When the irregularities become comparable to or smaller than the wavelength of incident light, the scattering problem becomes a diffraction problem and geometrical optics is no longer adequate. A great simplification occurs, however, if the scattering centers can be considered to act independently. Mie scattering theory (70), of which Rayleigh scattering (86) is a special case, can then be used. The scattering caused by so called microirregularity, has been studied by several workers based on the Kirchoff method in diffraction theory. The most comprehensive development of Kirchoff method has been given by Beckmann and Spizzichino (7).

F. MEASUREMENT AND CHARACTERIZATION OF SURFACE ROUGHNESS

Measurement of Surface Roughness

Quantitative evaluations of film surface roughness have been done mainly using the scanning electron microscope (41,42,94). Howells and Benbow (41) reported that the size of small defects on blown LDPE film surface, which is thought to be the main cause of haze, is about 1 μm. Stehling et al (94), based on SEM photographs, reported that these small scale defects form mounds which are a few microns in diameter and protrude from the surface by about 1 μm or less.

Elson, Bennett and Bennett (25) have developed methods of measuring the statistical character of rough optical surfaces. Statistical surfaces having fine scale roughness may be measured using stereo electron microscopy (18,84,85), multiple beam interferometry (9) or surface profiling instruments (10,24). Stereo electron microscopy involves making a replica of the surface for observation in a transmission electron microscope, and then measuring heights of surface features using a stereo viewer and parallax bar. Multiple beam interferometry is a method for obtaining statistics of surface features which have lateral separation of the order of several micrometers.

Surface profiling instruments (83) use a diamond stylus to trace over the surface. The radius of the standard (conical) stylus is about 8 μm, and several styluses having radii in the 0.5 to 2.5 μm range are available. The stylus loading is continuously adjustable from about 1 to 40 mg. A loading of 2 mg is generally used with standard stylus for optical surface measurement to insure good contact without permanently marking the surfaces (24).

Characterization of Random Rough Surfaces

The fine scale surface roughness of the blown films appear to be a random process. Random surfaces such as terrain, sea, atmospheric layers etc are best described by the values of appropriate statistical parameters (7,8).

Consider a one dimensional random surface profile (Figure 12), where X is the horizontal coordinate and h(x) is the height coordinate of the random surface. We define δ as the separation parameter according to following equation :

$$\delta = X_2 - X_1 \qquad (19)$$

where X_1 and X_2 are arbitrary sucessive points on X-axis. Assuming the random process of the surface roughness is stationary and ergodic, we can characterize the roughness of the surface using two statistical functions. That is, the statistical distribution of height deviation from a certain

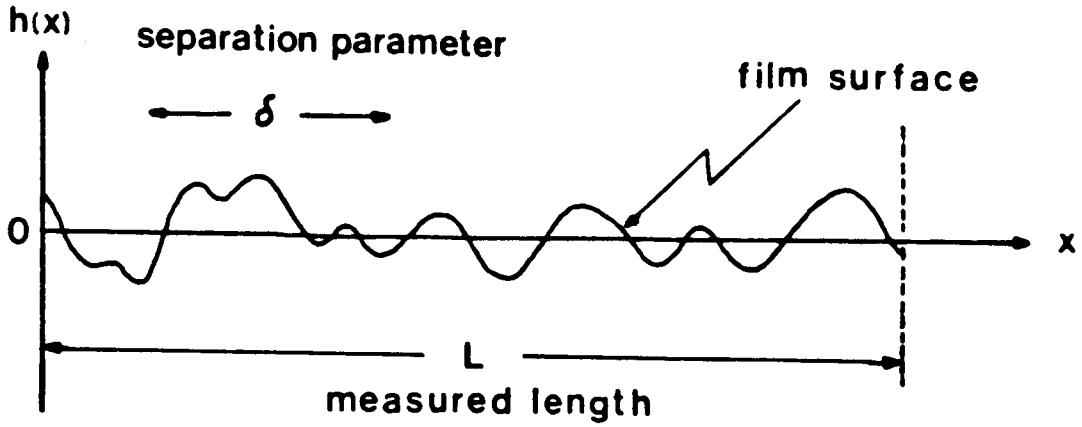

Figure 12. Coordinates of Random Surface Profile

mean level gives us information about heights of hills, and the correlation function or autocorrelation coefficient gives us information about how the hills and valleys of the surface are crowded close together or far apart. These functions are defined as follows.

The standard deviation σ of height h(x) is given as

$$\sigma^2 = \lim_{L\to\infty} 1/L \int_0^L [h(x) - \langle h(x)\rangle]^2 dx$$
$$= \langle h^2(x)\rangle - \langle h(x)\rangle^2 \qquad (20)$$

where $\langle h(x)\rangle$ is the mean value of height given by

$$\langle h(x)\rangle = \lim_{L\to\infty} 1/L \int_0^L h(x)d(x) \qquad (21)$$

The correlation function is

$$B(\delta) = \lim_{L\to\infty} 1/L \int h(x) \cdot h(x+\delta)d(x) \qquad (22)$$

And its normalised correlation function called the autocorrelation function is

$$C(\delta) = \frac{B(\delta) - \langle h(x)\rangle^2}{\langle h^2(x)\rangle \cdot \langle h(x)\rangle^2} \qquad (23)$$

For a purely random surface, C(δ) will decrease monotonously from its maximum value

$$C(0) = 1.0 \quad \text{to} \quad C(\infty) = 0.0 \qquad (24)$$

And the correlation distance Dc which can be thought of as a measure of the density or frequency of roughness on a horizontal scale is defined to be the distance at which $C(\delta)$ drops from its maximum value of 1.0 to 1/e (=0.3679) (Figure 13).

These statistical parameters, standard deviation (σ), autocorrelation coefficient $C(\delta)$ and correlation distance Dc can be evaluated from surface profile data obtained using a stylus.

G. EFFECT OF PROCESS AND POLYMER VARIABLES ON SURFACE ROUGHNESS AND OPTICAL PROPERTIES

Cause of Surface Roughness on Polymer Film

There appear to be two major type of optical irregularities on the surface of blown crystalline polymer film, although light will also be scattered at inhomogeneities such as grain, microgels and particulate additives. These arise from surface irregularities caused by melt flow phenomenon and those caused by crystallization behavior (41). The effect of these irregularities depends on two factors : the degree of optical path difference and their size and distribution. The optical path difference for a given film thickness results either from physical path variations or from refractive index (including birefringence) differences. The greater the thickness or

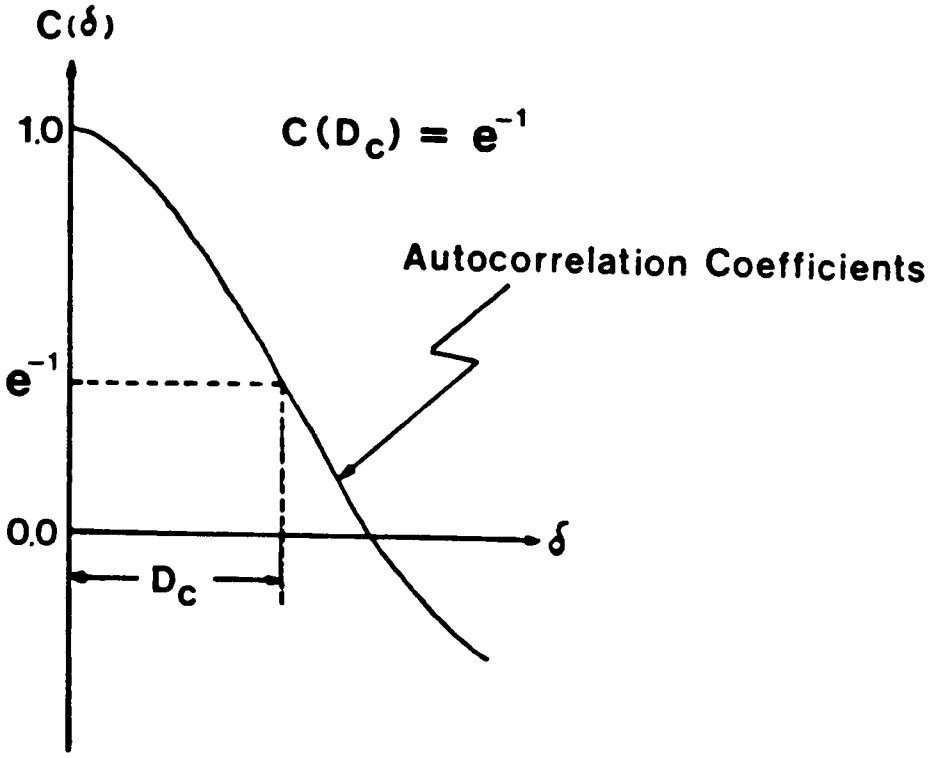

Figure 13. Definition of Correlation Distance

refractive index differences are, the more effective the irregularities will be in scattering light. Several kinds of irregularities, known as flow defects are observed and categorised :

(I) Extrudate distortion, described as "waviness", "knobliness" by Clegg (16) and as "melt fracture" by Tordella (105,106), is recognised as a departure from smooth flow which arises because polymer melts are viscoelastic in nature. This phenomenon has been studied extensively by several researchers (106,108).

(II) Surface irregularities, known as "shark-skin" or "matness" have depth of more than 50 μm. This phenomenon is considered as a surface defect arising at the die exit where a velocity discontinuity occurs owing to polymer metal adhesion. The correlation between "shark skin" and the cohesive failure of polymer melts was studied by Cogswell (17).

(III) Surface irregularities causing so called "extrusion haze" (42), is a structure about 1 μm in size. Although this kind of irregularity seems to be mainly related to haze of thin blown film as well as irregularities caused by crystallization behavior, it is still incompletely explained because of its fine structure.

McCallum (65) tabulated variation in size of irregularities covering several orders of magnitudes and pointed out their effects :

Unit Size	Effect
100 - 50,000°A	Haze and poor clarity
5 - 500 μm	Surface roughness
500 μm - 5 mm	Orange peel; ripple
5 mm or greater	Gross defects

Fine surface irregularities caused by crystallization behavior have been studied only briefly (41,42,94). Huck and Clegg (42) concluded that these surface irregularities arise from the growth and aggregation of crystallites at or near the surface which buckle the surface of the film. Stehling et al (94) suggested that so called crystallization haze is caused by stress induced crystallization close to the film surface during blown film operation.

Effect of Processing Conditions

Huck and Clegg (42), who first showed the existence of extrusion haze, suggested how the degree of surface roughness depends on the principal extrusion conditions in the blown film process for PE. According to their interpretation, during the film forming operation there will be change in the texture of the surface of melt because of a decrease in height of the extrusion defects and increase in

their length and breadth as the melt is drawn lengthways (draw down along MD) and blown sideways (blow-up along TD) and the overall magnitude of the extrusion defects will decrease under the influence of surface tension. On the other hand surface irregularities arising from the growth and aggregation of crystallites, which is mainly influenced by the temperature gradient at the frost line height, and the cooling time will increase as the frost line height (cooling time) increases. These two opposing effects should contribute to the total haze of blown film (Figure 14). The surface irregularities caused by extrusion defects originate from the complex elastic melt flow behavior in the extrusion die and are also influenced by the shear rate (output rate), the melt temperature and die profile. They show the effect of variables like extrusion temperature, output rate, blow-up ratio, and haul off speed in form of the characteristic haze curves.

Temperature. The effect of increasing temperature is to produce a film having lower haze, higher gloss and higher clarity. The reason being that the melt is smoother at the higher temperature and size of the crystalline aggregates get reduced because of higher cooling rates to maintain a given freeze-line distance.

Output Rate. An increase in the magnitude of frozen-in melt surface irregularities and so in percent haze might be

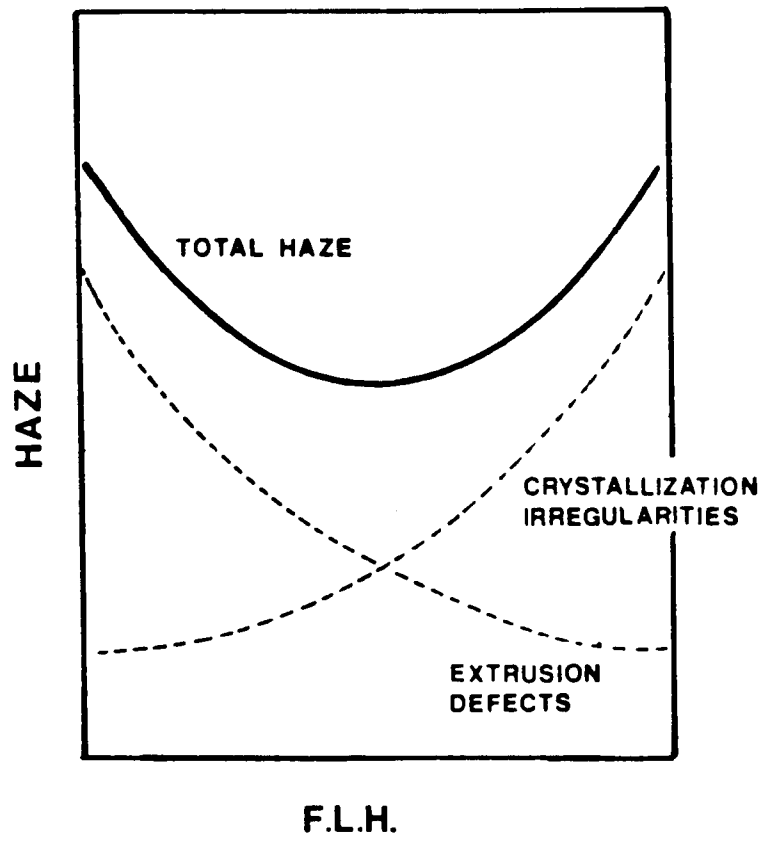

Figure 14. Haze Value as a function of Frost Line Height (FLH)

Source: Huck, N. D. and P. L. Clegg, SPE Trans., 1, 121(1961).

expected with increasing output rate. To maintain a constant freeze-line distance at an increased output rate, however, more air cooling is needed and the cooling rate through the freeze line increases reducing crystalline haze.

Blow-Up Ratio (82). An increase in blow-up ratio and consequent drawing of the melt reduces the size of extrusion defects finally frozen into the film; at the same time if this change is made at a constant output rate and the haul off speed is adjusted to maintain film thickness constant, there is an increase in the cooling time and so increase in crystallization haze.

Draw Down Ratio. Howells and Benbow (41) experimentally found that the surface haze which they associated with mainly the extrusion haze component, decreases with decreasing draw down ratio. They noted that this decrease in extrusion haze is partly accountable by the greater relaxation occuring between the die and the frost line at low draw down ratio. And they suggested that in order to generate extrusion haze it is necessary to apply both melt shear (as in the film die) and a simple melt deformation (as in the draw down and blow-up). They argue that one of these processes alone is not sufficient, and that extrusion haze may originate in the immediate vicinity of the die exit but relaxes rapidly unless a restraint is imposed.

Bubble Cooling Arrangements. Pilaro and Kremer (81) suggested that extruding blown tubing through an annealing chamber minimizes the surface roughness caused by melt fracture. Huck and Clegg also suggest use of annealing chamber but followed by a rapid quench at or near the freeze line to reduce the size of the crystallization irregularities.

Recently Stehling and his coworkers (94) carried out on-line haze measurement to confirm Huck and Clegg's hypothesis using flat film extruded from a slit die. It was assumed that for these films the mechanism of haze formation is similar to that of blown films. Haze was measured as a function of distance from the die. Their measurements on LDPE showed monotonically increasing haze from the die exit to far downstream instead of postulated initial decrease. They also carried out on line small angle light scattering measurements. They suggested that the spatial rearrangement of the surface features generated at the die exit possibly causes an increase rather than a decrease in haze after exit from the die.

Effect of Polymer Variables

It is well known that the haze of LDPE film can be reduced by subjecting the polymer melt to a mechanical deformation in an intensive mixer before extrusion (1).

Although this process is commonly used in the film industry, the mechanism is poorly understood. A number of workers have proposed that polymer melt elasticity is closely related to blown film haze. According to Huck and Clegg (42), the haze of LDPE film increases as extrudate die swell increases. Shida et al (90) used entrance pressure drop for flow into a capillary, Po, as a measure of melt elasticity and concluded that the haze of blown poly(ethylene co-vinyl acetate) film increased as Po increased. Howells and Benbow (41) reported, without supporting data, that mechanical treatment reduced LDPE melt elasticity without molecular weight changes. A better documented conclusion was obtained by Fujiki (28) and Rokudai (87), who further noted that reduction in elasticity (die swell and entrance drop) was accompanied by a decrease in film haze.

On the other hand Albright (1) attributed the reduction of film haze resulting from mechanical deformation of the melt to polymer chain scission, but he presented no data to support this view. Stehling et al (94) carried out haze measurement on LDPE blown films which were reextruded several times. From data obtained by GPC measurements and measurements of die swell recovery with different residence times in a capillary rheometer, they concluded that mechanical deformation reduces melt elasticity and haze by a reversible physical mechanism that generates a long-lived nonequilibrium melt structure.

Perron and Lederman (80) studied the effect of molecular weight distribution on PE blown film properties including haze and gloss. They concluded that broadening the MWD increases haze and reduces film gloss because of non-Newtonian behavior of melt. They also pointed out that increased molecular weight increases haze because of the influence of weight average molecular weight on melt viscosity and rheological properties. Foster (27) concluded that haze of LDPE blown film increased as the number of long chain branches in the resin increased. Stehling et al (94) reported from their GPC measurements that the haze of blown LDPE film increased with increase of MWD, the concentration of large size molecules and the number of long branches in a weight average molecule. They also suggested that by introducing more irregularity into the polymer chain by copolymerization or by increasing short chain branching, haze arising from crystallization may possibly be reduced. Williamson (113) studied clarity and haze of LDPE films of varying melt indices. He pointed out that the distortion or turbulence leading to large scale surface irregularities originates at the extrusion die entry and occurs at a critical shear stress or rate of shear. The easier flowing, high melt index PEs can be extruded below this critical point giving high clarity films.

Kuhre et al (54) studied crystallization modified polypropylene (PP) by incorporating nucleating agent (metal salts of organic acids). He suggested that certain metal salts have requisite properties such as molecular size, stereochemical structure and polarity to provide suitable nucleii for the growth of PP spherulites. He concluded that crystallization modified PP demonstrates good processing characteristics and improved mechanical and optical properties. This is the result of finer microstructure promoted by nucleation results. Kargin et al (45) studied effect of nucleating agents on the kinetics of crystallization of polymers and resulting properties. They concluded that artificial nucleating agents change not only the sizes of super molecular structure elements of the polymer, but also the rate of crystallization. The efficiency of the influence of a nucleating agent on the polymer structure and properties are greatest in those cases where the crystallization of the polymer without nucleating agent causes the growth of inhomogeneous large structures, whereas addition of small amount of dispersive solids causes polymers of a homogeneous structure.

CHAPTER 3

MATERIALS AND EXPERIMENTAL PROCEDURES

A. MATERIALS AND THEIR CHARACTERIZATION

PP resins used in our experiments were commercial polymers supplied by Gulf Chemical Company of varying melt flow rate, MFR,(from 2.3 to 27.4), molecular weight distribution (labled B-broad and N-narrow) with and without nucleating agent (0.2% sodium benzoate). All the resins contained a standard stabilizer package. We also used Hercules Pro-fax PD195 (MI-1.5, N-MWD) as a resin with low melt index. The nomenclature (as provided by Gulf) followed and details of MFR, MWD and nucleating agent additive are listed in Table I.

Intrinsic viscosities of decalin solutions of a few PP resins were determined using a Cannon-Ubbelhode viscometer immersed in a hot silicone oil bath maintained at 135°C. The possible shear rate dependence of the viscosity was assumed to be neglible. Intrinsic viscosity $[\eta]$ was obtained by extrapolating the plots of η_{sp}/c and $\ln \eta_r/c$ versus c according to following relations

$$[\eta] = \lim_{c \to 0} \frac{\ln \eta_r}{c} = \lim_{c \to 0} \frac{\eta_{sp}}{c} \tag{25}$$

where relative (η_r) and specific (η_{sp}) viscosities are given by

$$\eta_r = \frac{\eta}{\eta_o} \quad ; \quad \eta_{sp} = \eta_r - 1 \tag{26}$$

Table I. List of Resins and their Properties

Resin	Appr. MFR (g/10min)	MWD (B/N)	Additive	I.V.[η] (dl/g)	$\bar{M}v_{-5}$ X10
PD 195	1.5	N	none	1.78	2.06
6214	2.3	B	none	1.74	2.00
PX2777	2.6	B	NA(0.2%)	----	----
6414	3.9	B	none	1.65	1.87
PX2782	3.8	B	NA(0.2%)	----	----
PX2779	3.9	N	none	----	----
PX2778	4.5	N	NA(0.2%)	----	----
7214	14.40	B	none	1.54	1.72
PX2780	10.29	N	none	----	----
PX2784	27.40	B	none	1.25	1.32
PX2781	30.00	N	none	----	----
PX2785	24.50	B	NA(0.2%)	----	----

B-Broad, N-Narrow, NA-Nucleating agent
a - approximate MI data provided by Gulf.
b - I.V. measured in our laboratory.

where η and η_o are viscosities of a solution of a given concentration c (in g/dl) and the solvent, respectively.

Viscosity average molecular weight ($\bar{M}v$) of PP resins were calculated according to Mark-Houwink equation (69)

$$[\eta] = K \bar{M}_v^a \qquad (27)$$

where K and a are constants. The values of K and a used were $1.0X10^{-4}$ dl/g and 0.8 respectively. The measured values of $[\eta]$ and $\bar{M}v$ for PP resins are given in Table I.

B. BLOWN FILM EXTRUSION EQUIPMENT AND OPERATING CONDITIONS

Tubular blown film from all resins were produced using a 3/4 inch Raineville screw extruder with an annular blown film die (inside diameter = 1.43 cm and outside diameter = 1.59 cm). A schematic diagram of the die is shown in Figure 15.

Temperatures set on various zones of extruder and die varied from 160°C to 210°C depending on type of resins being blown. High MFR resins with B-MWD needed slightly lower temperature settings (200°C). Throughput rate was kept constant for all experiments (Q = 617 g/hr). Several samples of blown films were made varying blow-up ratios (BUR) (1.0 to 4.0), draw down ratios (4.0 to 10.0) and frost line heights (FLH) (2.5 cm to 18 cm). Variation of FLH was done at constant conditions of BUR = 3.0 and DDR = 7.0. For

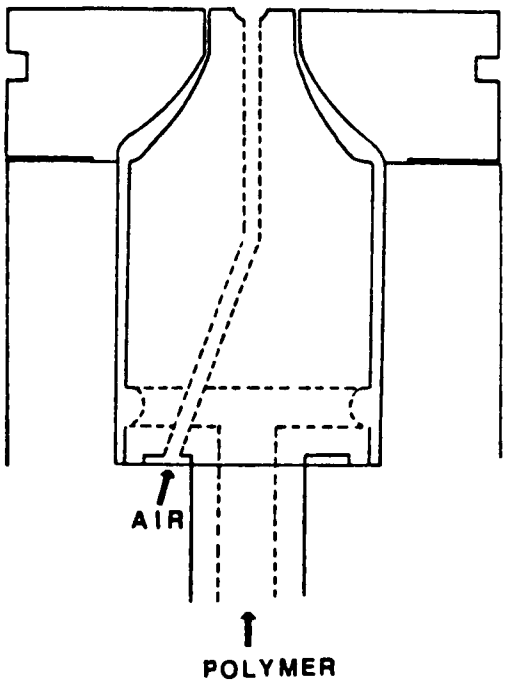

Figure 15. Schematic Diagram of the Blown Film Die

various resins any signs of bubble instability occuring were noted down qualitatively thus giving rise to operating space for stable bubbles in terms of BUR, DDR, and FLH. The temperature settings for various resins are listed in Table II. In Table III a list of film preparation conditions and the sample labelling is shown which will be used while characterizing the samples.

C. DEGREE OF CRYSTALLINITY OF FILMS

Degree of crystallinity of various PP films were determined by measuring their densities at 23°C using a distilled water-isopropyl alcohol density column with density range of 0.8800-0.9300 g/cc. The crystalline fraction was obtained through

$$X = \frac{\rho_c}{\rho}\left(\frac{\rho - \rho_a}{\rho_c - \rho_a}\right) \tag{28}$$

where X is the weight fraction of crystalline phase, ρ is the density of the sample film, ρ_a is the density of the amorphous phase (0.854 g/cc), and ρ_c is the density of the crystalline phase (0.932 g/cc).

The values of % crystallinity of various films are given in Table III.

D. DIRECT TRANSMISSION FACTOR MEASUREMENTS

The direct transmission factor of the blown film was measured using wide angle light scattering apparatus, Model

Table II. Temperature Setting on Extruder and Die Zones

Resin	Temperature on extruder and die zones (°C) Zone 1	Zone 2	Zone 3	Die
PD 195	190	200	210	215
6214	180	190	190	210
PX2777	180	190	190	210
6414	180	190	190	200
PX2782	180	190	190	200
PX2779	190	195	195	210
PX2778	190	195	195	210
7214	170	170	180	190
PX2780	170	180	190	200
PX2784	160	170	175	180
PX2781	170	175	180	190
PX2785	160	170	175	180

Table III. List of Film Preparation Conditions

Resin	Sample	BUR	DDR	FLH (cms)	Degree of crystallinity (%)
PD 195	PPN-11	1.0	4.0	8.0	64.84
	PPN-12	1.0	10.0	11.0	64.90
	PPN-13	3.0	7.0	3.0	64.80
PX2779	PPN-41	1.0	4.0	8.0	67.71
	PPN-42	1.0	10.0	11.0	66.34
	PPN-43	3.0	7.0	5.0	66.09
	PPN-44	3.0	7.0	10.0	-----
	PPN-45	3.0	7.0	15.0	-----
PX2780	PPN-101	1.0	4.0	8.0	67.71
	PPN-101	1.0	10.0	8.0	66.34
	PPN-103	3.0	7.0	4.0	63.59
6214	PPB-21	1.0	4.0	8.0	66.09
	PPB-22	1.0	10.0	11.0	66.34
	PPB-23	3.0	7.0	3.0	65.46
6414	PPB-41	1.0	4.0	8.0	67.71
	PPB-42	1.0	10.0	11.0	66.71
	PPB-43	3.0	7.0	5.0	66.09
	PPB-44	3.0	7.0	12.0	-----
	PPB-45	3.0	7.0	18.0	-----
7214	PPB-141	1.0	4.0	8.0	66.34
	PPB-142	1.0	10.0	11.0	66.34
	PPB-143	3.0	7.0	2.5	66.71
	PPB-144	3.0	7.0	5.0	-----
	PPB-145	3.0	7.0	8.0	-----
	PPB-146	3.0	7.0	10.0	-----
	PPB-147	3.0	7.0	13.0	-----
	PPB-148	3.0	7.0	15.0	-----
PX2784	PPB-271	1.0	4.0	8.0	66.46
	PPB-272	1.0	10.0	11.0	64.90
	PPB-273	3.0	7.0	4.0	66.46
PX2778	PPN-41NA	1.0	4.0	8.0	68.08
	PPN-42NA	1.0	10.0	11.0	68.08
	PPN-43NA	3.0	7.0	3.0	67.96
	PPN-44NA	3.0	7.0	10.0	-----
PX2777	PPB-21NA	1.0	4.0	8.0	67.34
	PPB-22NA	1.0	10.0	11.0	67.09
	PPB-23NA	3.0	7.0	3.0	66.46
PX2782	PPB-41NA	1.0	4.0	8.0	68.33
	PPB-42NA	1.0	10.0	11.0	68.08
	PPB-43NA	3.0	7.0	4.0	67.09
	PPB-44NA	3.0	7.0	8.0	-----
PX2785	PPB-251NA	1.0	4.0	8.0	69.20
	PPB-252NA	1.0	10.0	11.0	68.33
	PPB-253NA	3.0	7.0	3.0	67.96

Only for resin 7214 sample films were made varying BUR at increment of 0.5 and DDR at increment of 1.0 to study transmission factors.

7214	PPB-1411 (25 samples)	1.0-3.5	4.0-10.0	2.5-11.0

6000 Light Scattering Monophotometer (C-7). A source of monochromatic light whose wavelength is 5460 A° provided incident light. A schematic diagram of the apparatus is shown in Figure 16.

A polymer film can be thought of as having a bulk phase and a surface phase. The total direct transmission factor, T, of the film will be the product of transmission factors of bulk phase, Tb, and surface phase, Ts,

$$T = Tb \cdot Ts \tag{29}$$

Direct transmission factors T and Tb were obtained using the immersion method. First the total transmission factor of a single blown film, T, was measured by holding the film between a pair of glass miscroscope slides. Then surfaces of film were covered by immersion oil (silicone n = 1.515) whose refractive index is similar to that of PP (n = 1.490) thus giving transmission factor of bulk phase Tb. Using equation (29) we could calculate Ts once T and Tb are measured. T was normallised to take in to consideration the effect due to variation in thickness of various samples using Lambert's law :

$$Tb = \exp(-\tau t) \tag{30}$$

where τ is the turbidity and t is the thickness of the bulk phase (assumed to be equal to the thickness of the film). Equation (30) permits to calculate turbidity τ first which was utilised to normallize Tb for constant representative thickness.

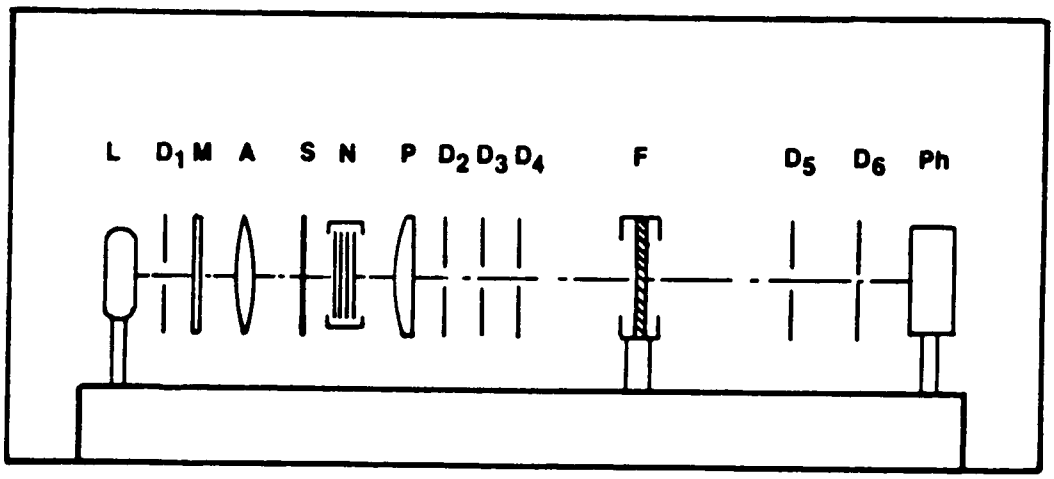

L: Mercury lamp
D: Diaphram
M: Monochromatic filter
A: Achromatic lens
S: Shutter
N: Neutral filter
P: Plano cylindrical lens
F: Film sample
Ph: Photomultipulier tube

Figure 16. Schematic Diagram of Light Scattering Monophotometer Model 6000

Ts could be further divided into transmission factors of inside surface phase, Tsi, and outside surface phase, Tso (considering bubble to be of cylindrical geometry). The method followed is similar to that used by Clampitt (14). Thus we can write

$$Ts = Tsi \cdot Tso \tag{31}$$

By placing the outside surfaces of two identical films together with immersion oil in between, the contributing surfaces will be the inside surfaces and vice versa, we could get transmission factors Tsi and Tso. Utilising schematic arrangement as shown in Figure 17 we can develop appropriate equations for separating Ts into Tsi and Tso.

For two films placed with the outside surfaces together using immersion oil in between them the transmission factor of the composite Tso-so will be

$$Tso\text{-}so = (Tsi)^2 \cdot (Tb)^2 \tag{32}$$

and for two films placed with inside surfaces together using immersion oil in between them, the transmission factor of composite Tsi-si will be

$$Tsi\text{-}si = (Tso)^2 \cdot (Tb)^2 \tag{33}$$

The equations (32) and (33) yield the values of Tsi and Tso if Tb is already calculated using single blown film. Thus

$$Tsi = \frac{(Tso\text{-}so)^{1/2}}{Tb} \tag{34}$$

and

$$Tso = \frac{(Tsi\text{-}si)^{1/2}}{Tb} \tag{35}$$

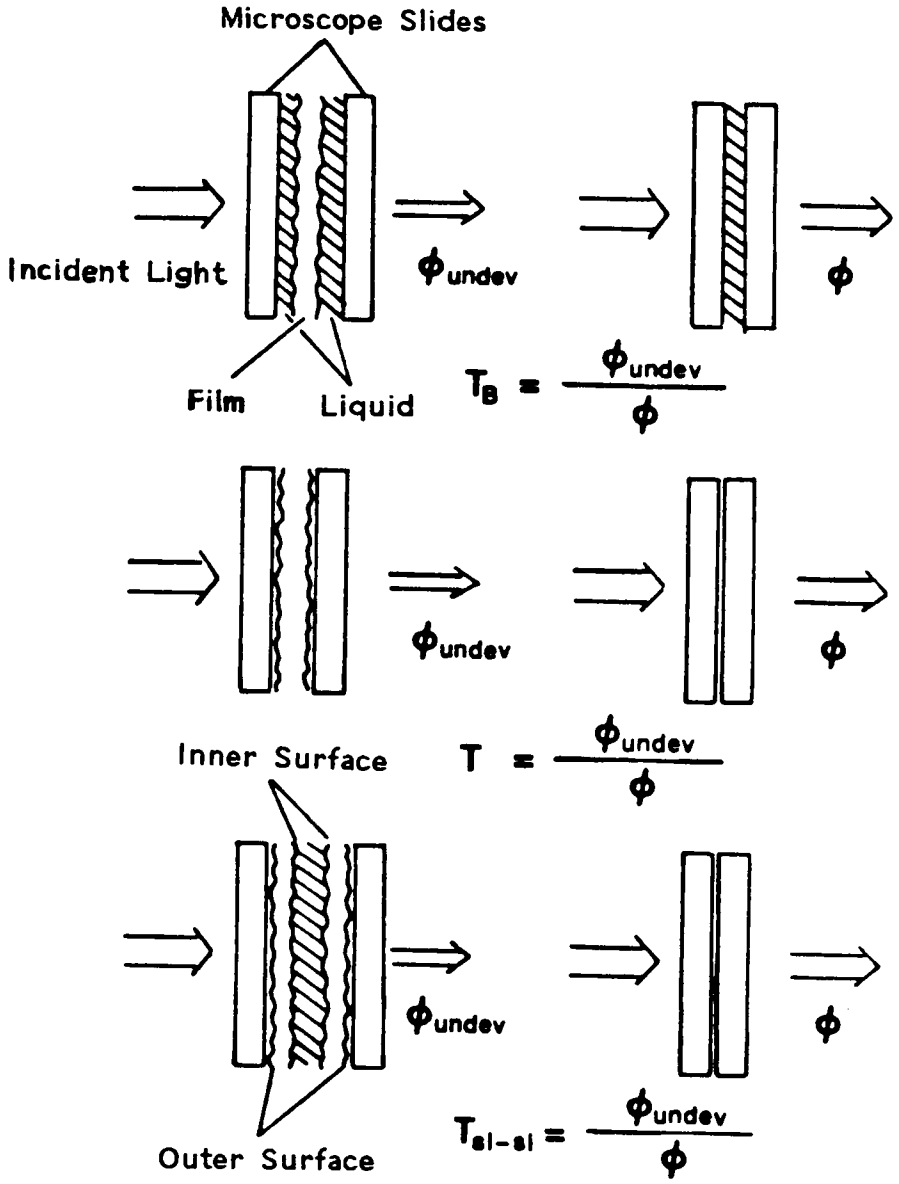

Figure 17. Sample Set Up for Measurement of Direct Transmission Factors

Experimentally for all film samples the transmission factors T, Tb, Tsi-si and Tso-so were measured. This provided the data to calculate Tsi, Tso and Ts. For measurement of T, Tb, Tsi-si and Tso-so the incident light flux ϕ through suitable filter and undeviated beam of transmitted flux ϕundev were measured. Depending on only film or surfaces of film covered by immersion oil or outside surfaces of two films placed together with immersion oil in between were held in microscope slides and inserted in incident beam we get ϕundev-film, ϕundev-b or ϕundev-so-so respectively (as shown in Figure 17). From ϕundev and ϕ we get transmission factors according to

$$T = \frac{\phi_{undev}}{\phi} \qquad (36)$$

E. SMALL ANGLE LIGHT SCATTERING MEASUREMENTS

For the SALS photographic patterns the instrument used was one similar to used by Stein and Rhodes (98). It was an assembly of a He-Ne laser light source, a polarizer, a shutter, pinhole holders, a sample holder, an analyser and a photographic cassette holder, mounted on a horizontal optical bench.

The film sample was held between a pair of glass microscope slides with immersion oil to eliminate surface scattering from the sample film. Photographic SALS Hv and Vv patterns were obtained using Polaroid films. Hv patterns

were used to calculate size of internal structure (spherulitic in PP) of film using the following equation :

$$Ro = \frac{1.025\ \lambda}{\pi \sin\left\{\frac{\Theta max}{2}\right\}} \qquad (37)$$

where λ = wavelength of laser beam in medium (632 nm for He-Ne laser source)

Ro = radius of spherulite

θ_{max} = radial maximum scattering angle

max is calculated by noting distance from film sample to photographic film (D) and from center of pattern to intensity maximum on lobe of Hv pattern (X). By geometry we have

$$\Theta max = \tan^{-1}\left(\frac{2X}{2D}\right) \qquad (38)$$

F. MEASUREMENT OF SURFACE PROFILE AND ITS CHARACTERIZATION

Measurement of Surface Profile

A profile of the surface roughness of each blown film was obtained using a Tencor Alpha-Step mechanical surface profiler (83). This profiler has a diamond stylus (conical) to trace over the surface placed on a sample station. The sample station can be moved in Y and Z directions. Y direction movement is used to place the sample in appropriate position and Z direction movement is used to get

the surface of sample in contact with stylus tip and to load stylus with appropriate loading. The stylus traces over the surface in the X direction and the profile is recorded on a chart recorder with 50 mm wide chart paper. Several different vertical magnifications (1000A° full scale to 1000KA° full scale) and three horizontal magnifications are available to obtain trace of various magnitudes of roughness. The profiler can be operated automatically or manually. In automatic operation the stylus first traverses on the surface to adjust automatic levelling of stylus with respect to the surface and then traces the profile on chart paper. In manual operation the trace of the profile is recorded on chart paper, and, if the profile slopes down or up the stylus is levelled manually. A list of vertical and horizontal magnifications and corresponding full scale ranges are given in Tables IV and V. The surface profiler is shown schematically in Figure 18.

The radius of the diamond stylus used in this experiment was 2.5 μm and the stylus loading was adjusted to 2.5 mg to produce good contact with the PP film surfaces. The total possible stylus travel across the sample is about 3 mm, but 0.4 mm long scans were generally used for the surface statistics.

Samples of film were laid as flat as possible on a glass microscope slide since otherwise the trace of profile has a tendency to show variation in slopes. The same result

Table IV. Horizontal Dimensions available on Profiler

Horizontal magnification setting	Spacing between 5mm vertical lines on chart (μm)	Scan speed (mm/sec)	Paper speed (mm/sec)
50X	100	0.1	5.0
500X	10	0.01	5.0
2500X	2	0.01	25.0

Table V. Vertical Dimensions available on Profiler

Full scale Dimensions	Vertical magnification	Spacing between 5mm horizontal lines
1000 A°	500,000X	100 A°
2500 A°	200,000X	250 A°
5000 A°	100,000X	500 A°
10 KA°	50,000X	1,000 A°
25 KA°	20,000X	2,500 A°
50 KA	10,000X	5,000 A°
100 KA°	5,000X	1 μm
250 KA°	2,000X	2.5 μm
500 KA°	1,000X	5 μm
1000 KA°	500X	10 μm

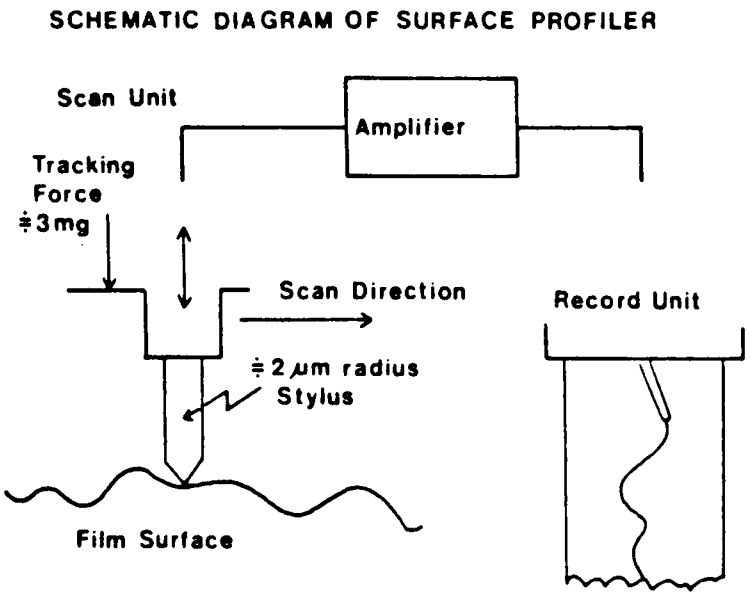

Figure 18. Schematic Diagram of Surface Profiler

is observed if thickness of the sample varies. Ten sets of data were taken from each sample, three sets along MD and three sets along TD at differnt places on the film and four sets with varying vertical magnifications. In our experiments manual operation of the profiler was used. Vertical magnifications of 10KA°, 25KA°, 50KA° and 100KA° were used depending on the degree of surface roughness. Horizontal magnification of 500X was used and this sets the scan and chart speed to 0.01 mm/sec and 5 mm/sec respectively.

The surface profiles obtained were digitized for statistical calculations using the TEKTRONIX 4953 Graphics Tablet system. The computer program used for this system is given in appendix A. The digitized data obtained are in tablet grid units and a calibration run was made on chart recorder paper to get digitized data in absolute units. Adjacent data points digitized were 2.0 μm apart on the X-axis and corresponding Y-axis coordinates were obtained. Y-axis coordinates essentially gave height deviation when used in the statistics program given in appendix B. On 0.4 mm long scans about 200 data points were digitized and typical data points in grid units are given in appendix C. Vertical spacings for each grid unit for different vertical full scale ranges are as shown below :

Full scale range	Vertical spacing for each grid unit
10KA°	0.00513 μm
25KA°	0.01282 μm
50KA°	0.02564 μm
100KA°	0.05128 μm

Characterization of Surface Roughness

Surface roughness of the blown film was assumed to be randomly as it appears from surface profiles (typical profiles are shown in Figure 19). The surface profiles were characterized in terms of standard deviation of height σ and autocorrelation coefficient $C(\delta)$ according to the following equations :

$$\sigma = \left[\frac{1}{N}\sum_{n=1}^{N}\left(h(n)\right)^2\right]^{1/2} \tag{39}$$

$$C(\delta) = \frac{B(\delta)}{\sigma^2} \tag{40}$$

$$C(\delta) = \frac{1/N \sum_{n=1}^{N} h(n) \cdot h(n+\delta)}{1/N \sum_{n=1}^{N} \left[h(n)\right]^2} \tag{41}$$

where $B(\delta)$ is correlation function, $n(=1,2,3\text{----})$ is each data point, N is total number of data points and δ is the separation factor between adjacent data points (2 μm in our case). It should be noted that for the above calculations the mean value of $h(n)$, $\langle h(n)\rangle$, is zero. Correlation distance Dc is the distance at which $C(\delta)$ drops to the value of 1/e according to relation

$$C(Dc) = e^{-1} \tag{42}$$

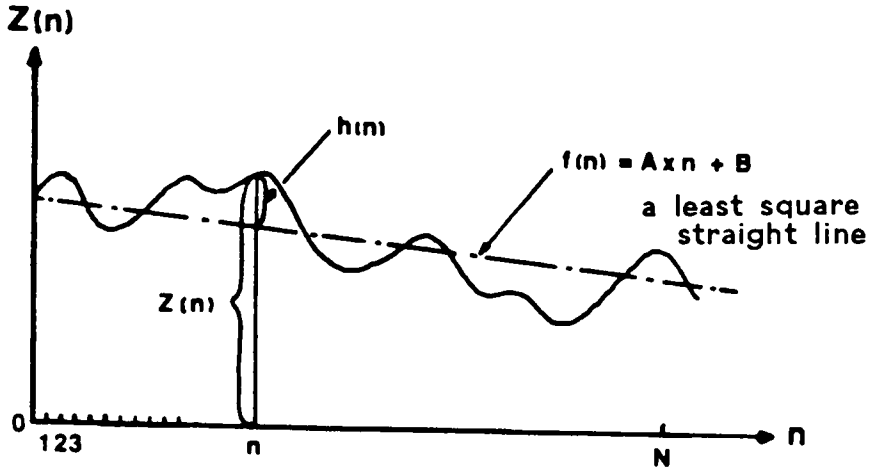

Actual Digitized Surface Profile Data Z(n)

$$h(n) = Z(n) - f(n)$$

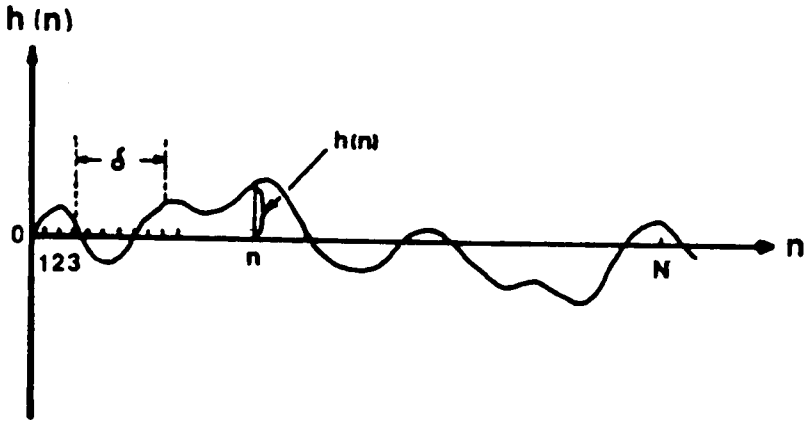

Basic Digitized Surface Profile Data h(n)

Figure 19. Treatment of Surface Profile Data

Evaluation of σ and $C(\delta)$ for each surface profile were made by using a fortran program (given in appendix B) on a DEC-10 computer system. In this statistics program digitized data of the surface profile were used. First a least square straight line was obtained by linear regression for a group of 20 data points (0.04 mm long scan) to elliminate effect of large bumps as well as instrument drift and sample tilt. The least square straight line is considered to be the mean surface level and differences of each data point from the mean surface were calculated. These differences were considered to be the height deviation h(n) for surface profile data (as shown in Figure 19). From the total number of data points and h(n), σ and $C(\delta)$ were calculated. Finally from a plot of $C(\delta)$ vs δ which is a typical monotonic decreasing plot from $C(0) = 1.0$ to $C(\infty) = 0.0$ (as already shown in Figure 13 on page 45), correlation distance Dc was calculated.

G. MICROSCOPIC EXAMINATIONS

A microscopic examination of both bulk phase and surface phases (inside and outside) of film were done using a Leitz polarizing optical microscope and a scanning electron microscope, AMR Model 900 high resolution electron microscope respectively.

Optical Microscopy

Film samples were held between a pair of glass microscope slides and the surfaces of film were covered with immersion oil to eliminate surface scattering effects. The microscope has a polarizer (acting as polarizing filter) attached to the condenser system with a lens. This lens illuminates the sample with a high numerical aperature beam of light suitable for higher magnifications (500X in our case). An analyser can be inserted between eye piece objective and sample to see the internal structure of the sample under crossed polarizers. A 35 mm camera was used to get optical photomicrographs.

Scanning Electron Microscopy

The film samples were examined on both inside and outside surfaces by SEM. The samples were coated with gold-palladium alloy in a vacuum chamber to elliminate charging of film surfaces by electrons. The scanning electron microscope was operated at 6KV and 40mA. This low voltage operation was chosen particularly to eliminate the destructive effects of the electron beam on the film surfaces. Magnification of 2000X was used for the observation of the film surfaces. SEM photographs were taken using Polaroid instant films in a photographic cassette.

CHAPTER 4

RESULTS AND DISCUSSION

A. OVERALL DIRECT TRANSMISSION FACTORS OF PP BLOWN FILMS

The values of the overall direct light transmission factors, T, were determined and separated into contribution by the bulk phase component (Tb) and surface phase component (Ts) for various PP films as described in chapter 3. The results for T are given in Table VI. Plots of T versus MFR of resins are shown in Figure 20. It is clear that the values of T are in the range of 37 to 55% (these low values of T for PP blown films were the basic reason of undertaking this study). From the plots shown in Figure 20 it appears that narrow MWD resins have larger T values than corresponding broad MWD resins, also T decreases with increasing MFR and the value of T is quite large for nucleated resins. Further, the above stated trend shows up in both low BUR/DDR and high BUR/DDR films. However, the films prepared at high BUR/DDR have larger value of T than those prepared at low BUR/DDR. It should be recalled that there was not much variation in % crystallinity values of these films (as already shown in Table III of chapter 3 on page 61).

Table VI. Total Transmission Factors of Films
Films - BUR 1.0-3.0, DDR 4.0-10.0

MI of Resin	Film Sample	T (%)	Film Sample	T (%)	Film Sample	T (%)
1.5	PPN-11	48.70	PPN-12	51.90	PPN-13	57.27
3.9	PPN-41	47.55	PPN-42	49.76	PPN-43	55.95
10.29	PPN-101	46.66	PPN-102	46.48	PPN-103	51.31
2.3	PPB-21	44.67	PPB-22	50.86	PPB-23	56.00
3.9	PPB-41	44.00	PPB-42	49.78	PPB-43	53.63
14.4	PPB-141	41.13	PPB142	45.52	PPB143	52.07
27.4	PPB-271	37.44	PPB-272	38.84	PPB-273	46.15
4.5	PPN-41NA	53.16	PPN-42NA	57.91	PPN-43NA	64.20
2.6	PPB-21NA	51.56	PPB-22NA	57.43	PPB-23NA	62.11
3.8	PPB-41NA	50.89	PPB-42NA	56.31	PPB-43NA	61.31
24.5	PPB-251NA	48.53	PPB-252NA	52.65	PPB-253NA	57.54

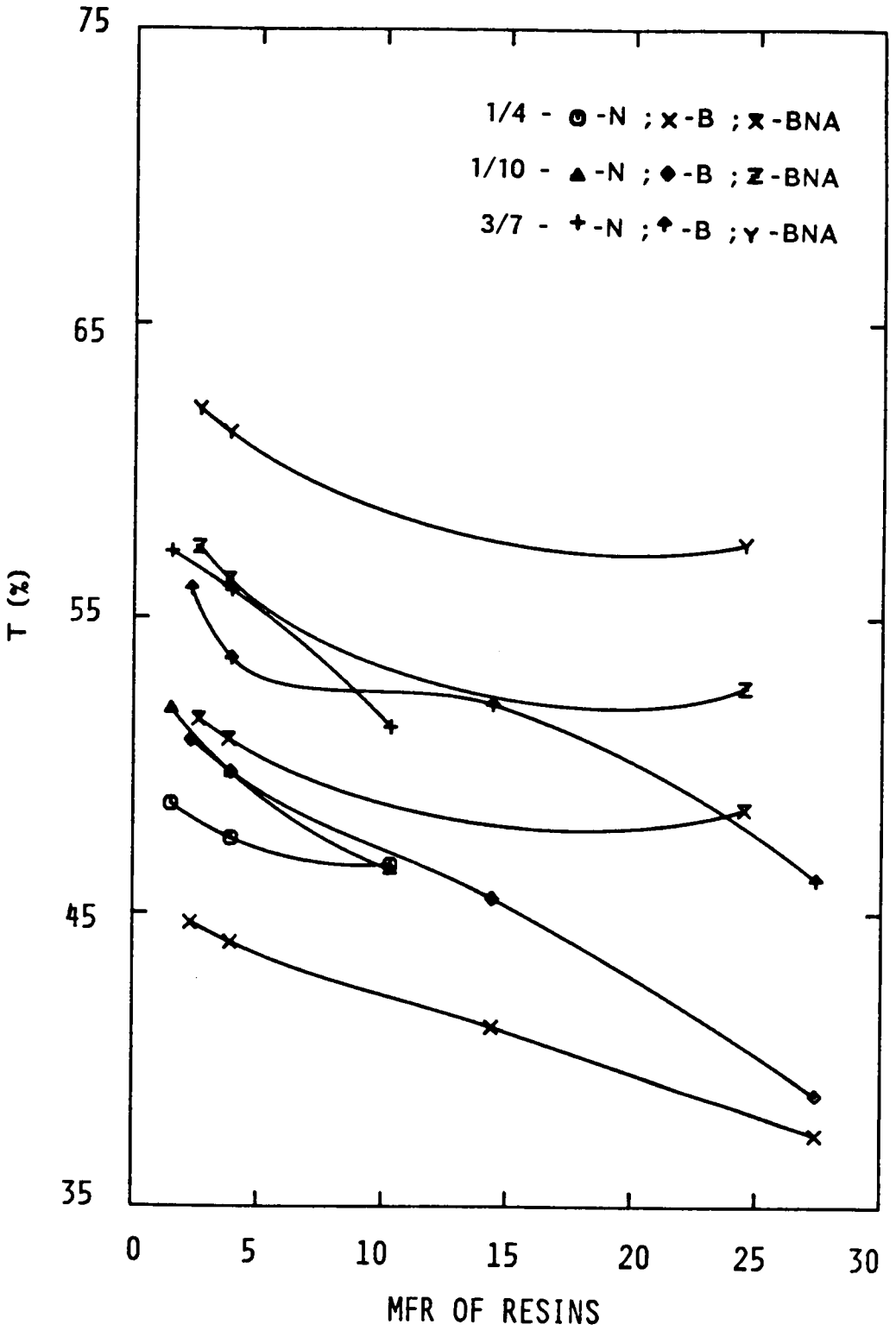

Figure 20. Overall Direct Transmission Factor (T) as a function of Melt Flow Rate

For the broad MWD resin with MFR = 14.4, the values of T were measured for the films with varying DDR (4.0 to 10.0), BUR (1.0 to 3.5) and FLH (2.5 to 15 cm at BUR = 3.0 and DDR = 7.0). The results are given in Tables VII, VIII and IX respectively and the respective plots are shown in Figure 21. These plots suggest a complex trend for variation of T with BUR and DDR and decrease in value of T with increase in FLH.

At this point we shall proceed without giving any discussion of the above results as it will be developed effectively in the following sections.

It is to be noted that the important notations used in figures and tables in this chapter are as follows:

N - Narrow MWD Resin	1/4 - BUR=1.0, DDR=4.0
B - Broad MWD Resin	1/10 - BUR=1.0, DDR=10.0
BNA - Broad MWD Resin with nucleating agent	3/7 - BUR=3.0, DDR=7.0

B. BULK PHASE OF FILMS

SALS Results

Hv-SALS patterns indicate that PP tubular blown films have spherulitic morphology, being 4 lobe clover leaf type of patterns. Typical patterns for resins (MFR = 4.0) with narrow/broad MWD with and without nucleating agent are as shown in Figures 22, 23, 24, 25 and 26. Qualitatively we see

Table VII. Total Transmission Factor of Films as a function of DDR
Resin - MFR 14.4, Broad MWD
Films - BUR 3.0, FLH 2.5 - 5.0 cm.

Film Sample	DDR	T (%)
PPB-1411	4.0	44.14
PPB-1412	5.0	42.67
PPB-1413	6.0	41.88
PPB-1414	7.0	52.01
PPB-1415	8.0	54.48
PPB-1416	9.0	57.92
PPB-1417	10.0	59.25

Table VIII. Total Transmission Factor of Films as a function of BUR
Resin - MFR 14.4, Broad MWD
Films - DDR 7.0

Film Sample	BUR	T (%)
PPB-1410	1.0	42.93
PPB-1415	1.5	41.56
PPB-1420	2.0	40.26
PPB-1425	2.5	37.90
PPB-1430	3.0	52.01
PPB-1435	3.5	53.48

Table IX. Total Transmission Factor of Films as a function of FLH
Resin - MFR 14.4, Broad MWD
Films - BUR 3.0, DDR 7.0

Film Sample	FLH (cms.)	T (%)
PPB-143	2.5	52.01
PPB-144	5.0	49.65
PPB-145	8.0	39.53
PPB-146	10.0	33.97
PPB-147	13.0	29.51
PPB-148	15.0	23.77

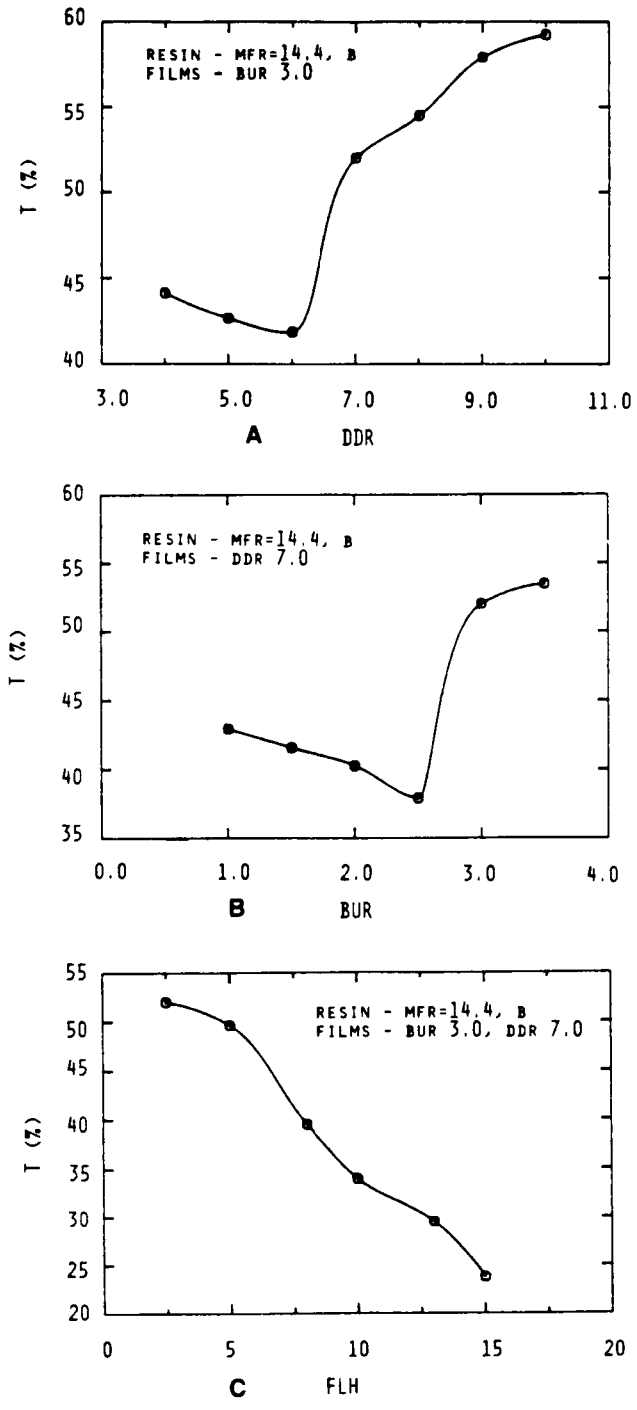

Figure 21. Overall Direct Transmission Factor (T) as a function of
A. Draw Down Ratio (DDR)
B. Blow-Up Ratio (BUR)
C. Frost Line Height (FLH)

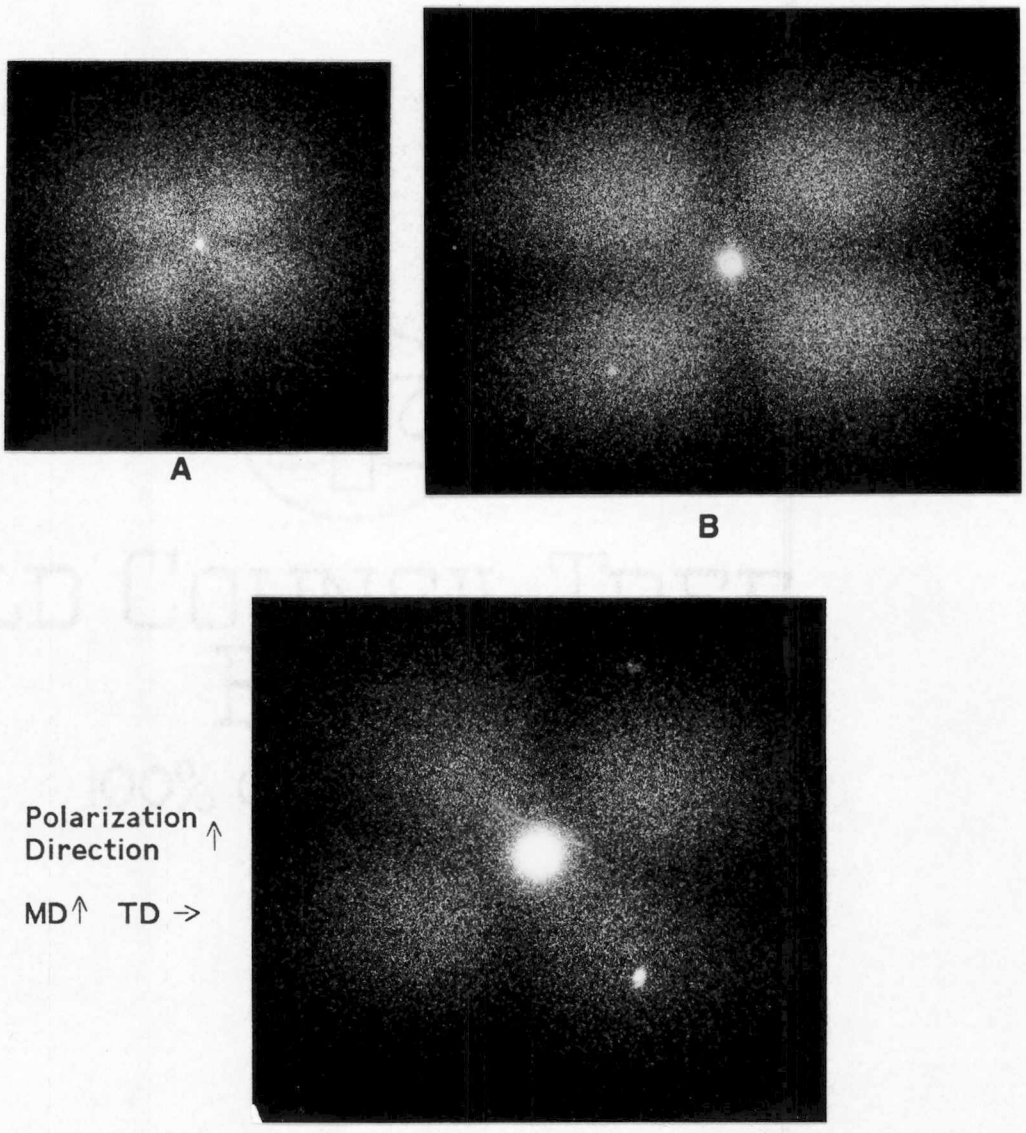

RESIN - MFR 3.9, B

A] FILMS - 1/4 ; Ro = 6.71μm
B] FILMS - 1/10 ; Ro = 3.32μm
C] FILMS - 3/7 ; Ro = 3.20μm

Figure 22. Typical SALS Hv Patterns, MFR 3.9, B

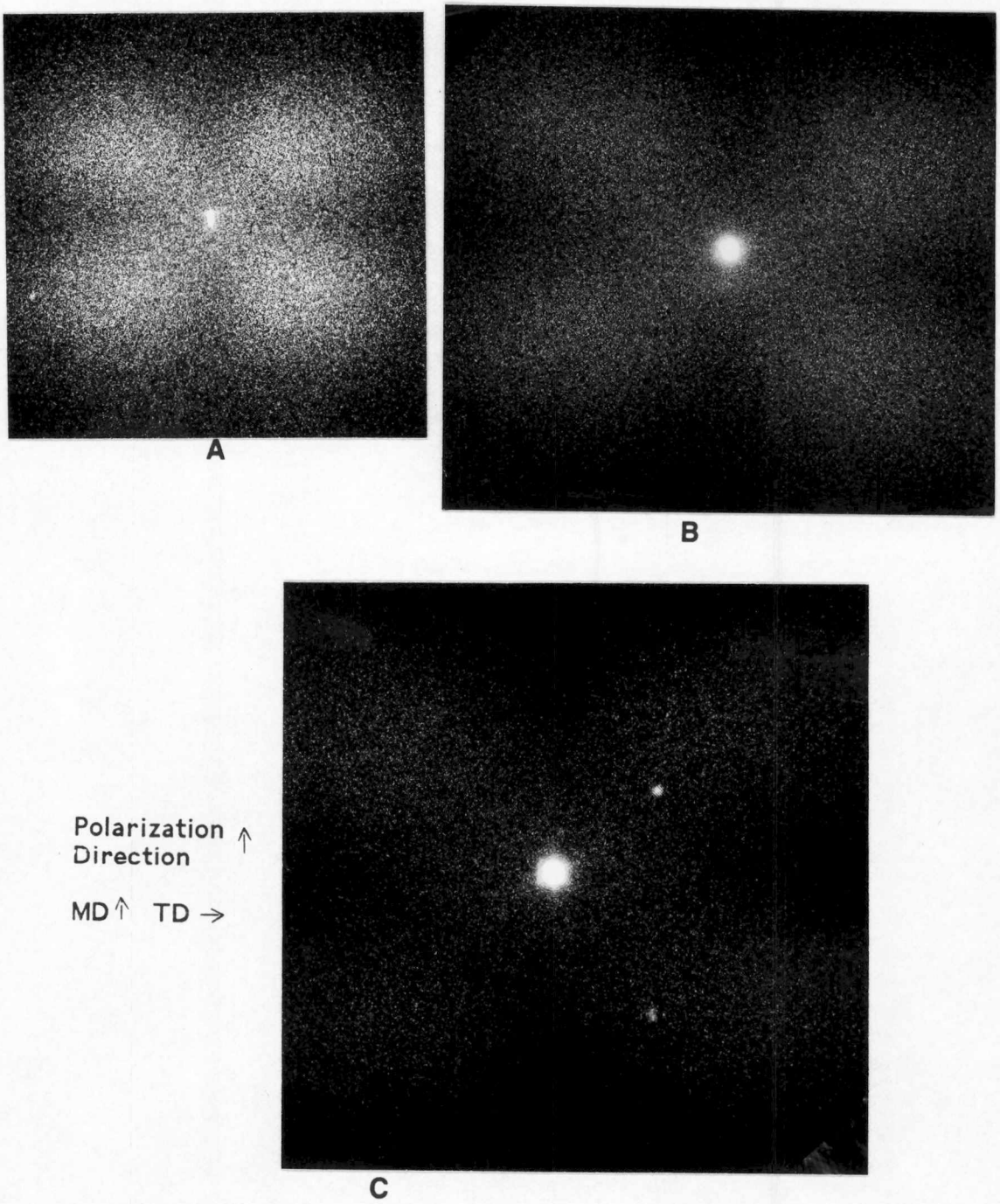

RESIN - MFR 3.8, BNA

A] FILMS - 1/4 ; Ro = 3.32 μm
B] FILMS - 1/10 ; Ro = 1.72 μm
C] FILMS - 3/7 ; Ro = 1.52 μm

Figure 23. Typical SALS Hv Patterns, MFR 3.8, BNA

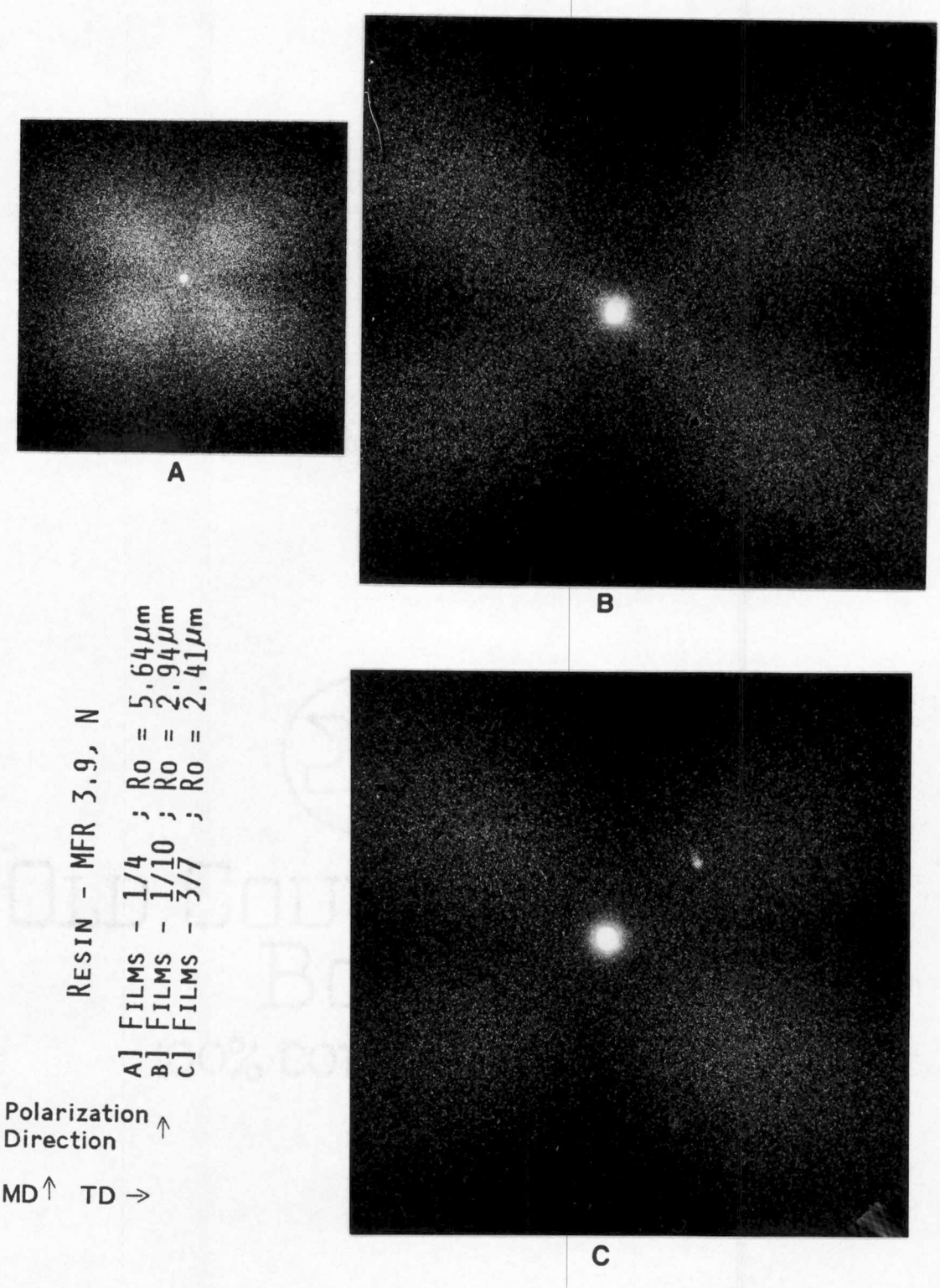

Figure 24. Typical SALS Hv Patterns, MFR 3.9, N

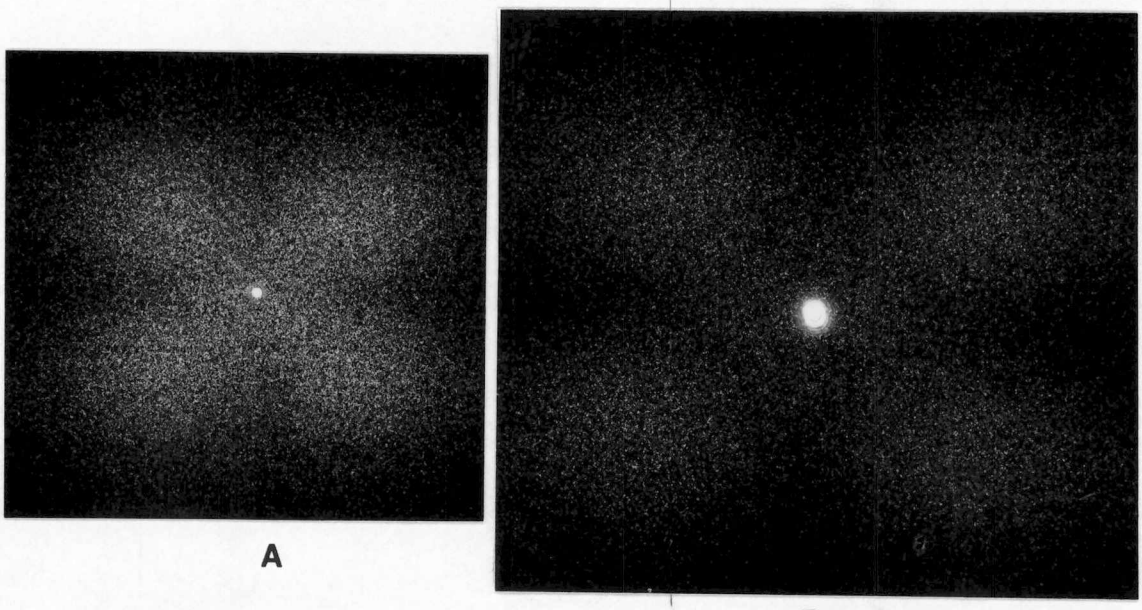

A

B

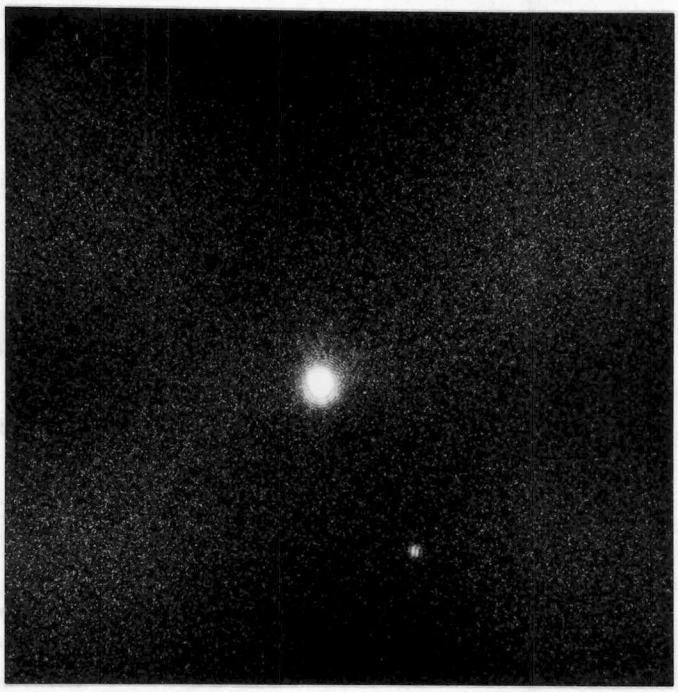

C

RESIN - MFR 4.5, NNA

A] FILMS - 1/4 ; Ro = 3.32 μm
B] FILMS - 1/10 ; Ro = 1.81 μm
C] FILMS - 3/7 ; Ro = 1.63 μm

Figure 25. Typical SALS HV Patterns, MFR 4.5, NNA

RESIN - MFR 3.9, B

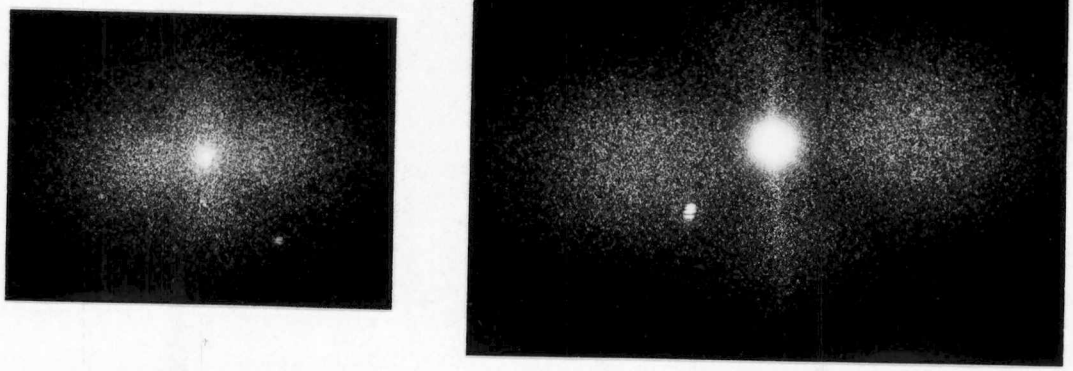

FILMS - BUR 1.0, DDR 4.0 FILMS - BUR 1.0, DDR 10.0

Polarization Direction ↑

MD↑ TD →

EFFECT OF FLH

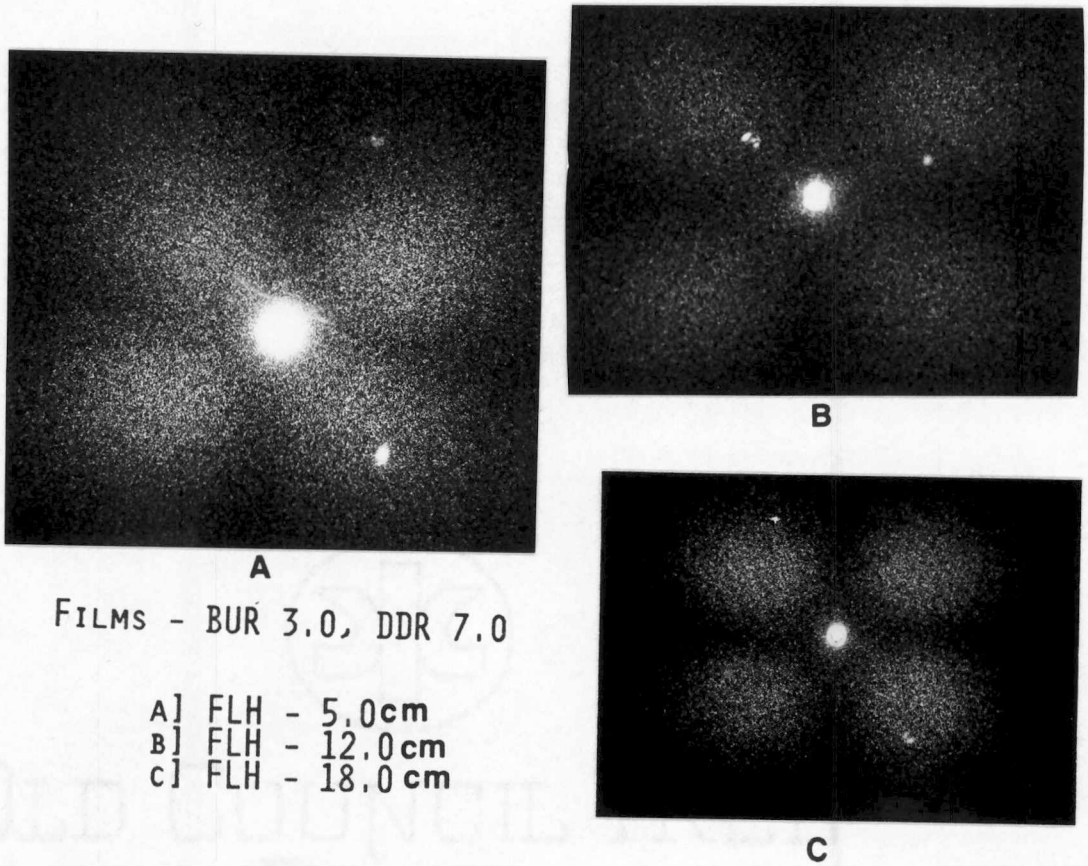

A B C

FILMS - BUR 3.0, DDR 7.0

A] FLH - 5.0cm
B] FLH - 12.0cm
C] FLH - 18.0cm

Figure 26. Typical SALS Vv Patterns and Effect of FLH on Hv Patterns

that at high DDR (BUR remaining constant) the lobes seem to be stretched perpendicular to the polarization direction whereas when both BUR and DDR are increased the lobes seem to be stretched both perpendicular and along the direction of polarization. Spherulite sizes have been calculated from these Hv-SALS patterns using the procedure described in chapter 3. The results for various resins under different film processing conditions are included in Tables X and XI. Spherulite sizes in terms of radius are plotted versus MFR in Figures 27 and 28. These plots show that at low BUR (1.0) and DDR (4.0) the spherulites are quite large (in the range of 5.0 to 7.0 μm in radius). They decrease in average radii as both BUR and DDR are increased. With increasing FLH the spherulites tend to grow quite effectively for high MFR resins. For all film preparation conditions spherulites tend to have larger sizes with increase in MFR up to MFR = 4.0, but beyond MFR = 4.0 the spherulite sizes are nearly independent of MFR. Broadening MWD produces larger spherulites than corresponding narrow MWD resins. Incorporating a nucleating agent in the resins, greatly reduces the spherulite size at all conditions of film preparation.

The final size of spherulites depends on cooling rates and concentration of nucleii. For nucleated resins it seems that smaller and more numerous spherulites are obtained due to a large concentration of nucleii. Whereas rapid cooling

Table X. Small Angle Light Scattering (SALS) Results
Films - BUR 1.0 - 3.0, DDR 4.0 - 10.0

Film Sample	Spherulite radius Ro (μm)	Film Sample	Spherulite radius Ro (μm)	Film Sample	Spherulite radius Ro (μm)
PPN-11	5.28	PPN-12	2.55	PPN-13	2.27
PPN-41	5.64	PPN-42	2.94	PPN-43	2.41
PPN-101	6.89	PPN-102	3.18	PPN-103	2.50
PPB-21	5.91	PPB-22	3.01	PPB-23	3.01
PPB-41	6.71	PPB-42	3.32	PPB-43	3.20
PPB-141	7.30	PPB-142	3.46	PPB-143	3.46
		PPB-272	3.56	PPB-273	3.46
PPN-41NA	3.32	PPN-42NA	1.81	PPN-43NA	1.63
PPB-21NA	2.97	PPB-22NA	1.70	PPB-23NA	1.40
PPB-41NA	3.32	PPB-42NA	1.72	PPB-43NA	1.52
		PPB-252NA	2.12	PPB-253NA	1.69

Table XI. Small Angle Light Scattering (SALS) Results
Films - BUR 3.0, DDR - 7.0, FLH 2.5 - 15 cm.

Film Sample	Spherulite Radius Ro (μm)
PPN-43	2.41
PPN-44	2.50
PPN-45	2.66
PPB-43	3.20
PPB-44	3.28
PPB-45	3.89
PPB-143	3.46
PPB-144	3.56
PPB-145	3.63
PPB-146	3.77
PPB-147	3.98
PPB-148	4.23
PPN-43NA	1.63
PPN-44NA	1.67
PPB-43NA	1.52
PPB-44NA	1.69

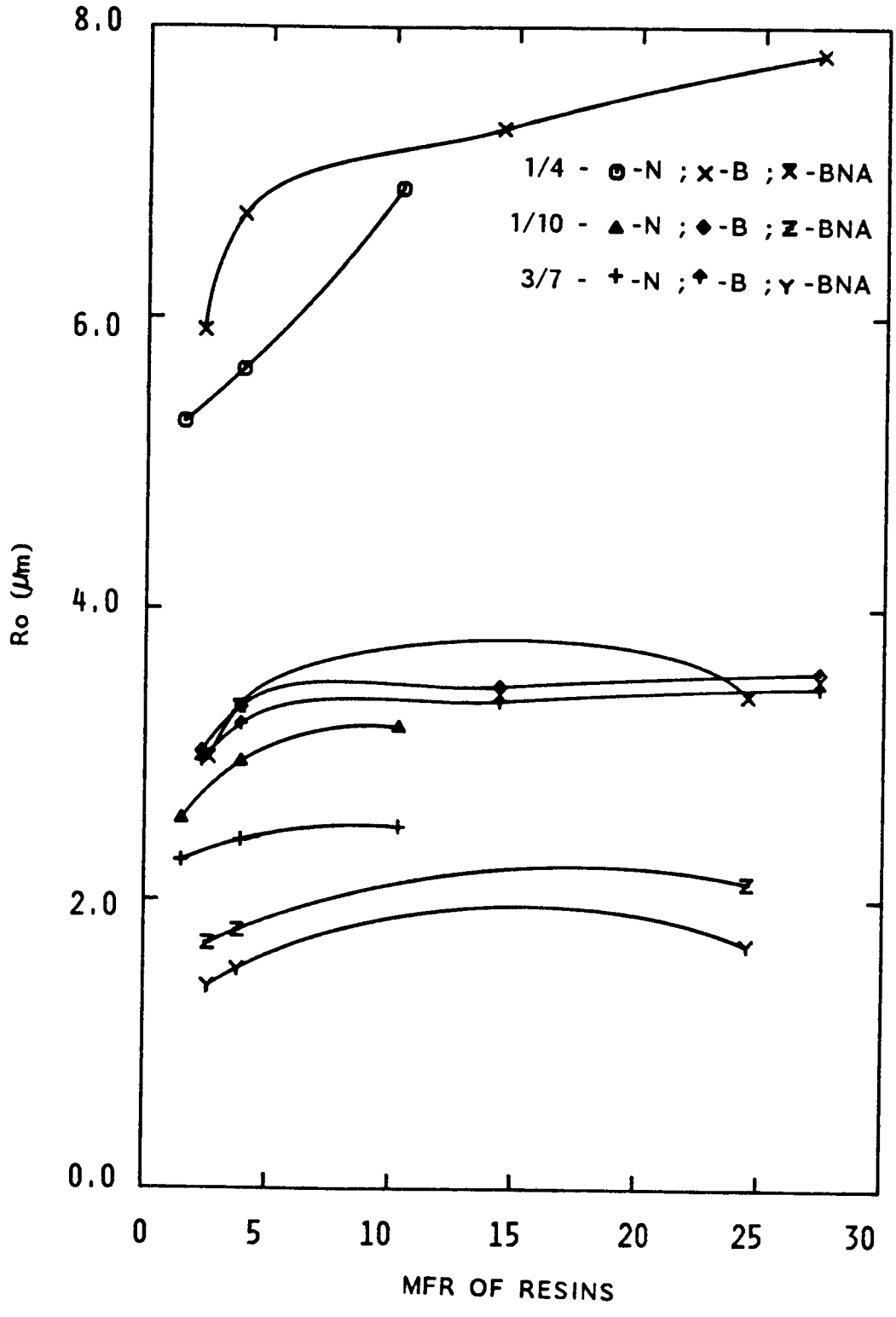

Figure 27. Spherulite Radius (Ro) as a function of Melt Flow Rate (MFR) of Resins

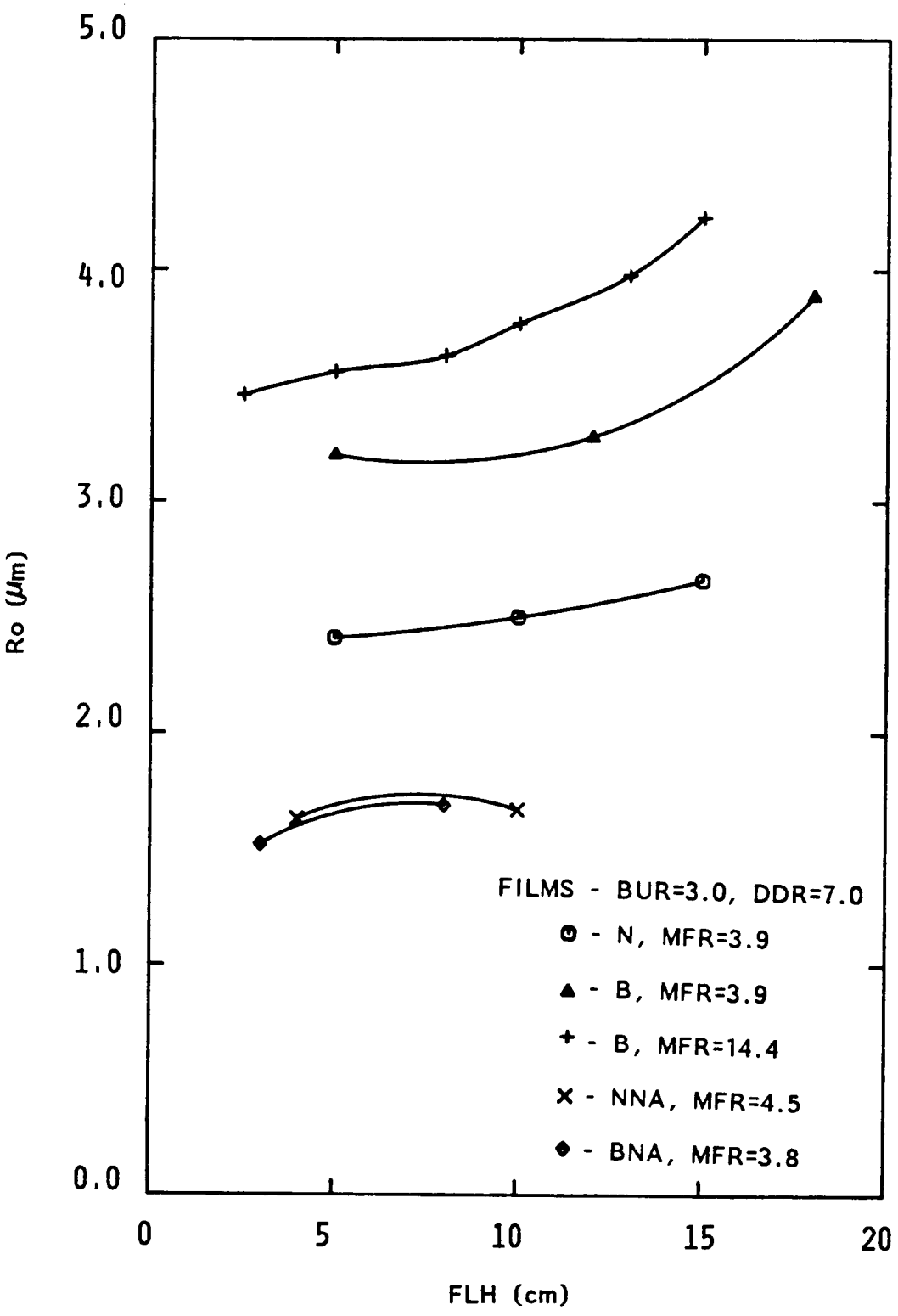

Figure 28. Spherulite Radius (Ro) as a function of Frost Line Height (FLH)

rates of bubble leads to smaller spherulites in case of unnucleated resins. This is a result of a larger undercooling prior to the onset of crystallization that results in greater nucleation rates. Slower cooling provides lower nucleation rates and more time for growth of the spherulites prior to impingement. At lower BUR and DDR, the films are rather thicker permitting lower cooling rates and hence larger spherulites. Similarly, increasing FLH lowers cooling rates and again produces larger spherulites. We thought that higher spherulite size for broader MWD resins might be due to the lower temperatures needed for extruding these resins (the temperature difference was 10°C) than for narrow MWD resins. Also for high MFR resins lower extrusion temperatures were needed than those for low MFR resins again probably giving higher spherulite sizes for high MFR resins due to the temperature differential. The temperature dependence of spherulite sizes was checked by extruding high MFR and broader MWD resin at the same temperature used for narrow and low MFR resin and the results are given in Table XII. From the results it is clear that the difference in extrusion temperature (10°C) does not have appreciable effect on spherulite size. The differences may therefore be ascribed to greater chain mobility in the lower molecular weight (higher MFR) resins which result in increased spherulite growth rates. Altrnatively, there may be somewhat greater nucleation rates for high molecular weight (low MFR)

Table XII. Small Angle Light Scattering (SALS) Results
Temperature Dependance of Spherulite Size

Film Sample	Spherulite size Ro(μm) @ 190°C	Spherulite size Ro(μm) @ 200°C	Film Sample	Spherulite size Ro(μm) @ 200°C
PPB-141	7.30	7.09	PPB-41	6.71
PPB-142	3.46	3.33	PPB-42	3.32
PPP-143	3.46	3.35	PPB-43	3.20

resins. It is not clear whether the effect of narrowing MWD is due to increased nucleation or decreased growth rate.

Direct Transmission Factors of Bulk Phase of Films

The direct transmission factors of the bulk phase Tb were determined by the procedure described in chapter 3. It was found that Tb is strongly dependent on thickness of film (thicker the film, lower the Tb) which should be apparently understood from Lambert's law. Typical values for Tb were in the range of 52-60% for films at lower BUR and DDR (1.0 and 4.0), 82-87% for films at lower BUR (1.0) and high DDR (10.0), 94-98% for films at high BUR (3.0) and high DDR (7.0). Typical thicknesses of these films were in the range of 200 μm, 75 μm and 38 μm respectively. These raw transmission factor values, referred to as absolute Tb values, are given in Tables XIII, XIV and XV for various films with varying resin characteristics and film preparation conditions. In order to elliminate the effect of thickness per se in the comparison we normallized the results for all films to a thickness of 50 μm (2.0 mils approximately). The values for Tbn (normallized Tb) range from 84 to 97%, the lower limit being for low BUR (1.0) and DDR (4.0) films and upper limit being for high BUR (3.0) and DDR (7.0) films. These Tbn values for all films are also given in Tables XIII, XIV and XV. In Figure 29 Tbn values are plotted versus MFR of the resins and the plot suggests

Table XIII. Absolute and Normallized Bulk Transmission Factors
Films - BUR 1.0, DDR 4.0

Film Sample	Turbidity cm^{-1}	Absolute bulk transmission factor Tba% (200μm thickness)	Normalised bulk transmission factor Tbn% (50μm thickness)
PPN-11	30.20	54.66	85.98
PPN-41	29.75	55.16	86.18
PPN-101	27.46	57.74	87.17
PPB-21	29.36	55.59	86.35
PPB-41	28.05	57.06	86.91
PPB-141	26.70	58.63	87.50
PPB-271	25.15	60.46	88.18
PPN-41NA	31.76	52.98	85.32
PPB-21NA	32.88	51.81	84.84
PPB-41NA	32.03	52.70	85.20
PPB-251NA	30.82	53.99	85.72

Table XIV. Absolute and Normallized Bulk Transmission Factors
Films - BUR 1.0, DDR 10.0

Film Sample	Turbidity cm^{-1}	Absolute bulk transmission factor Tba% (75μm thickness)	Normalised bulk transmission factor Tbn% (50μm thickness)
PPN-12	22.80	84.27	89.23
PPN-42	21.87	84.87	89.64
PPN-102	20.93	85.47	90.06
PPB-22	21.65	85.01	89.74
PPB-42	20.28	85.89	90.36
PPB-142	19.57	86.35	90.68
PPB-272	18.78	86.86	91.04
PPN-42NA	25.28	82.73	88.13
PPB-22NA	25.63	82.51	87.97
PPB-42NA	25.50	82.59	88.03
PPB-252NA	23.45	83.87	88.94

Table XV. Absolute and Normallized Bulk Transmission Factors
Films - BUR 3.0, DDR 7.0, FLH 2.5 - 15 cm.

Film Sample	Turbidity cm^{-1}	Absolute bulk transmission factor Tba% (38μm thickness)	Normalised bulk transmission factor Tbn% (50μm thickness)
PPN-13	10.52	96.07	94.88
PPN-43	8.32	96.88	95.93
PPN-44	14.04	94.79	93.22
PPN-45	16.81	93.80	91.94
PPN-103	7.80	97.07	96.18
PPB-23	7.12	97.32	96.50
PPB-43	6.90	97.41	96.60
PPB-44	15.35	94.32	92.61
PPB-45	20.24	92.58	90.38
PPB-143	3.43	98.70	98.30
PPB-144	11.35	95.77	94.48
PPB-145	18.51	93.19	91.16
PPB-146	22.76	91.69	89.24
PPB-147	23.04	91.60	89.12
PPB-148	24.40	91.10	88.52
PPB-273	5.06	98.09	97.50
PPN-43NA	11.04	95.88	94.63
PPN-44NA	17.14	93.68	91.79
PPB-23NA	15.98	94.09	92.32
PPB-43NA	13.98	94.81	93.25
PPB-44NA	18.29	93.27	91.26
PPB-253NA	12.73	95.27	93.83

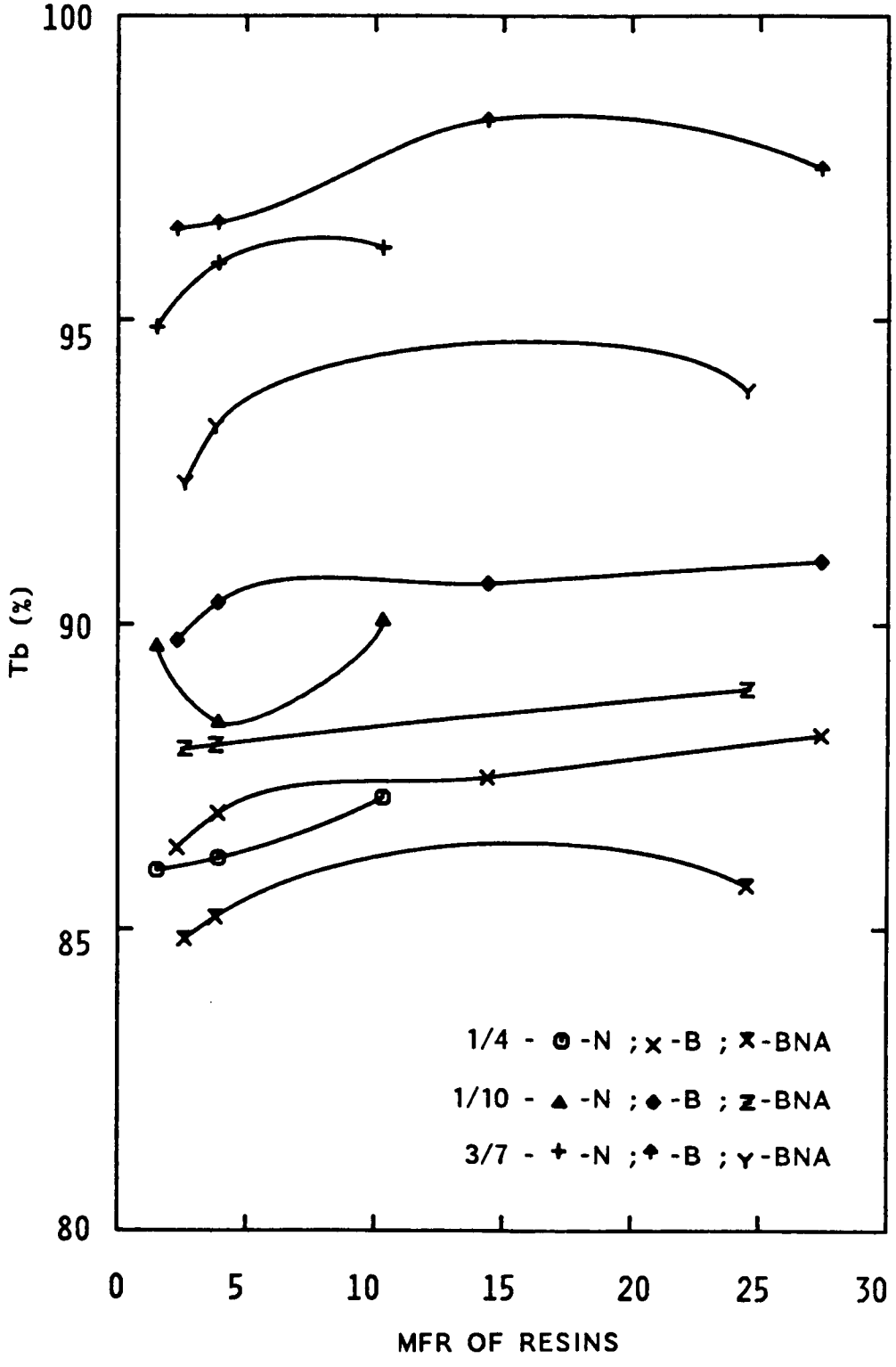

Figure 29. Bulk Phase Transmission Factor (Tb) as a function of Melt Flow Rate (MFR) of Resins

that varying MFR produces only a slight effect on Tbn. Broad MWD resins have higher Tbn values than narrow MWD resins. Further increasing BUR and DDR increases Tbn quite effectively. Nucleated resins have lower Tba and Tbn values than unnucleated resins.

Correlations between SALS Results and Transmission Factors of the Bulk Phase

The above discussed SALS and transmission factors of bulk phase results were correlated using normallized values of bulk transmission factors. Direct transmission factors of the bulk phase of film permit calculation of the turbidity τ of the films. In Figures 30 and 31 variation of Tbn and with sperulite size is shown for various film preparation conditions. It is seen that the larger the spherulite size, the higher is Tbn and lower is τ when compared for the same conditions of film preparation. But with increasing BUR or DDR or both together Tbn increases and τ decreases eventhough the spherulite size is smaller. Thus spherulite size alone does not control the transmission factors or light scattered but as pointed out by Stein et al (96,102) the absolute scattering power of a polymer film depends on orientation; the more oriented films exhibiting less scattering than unoriented films because of decrease in both local orientation and density fluctuations.

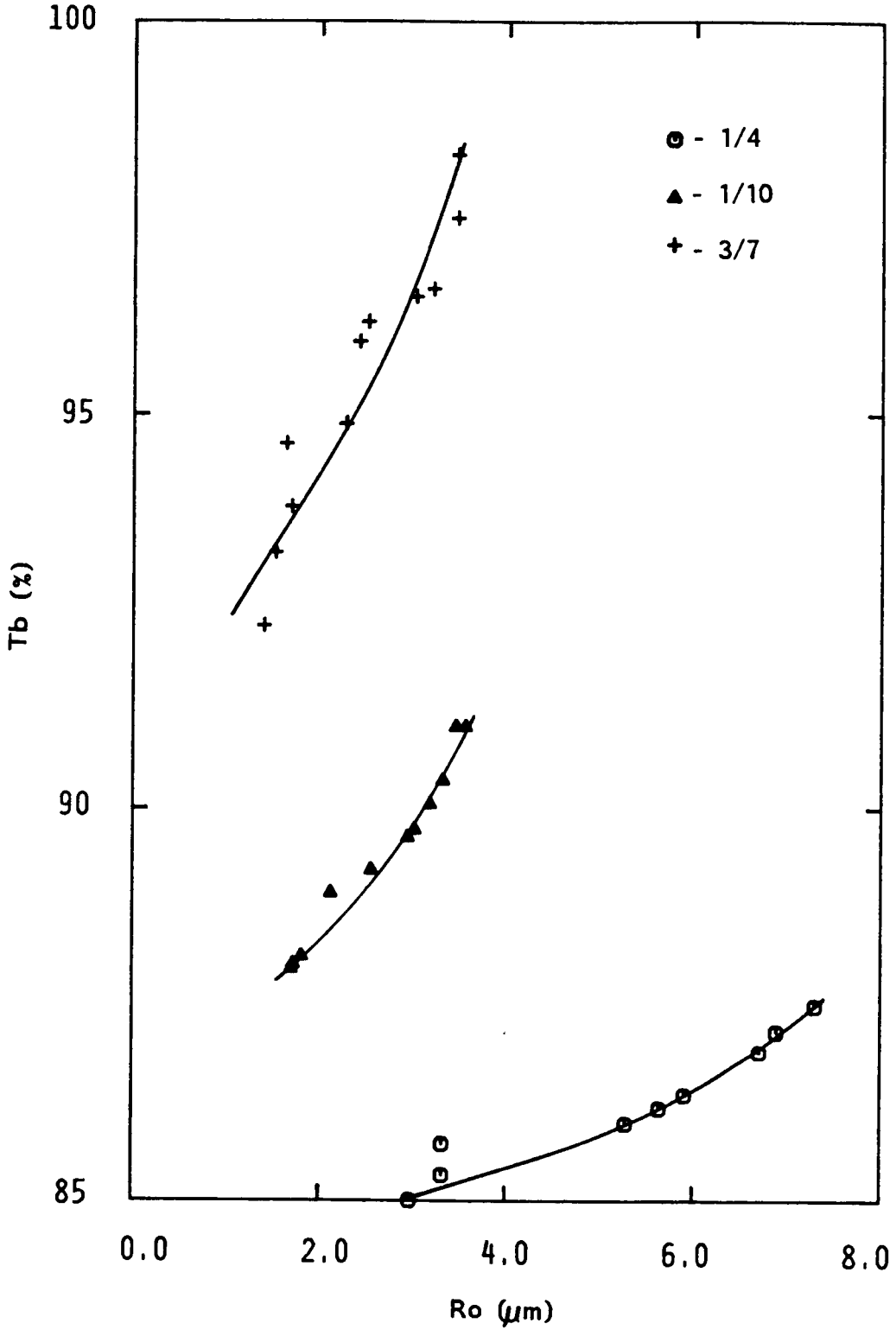

Figure 30. Bulk Phase Transmission Factor (Tb) as a function of Spherulite Radius (Ro)

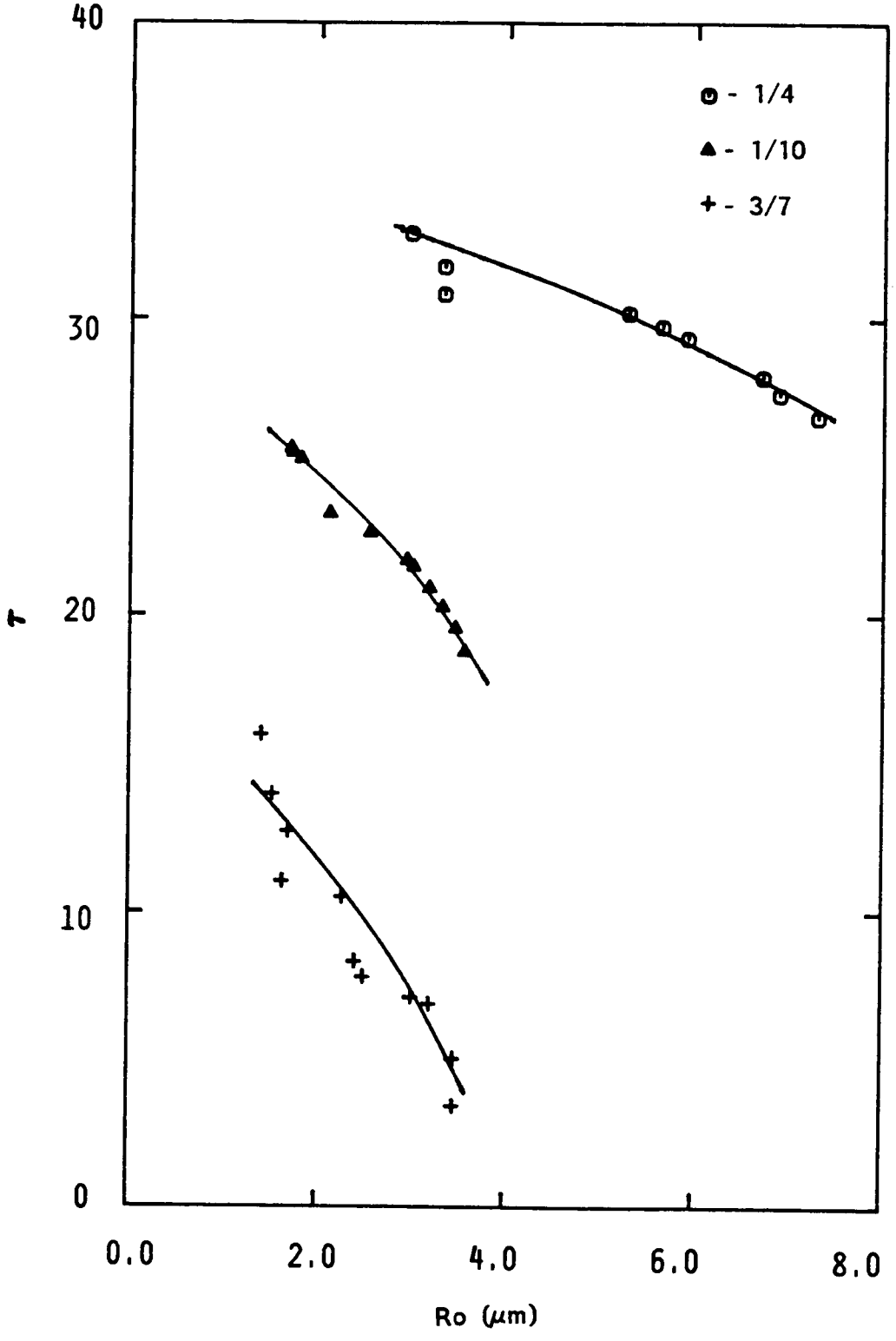

Figure 31. Turbidity (τ) as a function of Spherulite Radius (Ro)

Optical Microscopy Results

The optical photomicrographs of various films are shown in Figure 32. These photomicrographs taken under crossed polarizers seem to verify qualitatively that the bulk of film exhibits spherulitic structure. However, the overlap of the images and other difficulties make it very difficult to ascertain any detail from these photomicrographs. Better results could, perhaps, have been obtained from microtomed sections, but it was not deamed necessary to pursue the optical microscopy further. That which can be observed in Figure 32 seems consistent with the SALS results described in section B on page 82.

C. SURFACE TEXTURE OF FILMS AND SCATTERING FROM THE SO-CALLED SURFACE PHASE

Direct Transmission Factors of Surface Phases

Measurements of the inside surface transmission factors, Tsi, and the outside surface transmission factors, Tso, revealed the results that for every film sample Tsi is higher than Tso. It was found that both Tsi and Tso were lower at lower BUR (1.0) and DDR (4.0), the typical range was 72 to 80% for Tsi and 58 to 77% for Tso, while for higher BUR and DDR both Tsi and Tso were higher, the typical range was 75 to 86% for Tsi and 67 to 79% for Tso as given in Tables XVI, XVII and XVIII. Tsi and Tso are plotted versus MFR of resin in Figures 33, 34 and 35. These plots

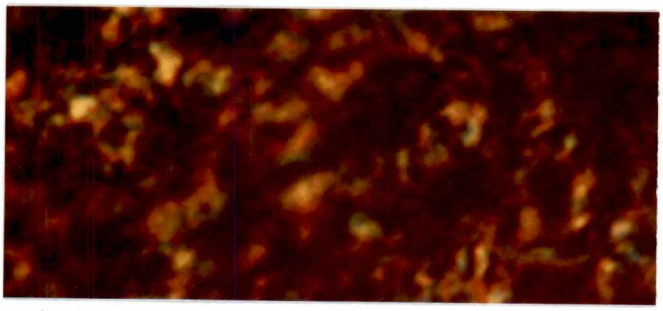

A

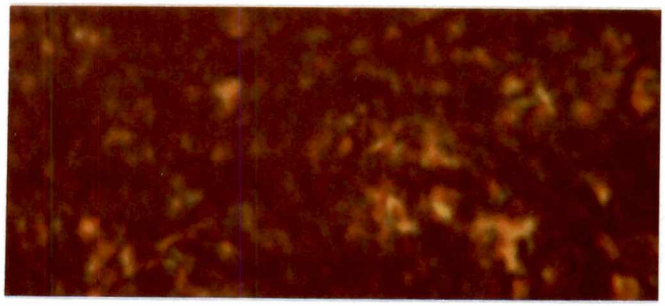

B

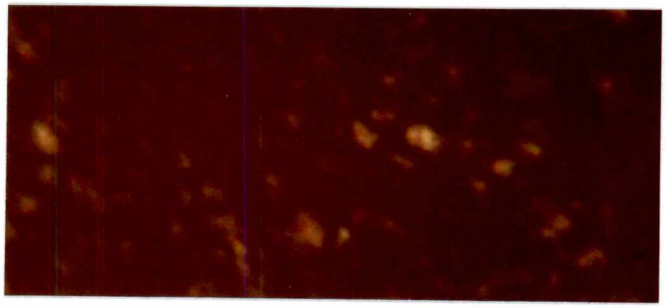

C

RESIN - MFR 3.9, B **500X**

A] FILMS - BUR 1.0, DDR 4.0, EXP. TIME - 75 SEC.
B] FILMS - BUR 1.0, DDR 10.0, EXP. TIME - 90 SEC.

RESIN - MFR 3.8, BNA

C] FILMS - BUR 1.0, DDR 4.0, EXP. TIME - 100 SEC.

Figure 32. Typical Optical Photomicrographs of Bulk Phase of PP Films

Table XVI. Direct Transmission Factors of Surface Phases Tsi and Tso
Films - BUR 1.0, DDR 4.0

Film Sample	MI of Resin	Tsi (%)	Tso (%)
PPN-11	1.5	80.55	70.32
PPN-41	3.9	79.32	69.56
PPN-101	10.29	78.50	68.19
PPB-21	2.3	78.00	66.32
PPB-41	3.9	77.00	65.75
PPB-141	14.40	75.69	62.10
PPB-271	27.40	72.83	58.29
PPN-41NA	4.5	81.10	76.83
PPB-21NA	2.6	80.40	75.59
PPB-41NA	3.8	79.51	75.12
PPB-251NA	24.5	76.30	74.20

Table XVII. Direct Transmission Factors of Surface Phases Tsi and Tso
Films - BUR 1.0, DDR 10.0

Film Sample	MI of Resin	Tsi (%)	Tso (%)
PPN-12	1.5	82.84	69.89
PPN-42	3.9	81.08	69.44
PPN-102	10.29	77.74	66.39
PPB-22	2.3	79.26	71.50
PPB-42	3.9	77.92	70.70
PPB-142	14.40	73.45	68.35
PPB-272	27.40	65.34	65.30
PPN-42NA	4.5	83.60	78.60
PPB-22NA	2.6	83.57	78.12
PPB-42NA	3.8	82.48	77.56
PPB-252NA	24.5	78.30	75.60

Table XVIII. Direct Transmission Factors of Surface Phases Tsi and Tso
Films - BUR 3.0, DDR 7.0, FLH 2.5 - 15 cm.

Film Sample	MI of Resin	Tsi (%)	Tso (%)
PPN-13	1.5	83.46	72.32
PPN-43	3.9	82.35	70.82
PPN-103	10.29	79.13	67.42
PPB-23	2.3	80.55	72.04
PPB-43	3.9	79.54	69.80
PPB-143	14.40	78.34	67.54
PPB-144		77.87	67.49
PPB-145		73.42	59.05
PPB-146		69.35	54.90
PPB-147		65.66	50.42
PPB-148		59.91	44.82
PPB-273	27.40	70.23	67.40
PPN-43NA	4.5	85.75	79.12
PPB-23NA	2.6	85.35	78.83
PPB-43NA	3.8	84.32	77.98
PPB-253NA	24.5	80.56	76.12

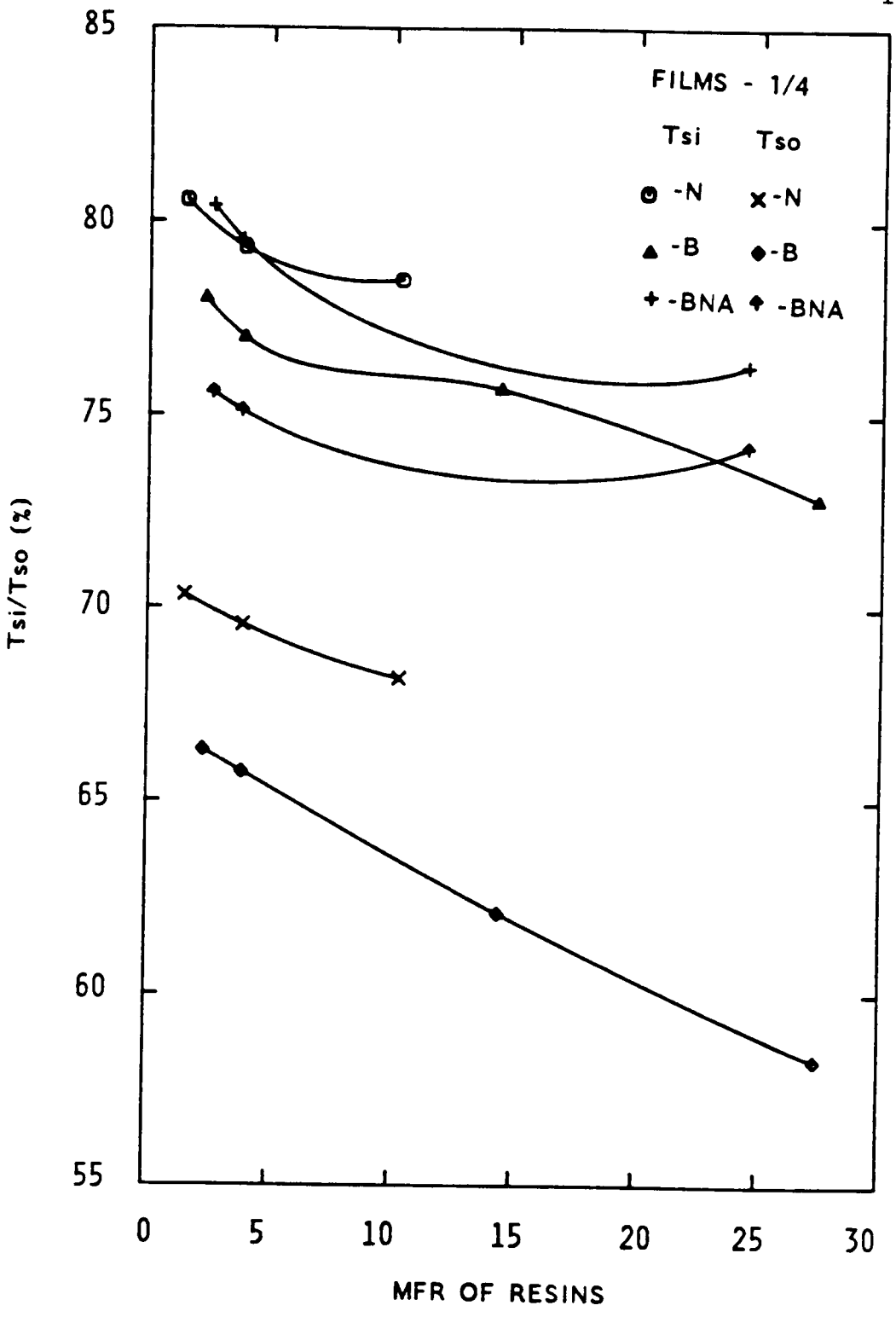

Figure 33. Surface Phase Transmission Factors (Tsi/Tso) as a function of Melt Flow Rate (MFR) of Resins, Films - 1/4

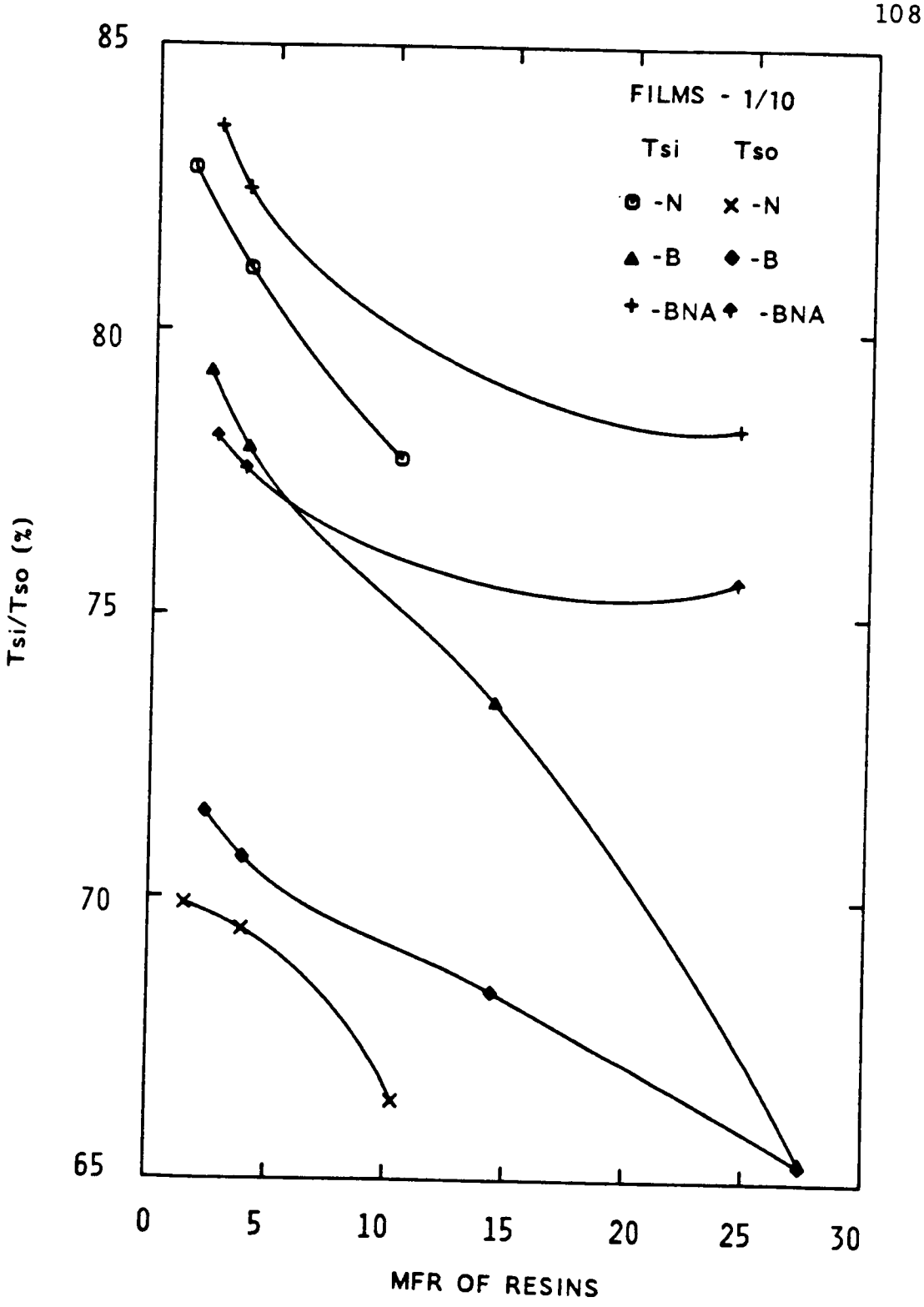

Figure 34. Surface Phase Transmission Factors (Tsi/Tso) as a function of Melt Flow Rate (MFR) of Resins, Films - 1/10

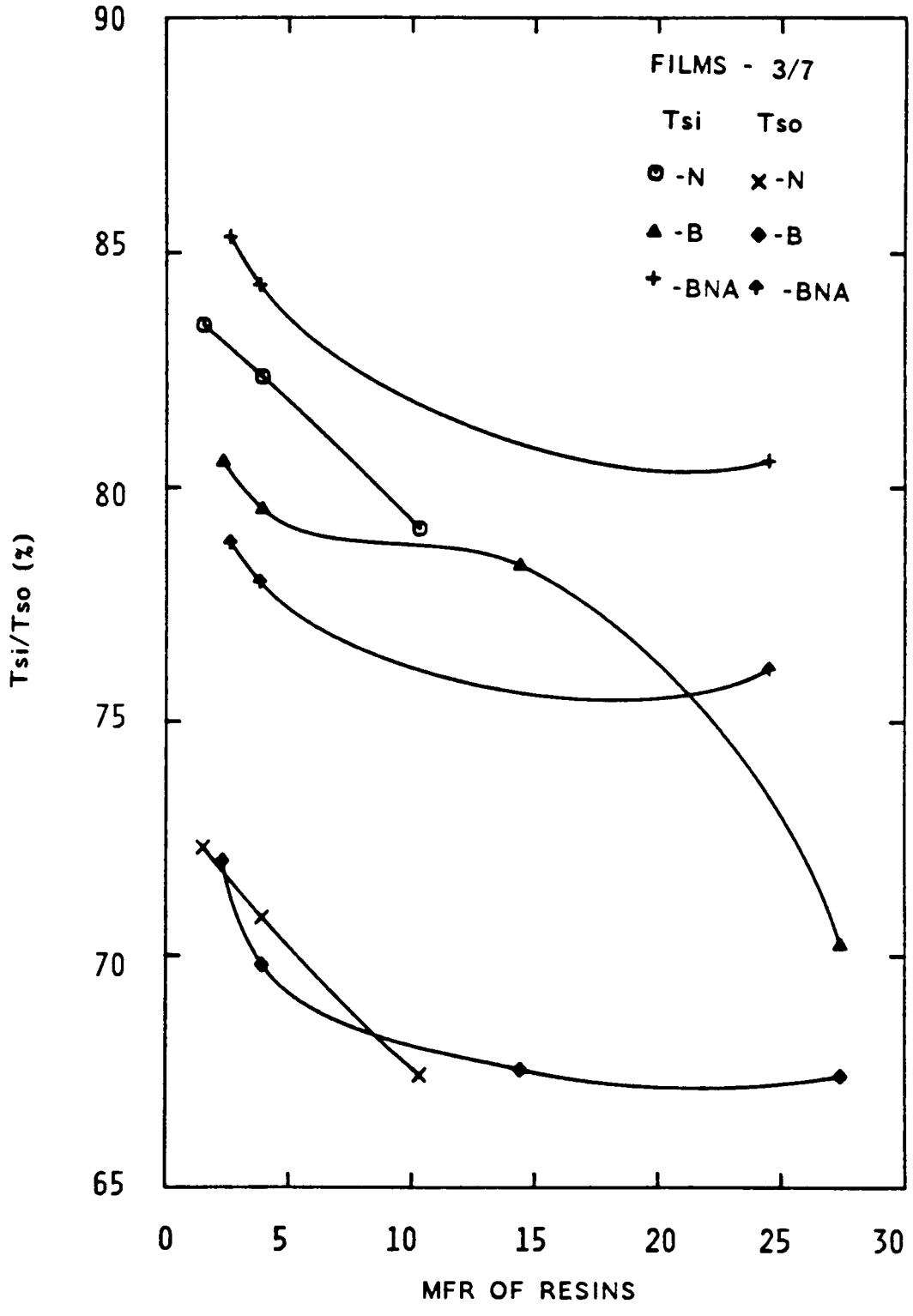

Figure 35. Surface Phase Transmission Factors (Tsi/Tso) as a function of Melt Flow Rate (MFR) of Resins, Films - 3/7, FLH 2.5-5 cm

indicate that generally Tsi was higher than Tso but the difference between them becomes smaller for films from nucleated resins. Further both Tsi and Tso are higher for films from narrow MWD resins than those from broad MWD resins. With increasing MFR both Tsi and Tso decrease, but this decrease is not as large for nucleated resins as that for unnucleated resins.

The difference in Tsi and Tso probably arises from the fact that inside the bubble the air (inflating the tube exiting from die) is stationary and outside the bubble the air is moving with a certain velocity for effective cooling of the bubble. It seems that the surface irregularities on the outside surface get frozen more quickly than for the inside surface causing inside surface to be smoother.

Surface irregularities are caused by "extrusion haze" and "crystallization haze" mechanisms as described by Huck and Clegg (42). Broad MWD resins exhibit higher non-Newtonian behavior in terms of their rheological characteristics and this behavior may be causing higher extrusion or flow irregularities as compared to narrow MWD resins. Also from SALS results it was found that films from narrow MWD resins have smaller spherulite size than those from broad MWD resins. Thus both mechanisms seem to be leading to smoother films from narrow MWD resins. Further with increasing MFR spherulite size increases and melt elasticity increases increasing die swell character (87,90)

and thus decreasing both Tsi and Tso. For nucleated resins spherulite sizes are quite small causing smaller surface irregularities.

Effect of FLH on surface transmission was studied for only broad MWD resin with MFR = 14.4. The results given in Table XVIII and plotted in Figure 36 indicate that as FLH increases both Tsi and Tso decrease substantially. SALS results on the same films indicate that the spherulite size increases with increasing FLH. This suggests that larger spherulites produce larger surface irregularities. These in turn scatter more light.

Surface Profile Statistics Results

The typical surface profiles of various films from resins of MFR approximately 4.0 with and without nucleating agent are shown in Figures 37, 38, 39 and 40. From these profiles it appears that at low BUR and DDR there are quite large hills and valleys and they become quite smooth at high BUR and DDR. Digitized data of the surface profiles were given statistical treatment with a group of 20 data points taken at a time. Effect of taking higher number of data points (50) at a time was examined and the results are given in Table XIX which indicate that standard deviation was higher for lower BUR and DDR films for group of 50 data points. This may be due to the variation in slope of profile.

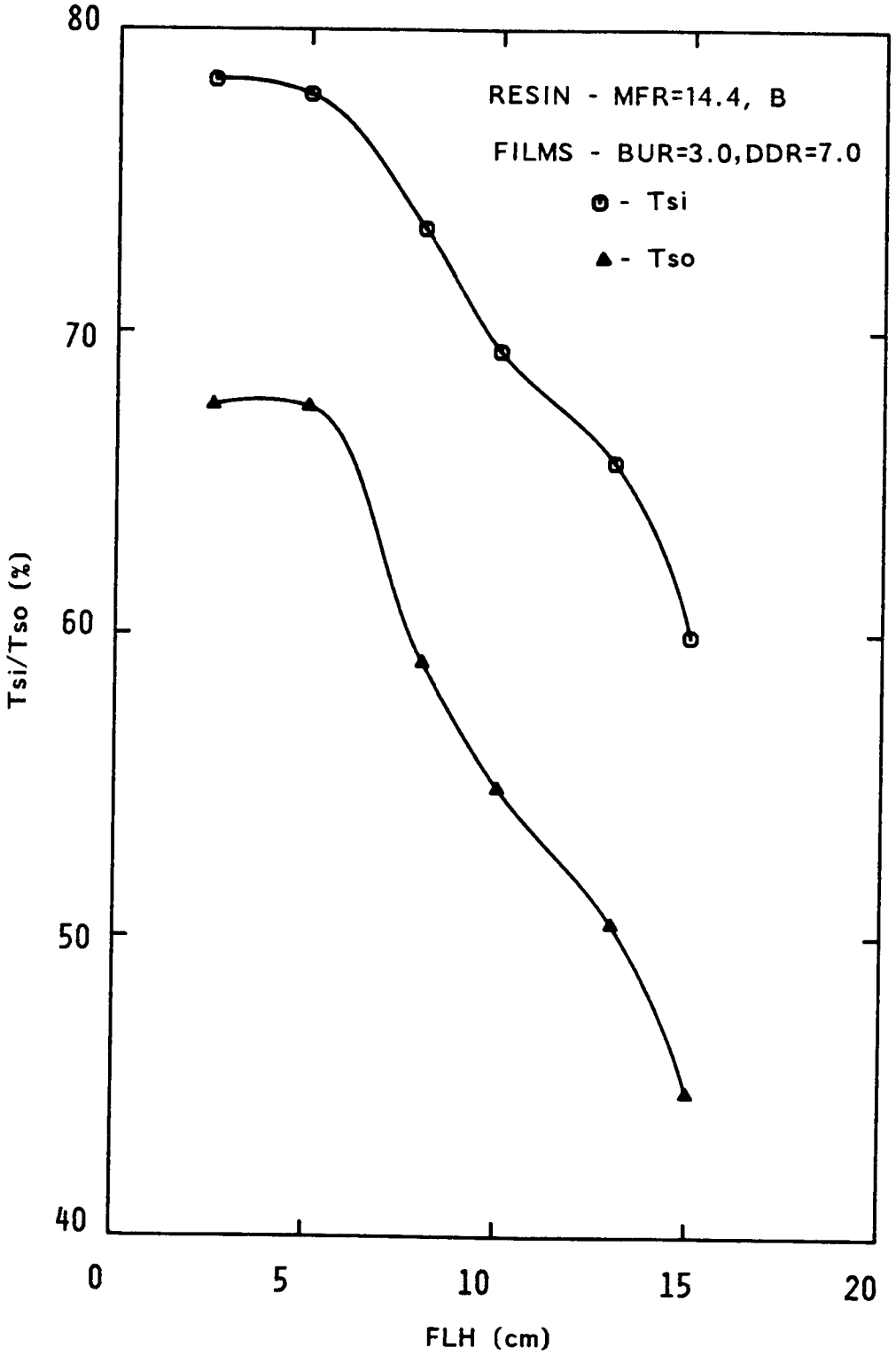

Figure 36. Surface Phase Transmission Factors (Tsi/Tso) as a function of Frost Line Height (FLH)

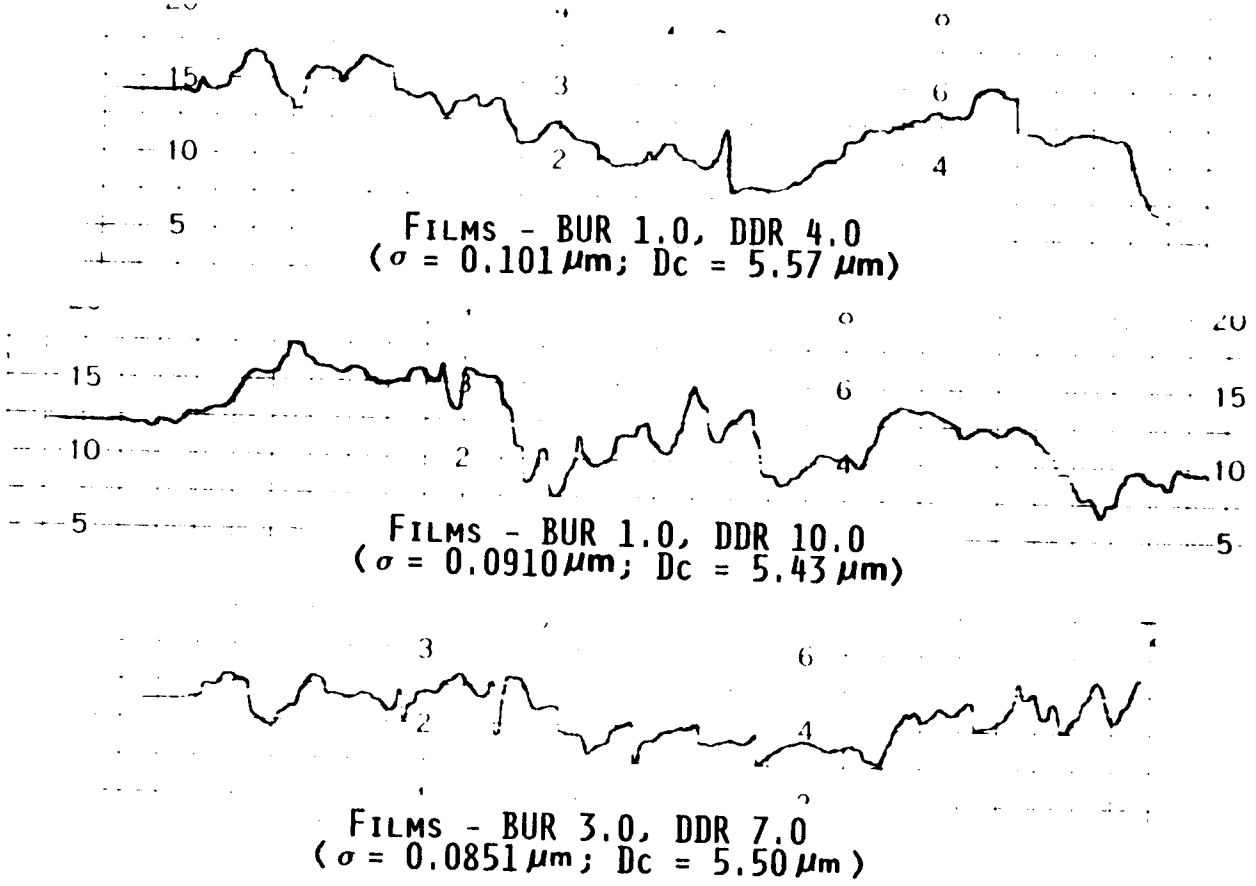

Figure 37. Typical Surface Profiles, MFR - 3.9, B

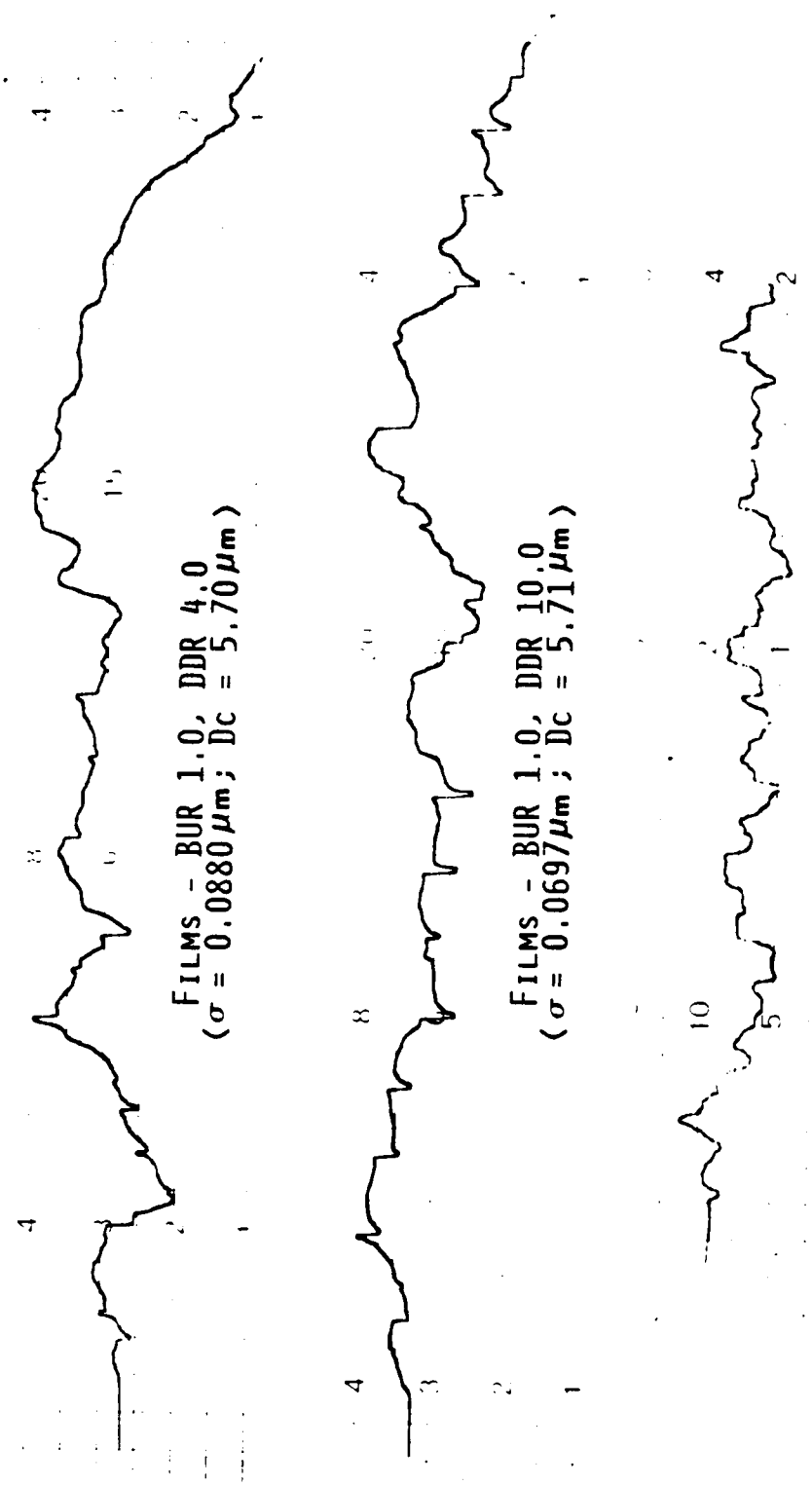

Figure 38. Typical Surface Profiles, MFR - 3.8, BNA

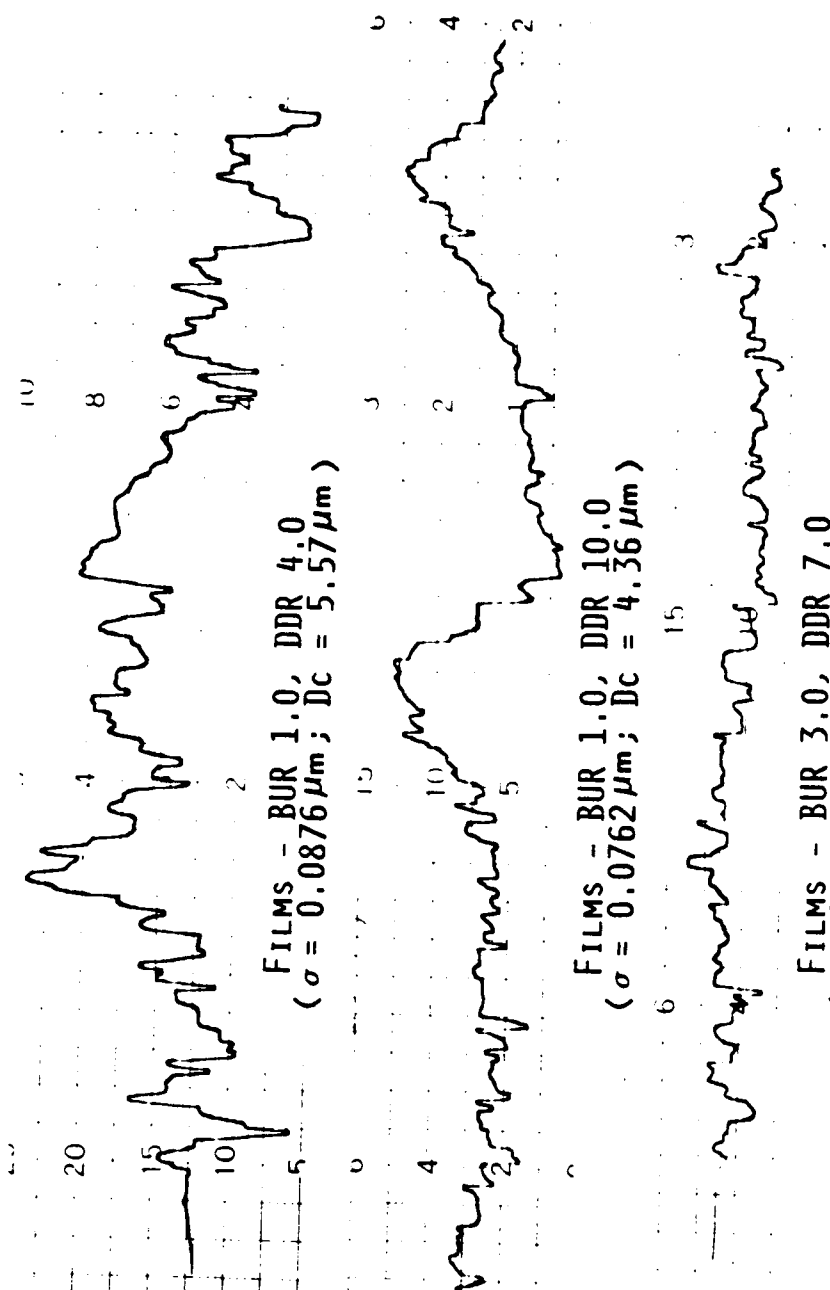

Figure 39. Typical Surface Profiles, MFR - 3.9, N

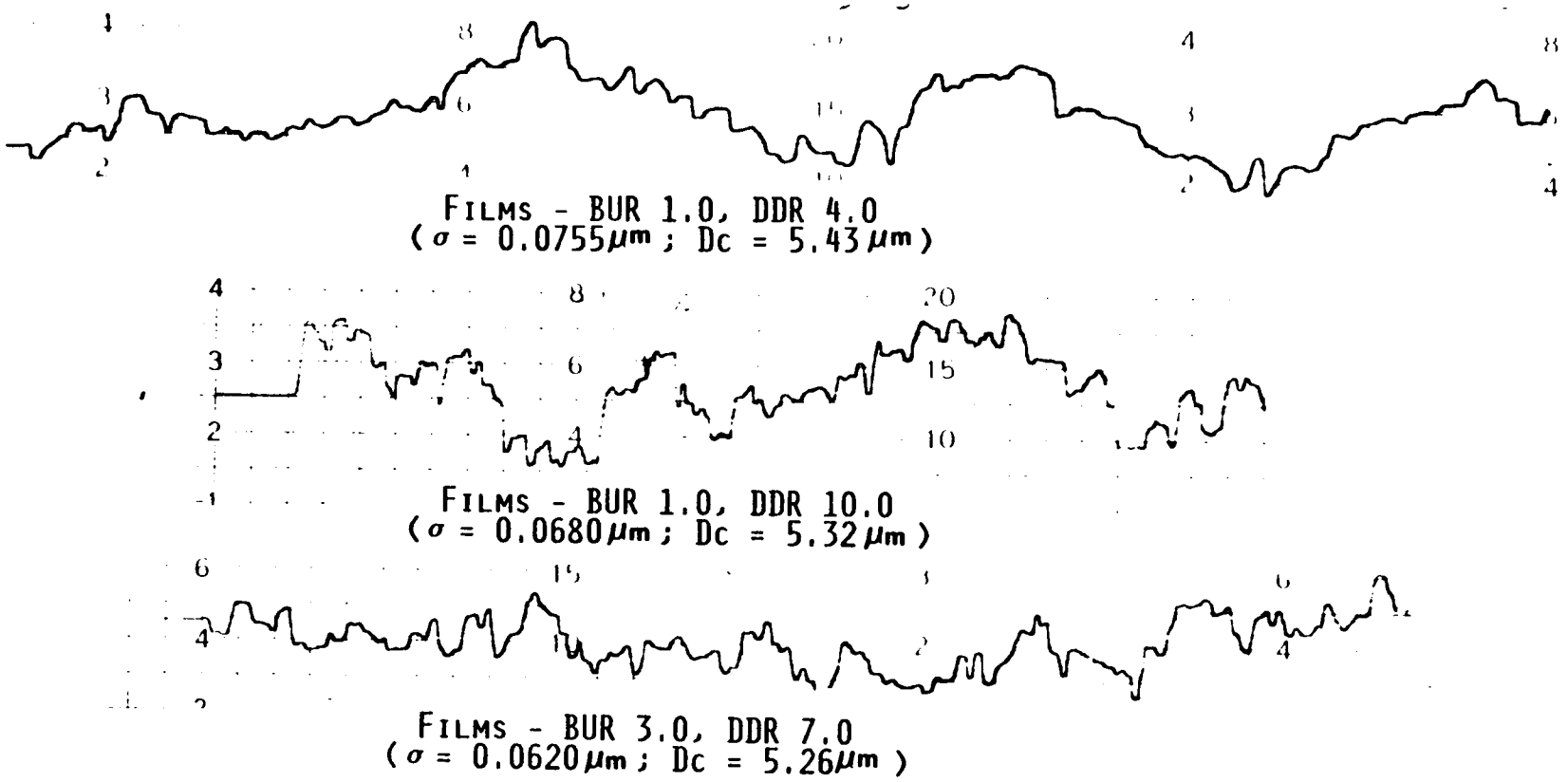

Figure 40. Typical Surface Profiles, MFR - 4.5, NNA

Table XIX. Effect of different group of data points on Standard Deviation

Film Sample	Standard deviation for group of 20 data points inside(μm)	outside(μm)	Standard deviation for group of 50 data points inside(μm)	outside(μm)
PPB-41	0.101	0.203	0.135	0.238
PPB-42	0.091	0.120	0.120	0.136
PPB-43	0.0851	0.127	0.0919	0.137
PPB-41NA	0.0880	0.105	0.130	0.173
PPB-42NA	0.0697	0.0893	0.0832	0.112
PPB-43NA	0.0662	0.0908	0.0803	0.103

It was found that the magnitude of standard deviation typically ranges from 0.06 μm to 0.5 μm and that of correlation distance ranges from 4.0 μm to 7.0 μm. These statistical parameters were measured for both inside and outside surfaces of films. The results of various films are given in Tables XX, XXI, XXII and XXIII. These results indicate that was comparatively lower for inside surface than that for outside surface of films. Correlation distance Dc did not show any particular trend except that for outside surface the value of Dc was generally higher. Evaluation of Dc was made by plotting autocorrelation coefficient as a function of separation parameter (δ). A typical plot is shown in Figure 41 and it is seen that autocorrelation coefficient is a monotonic decreasing function of δ with maximum value of 1.0 as expected. From the statistics program the height deviation of individual data points from mean surface was calculated and histograms of height deviation were made in order to examine their distribution. A typical histogram is shown in Figure 42. A Gaussian distribution curve is also shown on the histogram and it appears that the height deviation is not as close to Gaussian in distribution as it was in case of PE blown films as described by Ashizawa (4).

Table XX. Statistical Parameters of Film Surfaces
Films - BUR 1.0, DDR 4.0

Film Sample	INSIDE SURFACE Standard deviation (μm)	INSIDE SURFACE Correlation distance (μm)	OUTSIDE SURFACE Standard deviation (μm)	OUTSIDE SURFACE Correlation distance (μm)
PPN-11				
MD	0.0675	5.88	0.0932	6.00
TD	0.0875	5.93	0.153	6.10
Avg.	0.0775	5.91	0.123	6.05
PPN-41				
MD	0.0793	5.51	0.0995	5.86
TD	0.0959	5.63	0.167	6.01
Avg.	0.0876	5.57	0.133	5.94
PPN-101				
MD	0.0883	7.01	0.0950	6.49
TD	0.102	5.71	0.177	6.62
Avg.	0.0951	6.36	0.136	6.56
PPB-21				
MD	0.0913	4.69	0.0985	6.03
TD	0.106	6.08	0.246	6.48
Avg.	0.0985	5.39	0.172	6.26
PPB-41				
MD	0.0982	5.39	0.103	6.56
TD	0.104	5.03	0.303	7.09
Avg.	0.101	5.21	0.203	6.83
PPB-141				
MD	0.0905	5.31	0.103	6.93
TD	0.120	4.95	0.403	6.58
Avg.	0.105	5.13	0.253	6.76
PPB-271				
MD	0.0925	5.82	0.121	6.01
TD	0.130	5.39	0.525	7.39
Avg.	0.111	5.61	0.323	6.70
PPN-41NA				
MD	0.0710	5.28	0.0835	6.28
TD	0.0810	5.57	0.1105	4.82
Avg.	0.0755	5.43	0.0970	5.55
PPB-21NA				
MD	0.0683	4.85	0.0932	6.43
TD	0.0869	6.44	0.113	6.12
Avg.	0.0776	5.65	0.103	6.28
PPB-41NA				
MD	0.0830	5.50	0.0975	6.20
TD	0.0930	5.90	0.1125	6.85
Avg.	0.0880	5.70	0.105	6.53
PPB-251NA				
MD	0.0952	5.63	0.0987	6.32
TD	0.109	6.14	0.117	6.90
Avg.	0.102	5.89	0.108	6.61

Table XXI. Statistical Parameters of Film Surfaces
Films - BUR 1.0, DDR 10.0

Film Sample	INSIDE SURFACE Standard deviation (μm)	INSIDE SURFACE Correlation distance (μm)	OUTSIDE SURFACE Standard deviation (μm)	OUTSIDE SURFACE Correlation distance (μm)
PPN-12				
MD	0.0683	4.83	0.1180	6.41
TD	0.0741	5.04	0.140	5.71
Avg.	0.0712	4.94	0.129	6.06
PPN-42				
MD	0.0701	3.38	0.1250	6.17
TD	0.0824	5.33	0.143	5.90
Avg.	0.0762	4.36	0.134	6.04
PPN-102				
MD	0.0801	5.25	0.1300	5.04
TD	0.104	4.91	0.212	5.49
Avg.	0.0923	5.08	0.171	5.27
PPB-22				
MD	0.0790	5.88	0.0898	5.84
TD	0.0952	5.28	0.136	5.81
Avg.	0.0871	5.58	0.113	5.83
PPB-42				
MD	0.0821	5.64	0.0987	5.61
TD	0.0999	5.22	0.141	5.42
Avg.	0.0910	5.43	0.120	5.52
PPB-142				
MD	0.0841	5.16	0.112	6.01
TD	0.114	5.80	0.130	6.30
Avg.	0.0990	5.48	0.140	6.16
PPB-272				
MD	0.0952	5.23	0.163	6.15
TD	0.201	5.95	0.239	6.20
Avg.	0.148	5.59	0.201	6.18
PPN-42NA				
MD	0.0632	5.48	0.0730	5.57
TD	0.0728	5.15	0.1050	6.02
Avg.	0.0680	5.32	0.0890	5.80
PPB-22NA				
MD	0.0584	5.19	0.0883	6.57
TD	0.0770	5.46	0.0921	5.08
Avg.	0.0677	5.33	0.0902	5.83
PPB-42NA				
MD	0.0603	5.99	0.0755	6.09
TD	0.0791	5.42	0.1030	5.99
Avg.	0.0697	5.71	0.0893	6.04
PPB-252NA				
MD	0.0880	5.36	0.0892	6.10
TD	0.092	5.70	0.119	6.03
Avg.	0.0900	5.53	0.104	6.07

Table XXII. Statistical Parameters of Film Surfaces
Films - BUR 3.0, DDR 7.0, FLH 2.5-5 cm.

Film Sample	INSIDE SURFACE Standard deviation (μm)	INSIDE SURFACE Correlation distance (μm)	OUTSIDE SURFACE Standard deviation (μm)	OUTSIDE SURFACE Correlation distance (μm)
PPN-13				
MD	0.0563	5.60	0.0970	5.86
TD	0.0817	5.51	0.129	5.59
Avg.	0.0690	5.56	0.113	5.73
PPN-43				
MD	0.0594	4.72	0.0941	4.66
TD	0.0894	4.75	0.140	5.24
Avg.	0.0744	4.74	0.151	4.95
PPN-103				
MD	0.0734	5.04	0.1120	5.23
TD	0.0998	5.49	0.190	5.17
Avg.	0.0866	5.27	0.151	5.20
PPB-23				
MD	0.0634	5.17	0.0932	6.23
TD	0.0926	5.83	0.137	5.31
Avg.	0.0780	5.50	0.115	5.77
PPB-43				
MD	0.0732	5.89	0.1060	5.22
TD	0.0970	5.10	0.148	5.67
Avg.	0.0851	5.50	0.127	5.45
PPB-143				
MD	0.0840	5.56	0.105	5.73
TD	0.0936	5.56	0.155	5.52
Avg.	0.0888	5.67	0.127	5.45
PPB-273				
MD	0.1030	5.63	0.123	5.23
TD	0.135	5.45	0.181	5.89
Avg.	0.119	5.54	0.152	5.56
PPN-43NA				
MD	0.0521	5.62	0.0753	4.47
TD	0.0719	4.89	0.0987	5.81
Avg.	0.0620	5.26	0.0870	5.14
PPB-23NA				
MD	0.0534	6.07	0.0778	5.62
TD	0.0730	5.39	0.0968	5.74
Avg.	0.0632	5.73	0.0873	5.68
PPB-43NA				
MD	0.0583	5.36	0.0812	5.08
TD	0.0741	4.95	0.1004	5.90
Avg.	0.0662	5.16	0.0908	5.49
PPB-253NA				
MD	0.0694	5.16	0.0868	5.05
TD	0.0878	4.85	0.112	5.35
Avg.	0.0786	5.01	0.0993	5.20

Table XXIII. Statistical Parameters of Film Surfaces Films - BUR 3.0, DDR 7.0, FLH 2.5-15 cm.

Film Sample	INSIDE SURFACE Standard deviation (μm)	INSIDE SURFACE Correlation distance (μm)	OUTSIDE SURFACE Standard deviation (μm)	OUTSIDE SURFACE Correlation distance (μm)
PPB-143				
MD	0.0840	5.56	0.105	5.73
TD	0.0936	5.56	0.155	5.52
Avg.	0.0888	5.67	0.127	5.45
PPB-144				
MD	0.0827	5.47	0.109	5.83
TD	0.106	5.72	0.161	5.72
Avg.	0.0944	5.60	0.135	5.78
PPB-145				
MD	0.113	5.23	0.302	5.62
TD	0.117	5.46	0.408	5.43
Avg.	0.115	5.35	0.355	5.53
PPB-146				
MD	0.154	5.04	0.341	5.31
TD	0.154	4.98	0.431	5.85
Avg.	0.154	5.01	0.386	5.58
PPB-147				
MD	0.208	4.95	0.355	5.27
TD	0.258	5.06	0.441	5.99
Avg.	0.233	5.01	0.398	5.63
PPB-148				
MD	0.255	5.03	0.331	5.93
TD	0.392	5.13	0.495	5.02
Avg.	0.324	5.08	0.413	5.48

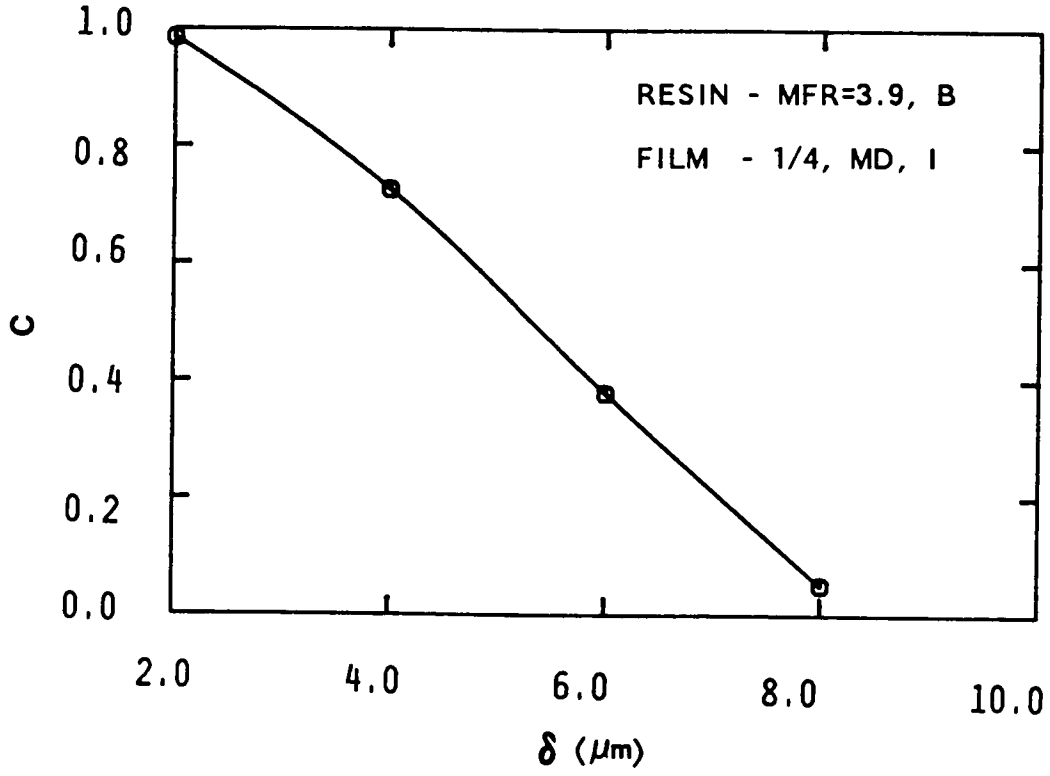

Figure 41. Autocorrelation Coefficient (C(δ)) as a function of Separation Parameter (δ)

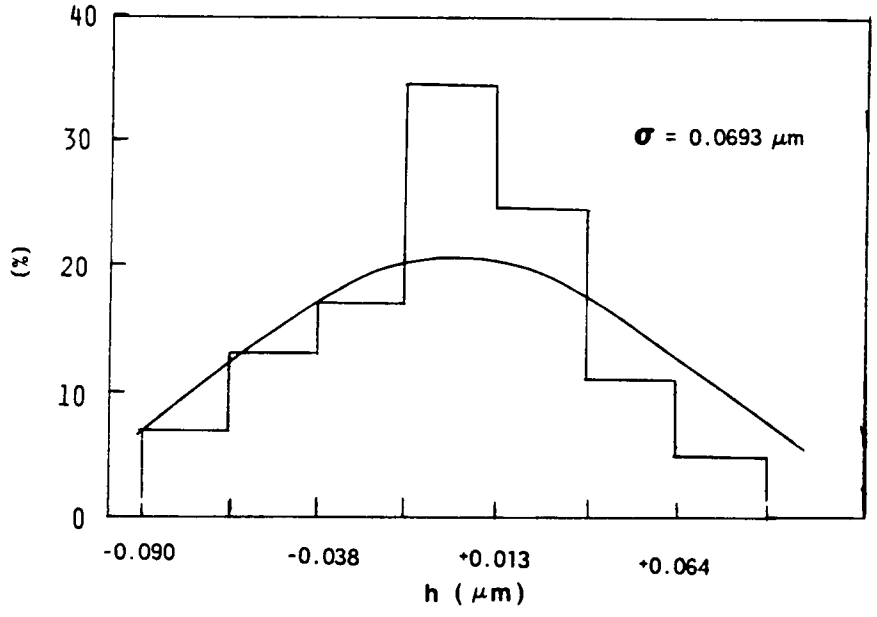

Figure 42. Histogram of Height Deviations

Correlation of Transmission Factors of Surface Phases and Standard Deviation

Tsi and Tso are plotted versus σ for all sample films for which σ was measured in Figure 43. Figure 43 shows that there is a good correlation of the surface transmission factors with the measured standard deviation of surface heights. It is seen that as σ increases Tsi/Tso decreases. Further, as the value of σ approaches the wavelength of light (5460 A = 0.546 μm) the transmission values are quite low indicating significant light scattering. On the plot of Figure 43 regions of film preparation conditions are also shown and it appears that films made at lower BUR and DDR tend to lie in the region of higher values of than those made at higher BUR and DDR. However, the regions overlap each other for some resins.

In Figure 44 Tsi/Tso are plotted versus as a function of BUR/DDR. It is seen that as σ increases Tsi/Tso decrease. Further the values of σ range from 0.08 to 0.20 μm.

In Figure 45 Tsi/Tso and FLH are plotted versus for films from broad MWD resin (MFR = 14.4). Again it is seen that as σ increases Tsi/Tso decreases indicating a good correlation. Further, as FLH increases σ increases. For these films it was found that spherulite size increases with increasing FLH. The increase in spherulite size at or near the film surface seem to cause higher standard deviation of surface heights.

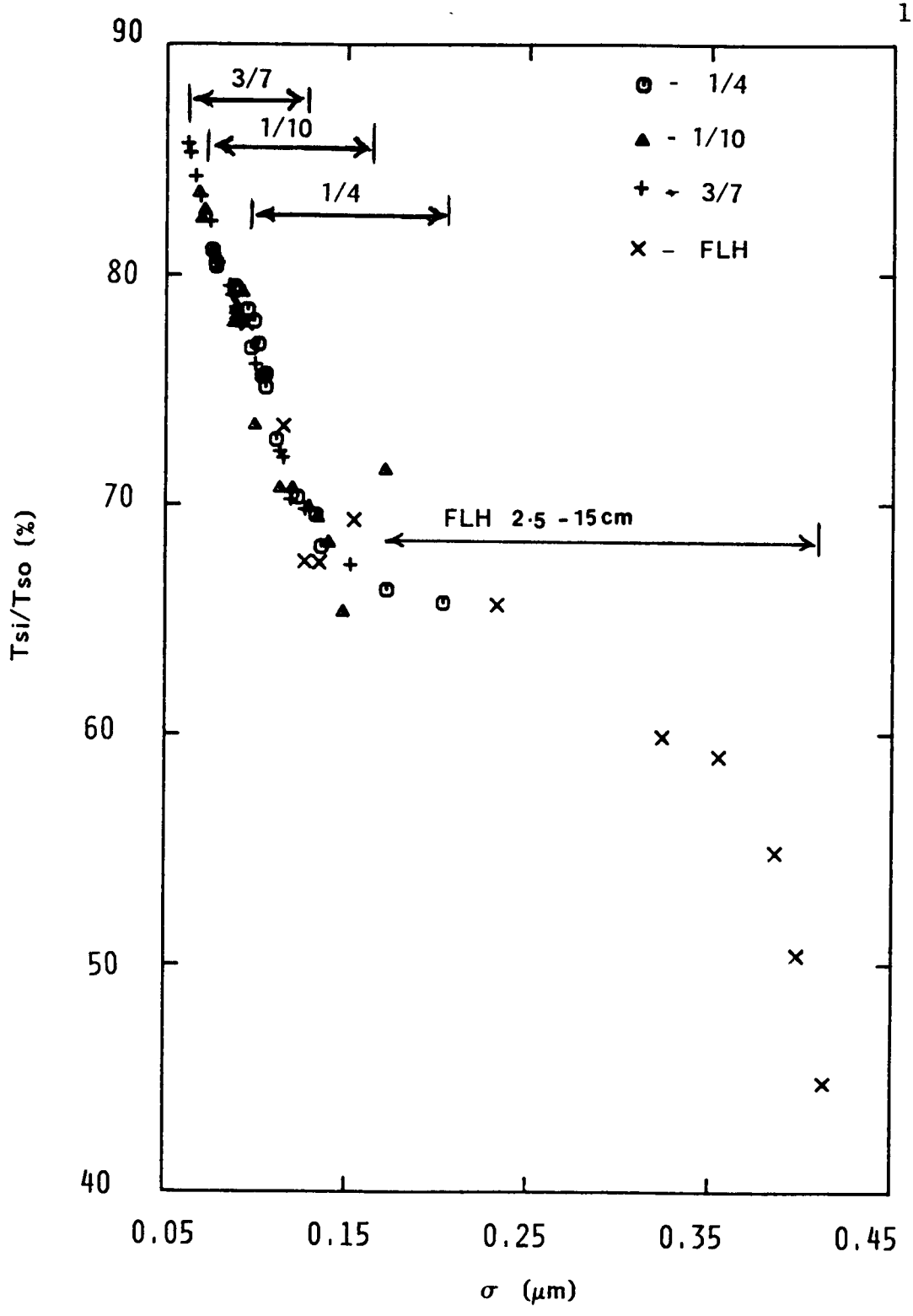

Figure 43. Surface Phase Transmission Factors (Tsi/Tso) versus Standard Variation of Surface Heights (σ) for all Films

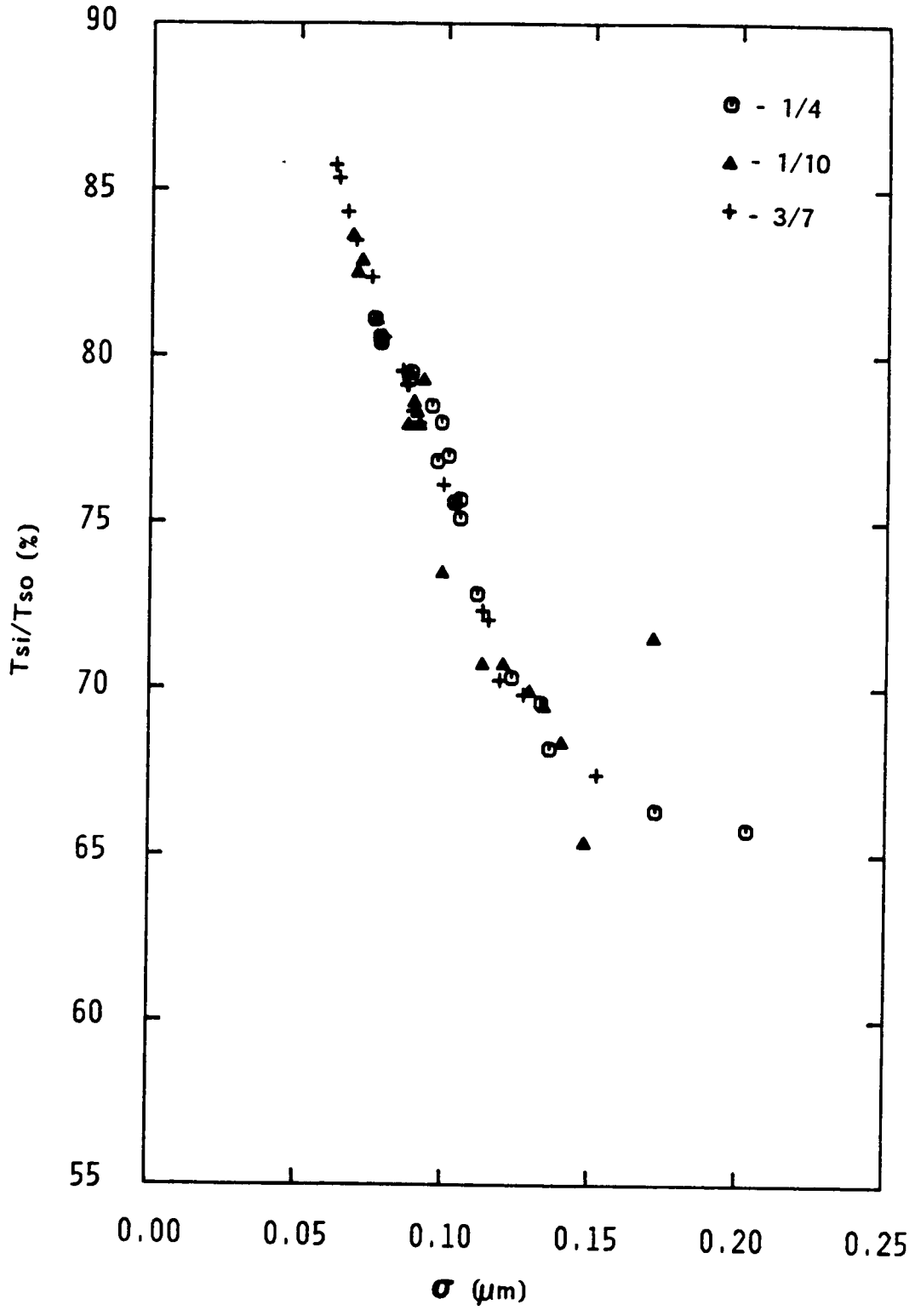

Figure 44. Surface Phase Transmission Factors (Tsi/Tso) versus Standard Variation of Surface Heights (σ) as a function of BUR/DDR

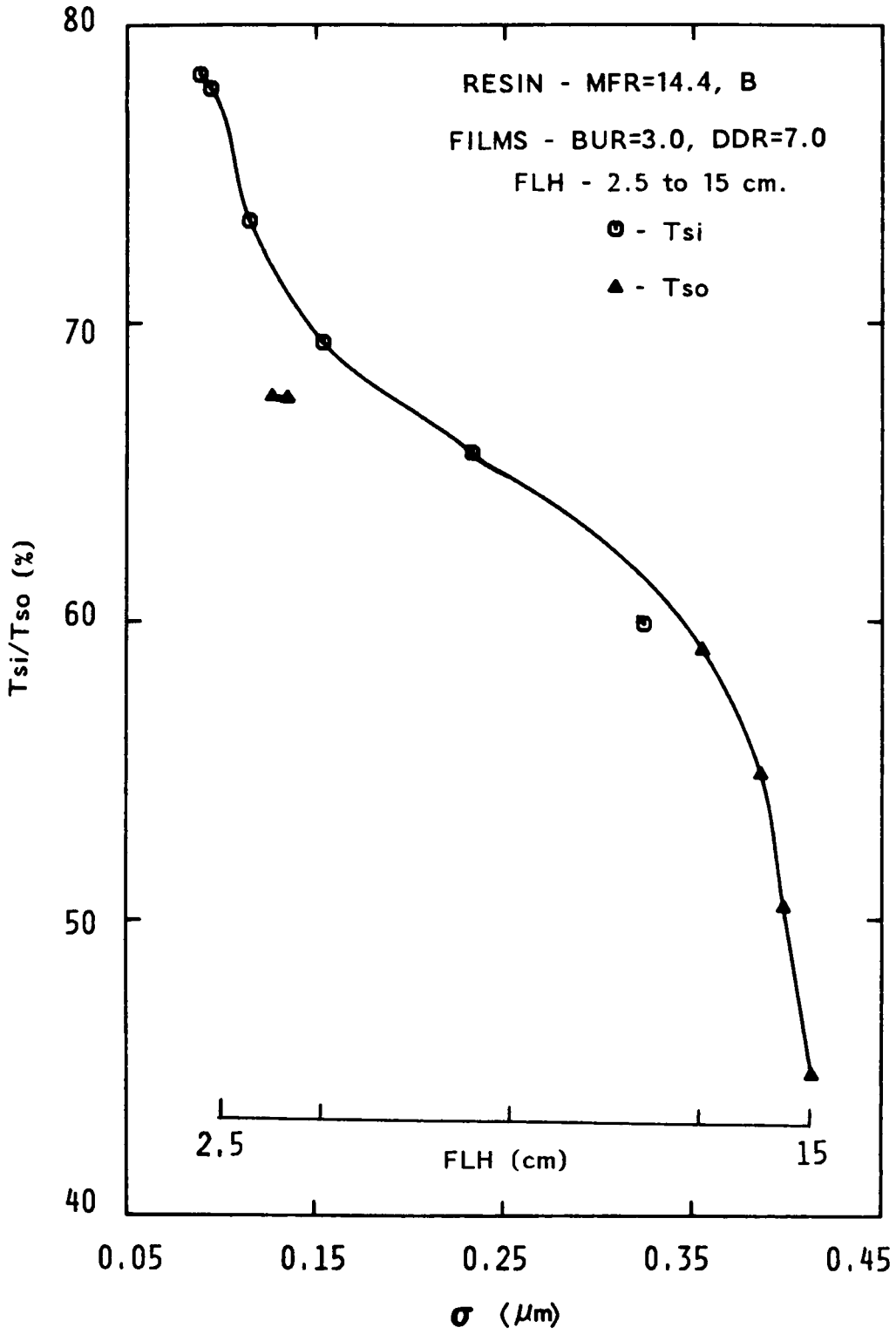

Figure 45. Surface Phase Transmission Factors (Tsi/Tso) versus Standard Variation of Surface Heights (σ) as a function of FLH

Recently Tang (103) has investigated theoretically and experimentally the surface scattering phenomenon of polystyrene (PS) crazes by small angle X-ray scattering (SAXS). The generallised theory of scattering of electromagnetic waves from rough surfaces presented by her is of interest in discussion of our results. This interest is due to the reason that we have studied light scattering by PP blown films in terms of transmitted light flux which is the difference between total incident flux and total scattered flux. The theory reviewed by her involves the discussion of scattered intensity using vector scattering theory.

A rough surface is best described by the statistical distribution of the deviation of the surface height from its mean level. The surface scattering factor leads to the surface correlation function

$$G(\vec{r_p}) = \frac{\overline{\sigma(\vec{Rp})}^2}{\bar{\sigma}^2 S} \qquad (43)$$

where S is area of irradiation and $\bar{\sigma}^2$ is the average value of the square of surface roughness. $\vec{r_p}$ and $\vec{Rp}$ are position vectors of scattered rays in an appropriately defined co-ordinate system. Thus, dimensionality in surface scattering is two and the contributing factor is the surface roughness distribution function $\sigma(\vec{Rp})$. The term $\bar{\sigma}^2 S$ is the invariant of surface scattering Ks

$$K_S = \bar{\sigma}^2 S = \frac{1}{(2\pi)^2}\int g(\vec{s_p})\, d^2 s_p \qquad (44)$$

where $g(\vec{s_p})$ is the surface scattering factor described in terms of surface scattering amplitudes.

For the circular symmetry of roughness distribution function about its average normal direction the invariant of surface scattering becomes

$$K_s = \bar{\sigma}^2 S = \frac{1}{(2\pi)^2} \int 2\pi s_p g(s_p) ds_p \tag{45}$$

and for an isotropic Gaussian approach for the correlation function $G(r_p)$ becomes

$$G(r_p) = \exp\left[\frac{-r_p^2}{\tau^2}\right] \tag{46}$$

where τ is the distance at which the correlation function $G(r_p)$ drops to the value of 1/e and popularly termed as correlation distance.

The total surface scattering intensity depends on the wavelength of incident radiation, optical proprties of the media and angles of incidence and scattering whereas surface scattering factor depends only on statistical properties of the surface. Thus total surface scattering intensity is product of two terms, namely, optical factor and scattering factor. The surface scattering intensity distribution on two dimensional detector plane for a PS-void interface were calculated by Tang using an isotropic Gaussian approach for the surface correlation function. The results were studied for two different values of correlation distance τ = 10 μm and 0.1 μm. The toatal scattered intensity (area under scattered intensity distribution curve) in both cases were

found to be same, however, distribution of scattered intensity varies, showing a sharp and narrower peak for higher value of τ. But the total scattered intensity varies with variation in surface height deviation from mean level.

Our results described earlier in terms of transmission factors of surfaces also showed a good correlation with standard variation of surface heights but no significant trend or variation in correlation distance. Thus our experimental results have a reinforcing effect from above theory or the assumptions made in the theory seem to be valid.

Scanning Electron Microscopy (SEM) Results

In Figures 46, 47 and 48 SEM photomicrographs of inside and outside surfaces of various films are shown. These micrographs typically show what appears to be the spherulite boundaries on the surfaces of the films. These boundaries show that at lower BUR and DDR the films have larger spherulite sizes compared to high BUR and DDR in agreement with the SALS results. These larger spherulites lead to rougher surfaces of films at lower BUR and DDR. The important result of SEM seems to be the streaks parallel to MD for the outside surface of the films. These streaks may be due to the die making the outside surface of the film rougher than the inside surface. Films from narrow MWD and nucleated resins have much smoother surfaces.

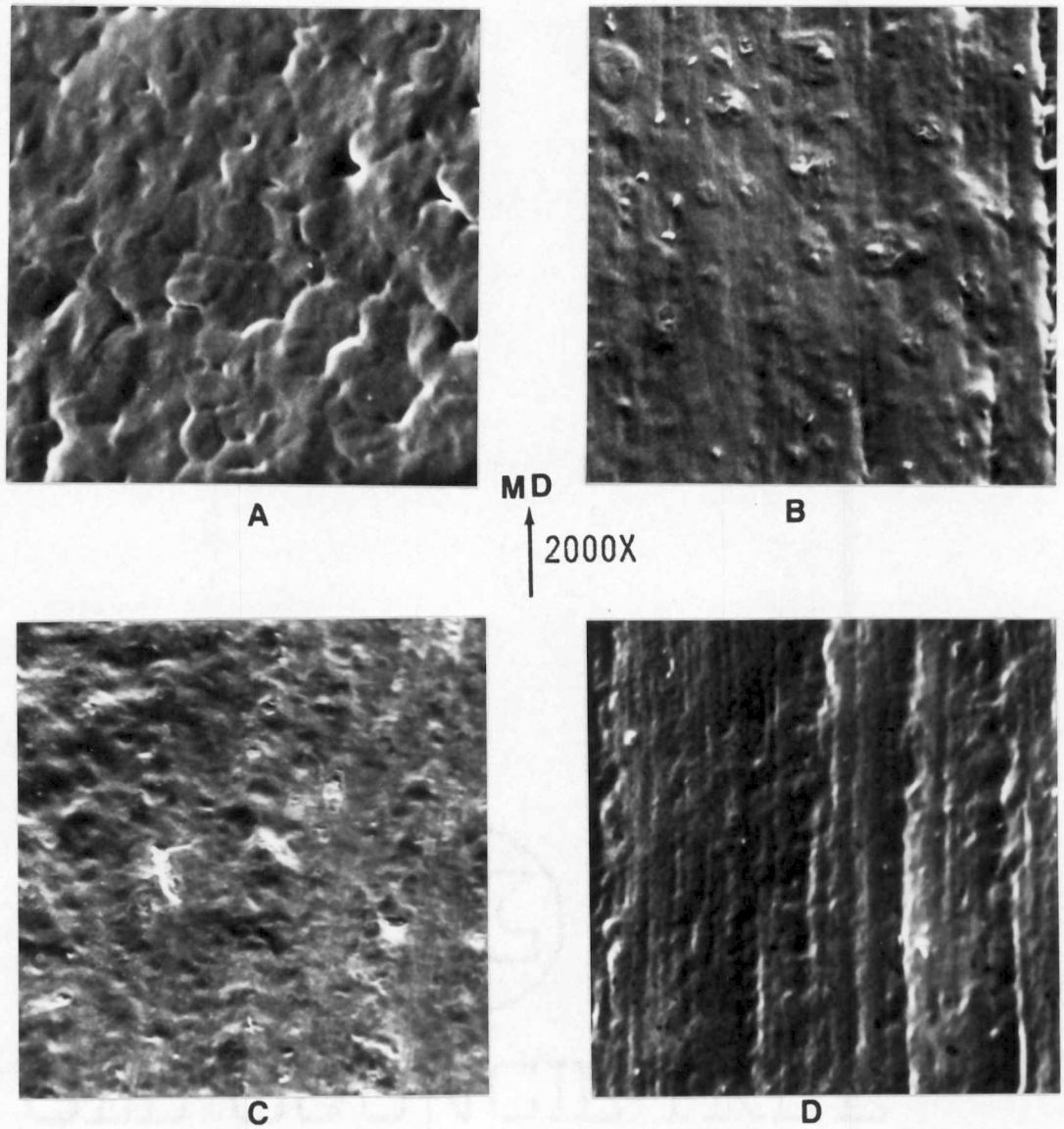

FILMS - BUR 1.0, DDR 4.0

RESIN - MFR 3.9, B

A] INSIDE SURFACE
B] OUTSIDE SURFACE

RESIN - MFR 3.8, BNA

C] INSIDE SURFACE
D] OUTSIDE SURFACE

Figure 46. Typical SEM Photomicrographs
Films - BUR 1.0, DDR 4.0

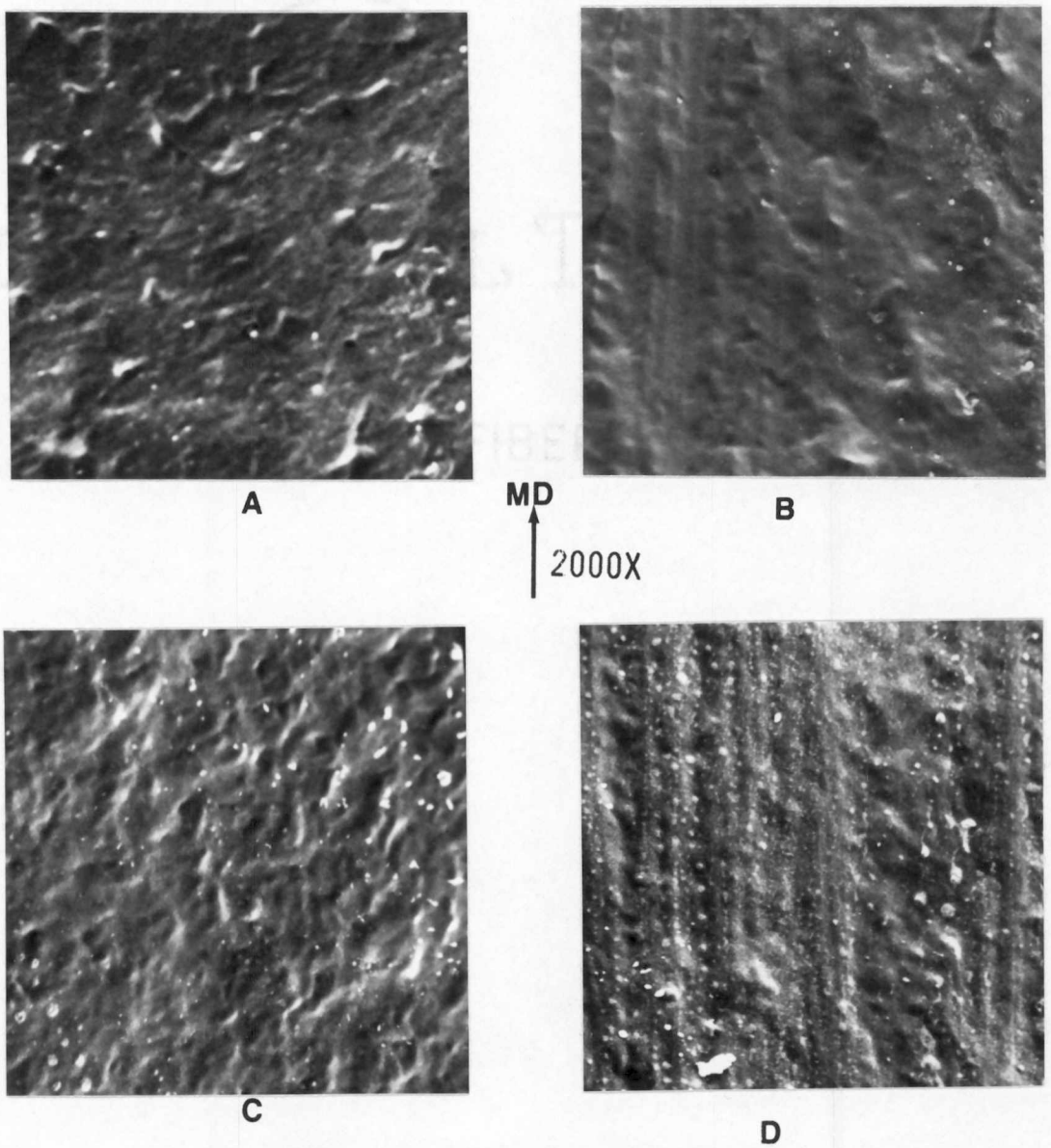

FILMS - BUR 1.0, DDR 10.0

RESIN - MFR 3.9, B

A] INSIDE SURFACE
B] OUTSIDE SURFACE

RESIN - MFR 3.8, BNA

C] INSIDE SURFACE
D] OUTSIDE SURFACE

Figure 47. Typical SEM Photomicrographs
Films - BUR 1.0, DDR 10.0

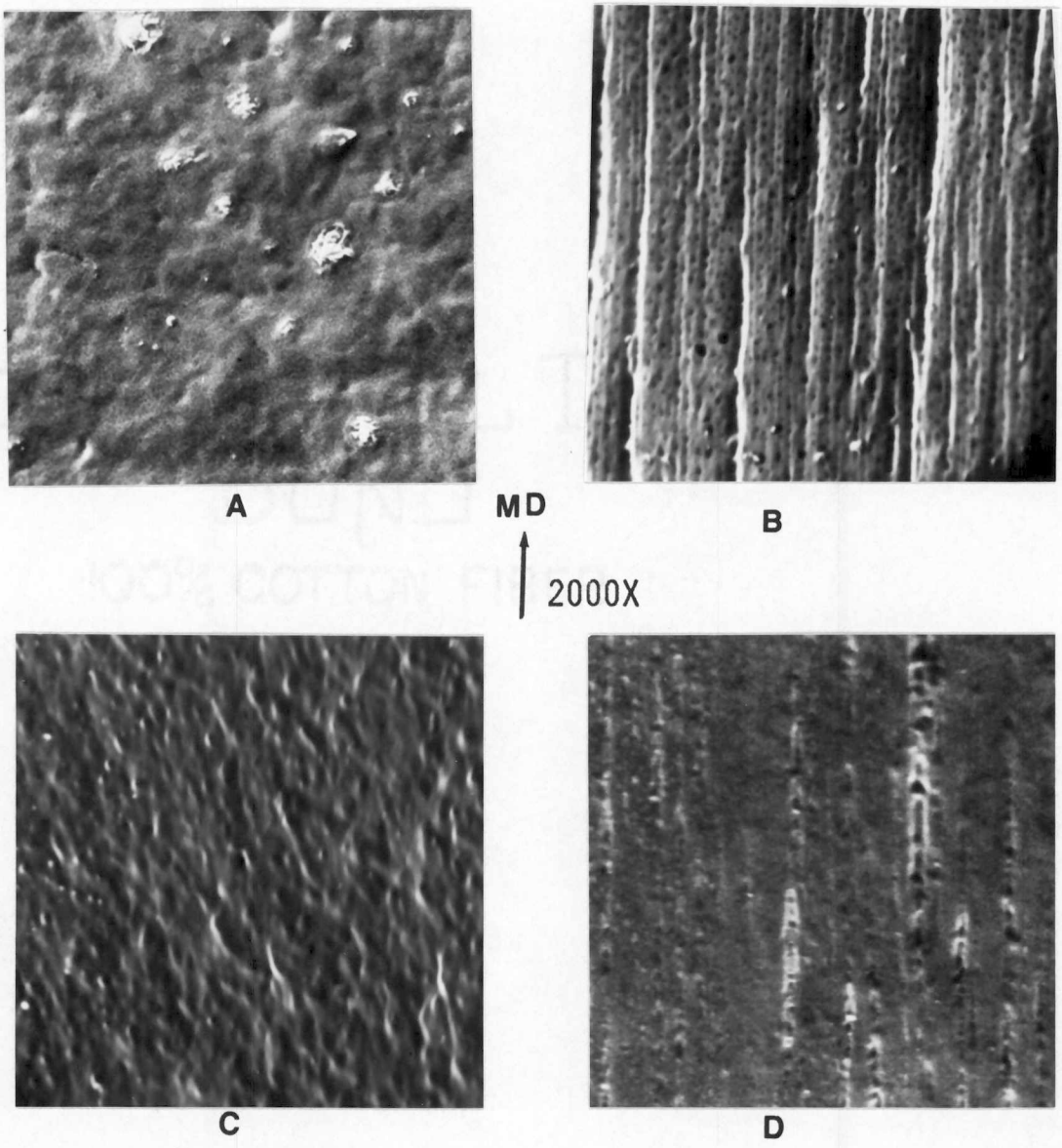

FILMS - BUR 3.0, DDR 7.0

RESIN - MFR 3.9, B

A] INSIDE SURFACE
B] OUTSIDE SURFACE

RESIN - MFR 3.8, BNA

C] INSIDE SURFACE
D] OUTSIDE SURFACE

Figure 48. Typical SEM Photomicrographs
Films - BUR 3.0, DDR 7.0

D. BUBBLE INSTABILITIES IN PP BLOWN FILMS

It was found that narrow MWD resins were more unstable than the broad MWD resins at various film preparation conditions. Also high MFR resins (beyond 14) were quite unstable at low BUR and DDR. In general for all resins the bubbles were unstable for BUR in the range 1.5 to 2.5. As pointed out by Kanai and White (44) the differing bubble stabilities depend on elongational flow behavior of the resins. In the Figures 49 and 50 we show operating space for PP tubular blown film process in terms of BUR, DDR and FLH for various resins. Qualitatively the typical unstable bubbles are shown in Figure 51. As pointed out by Han et al (37) we also found "wave" type of bubble instabilities for PP blown film process. All of the samples whose light transmission properties were studied in this thesis were prepared under stable operating conditions.

E. FACTORS AFFECTING TOTAL TRANSMISSION FACTORS OF PP FILMS

Now we turn to the discussion for the results given in section A on page 76. For various films the values of bulk phase, surface phase and total transmission factors are given in Tables XXIV, XXV and XXVI. Plots of Tb, Ts and T versus MFR for broad MWD resins are shown in Figure 52. These plots suggest that Tb increases with increase in MFR but both Ts and T decrease with MFR. Further, the trend for

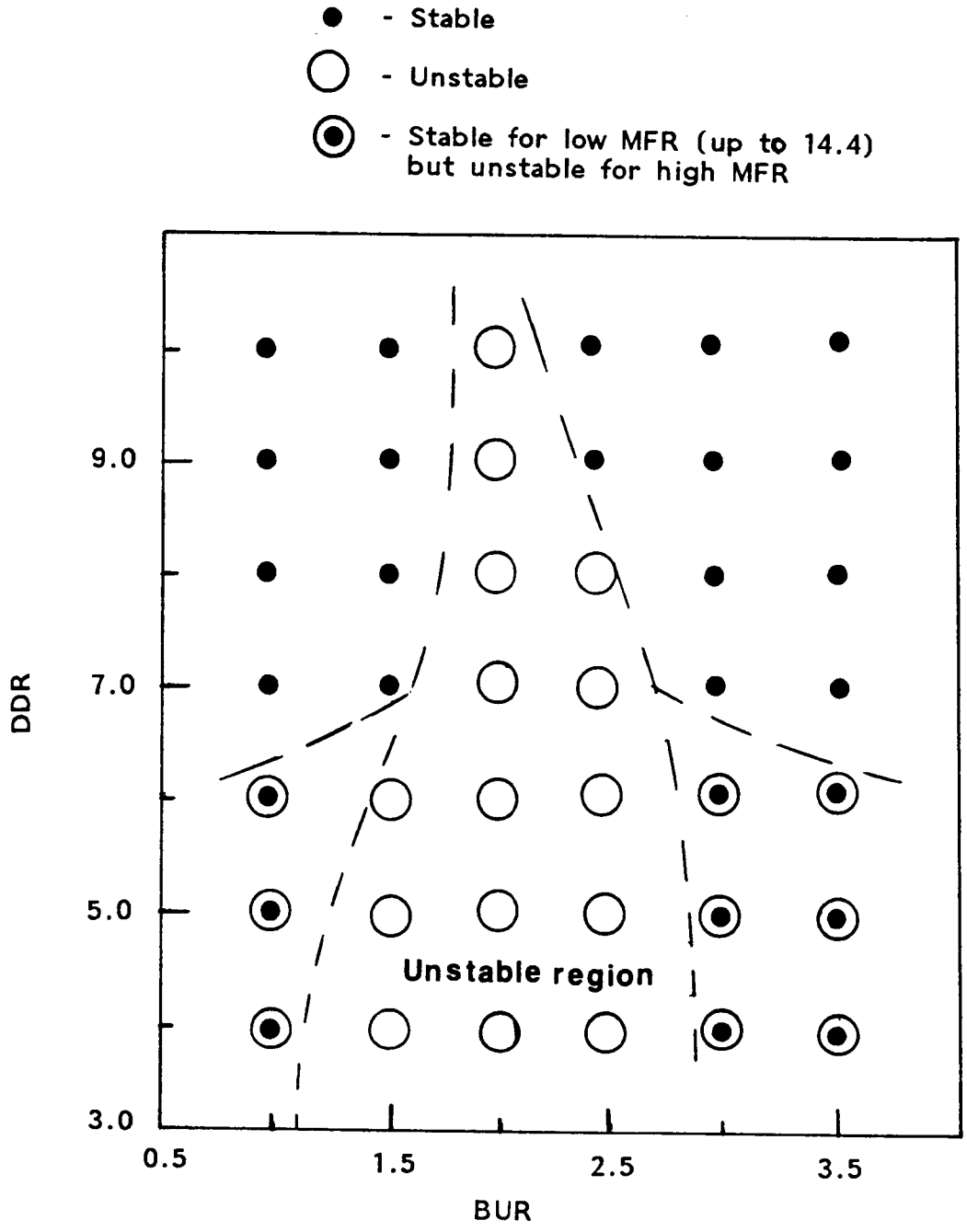

Figure 49. Operating Space for Blowing Films from Broad MWD, PP Resin

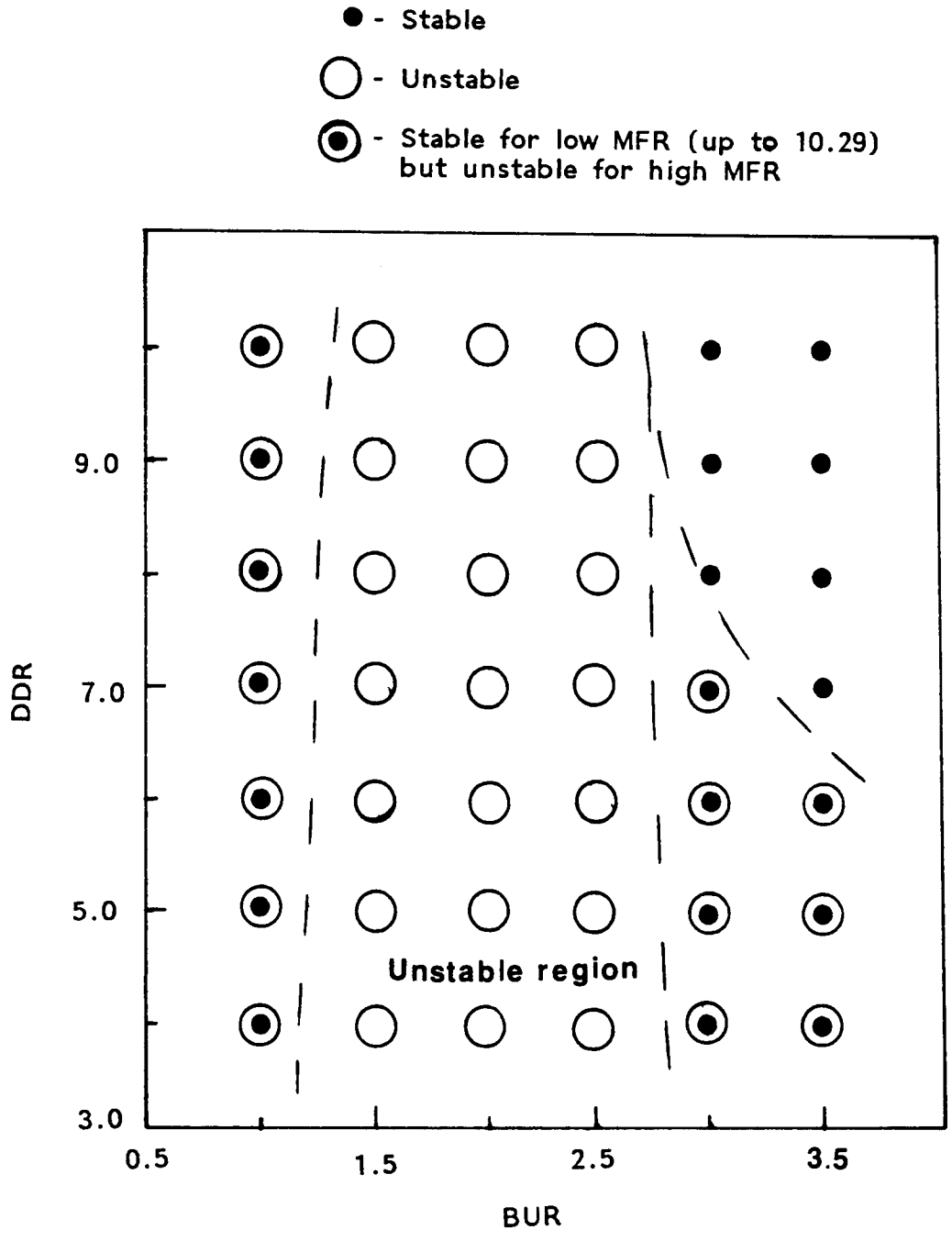

Figure 50. Operating Space for Blowing Films from narrow MWD, PP Resin

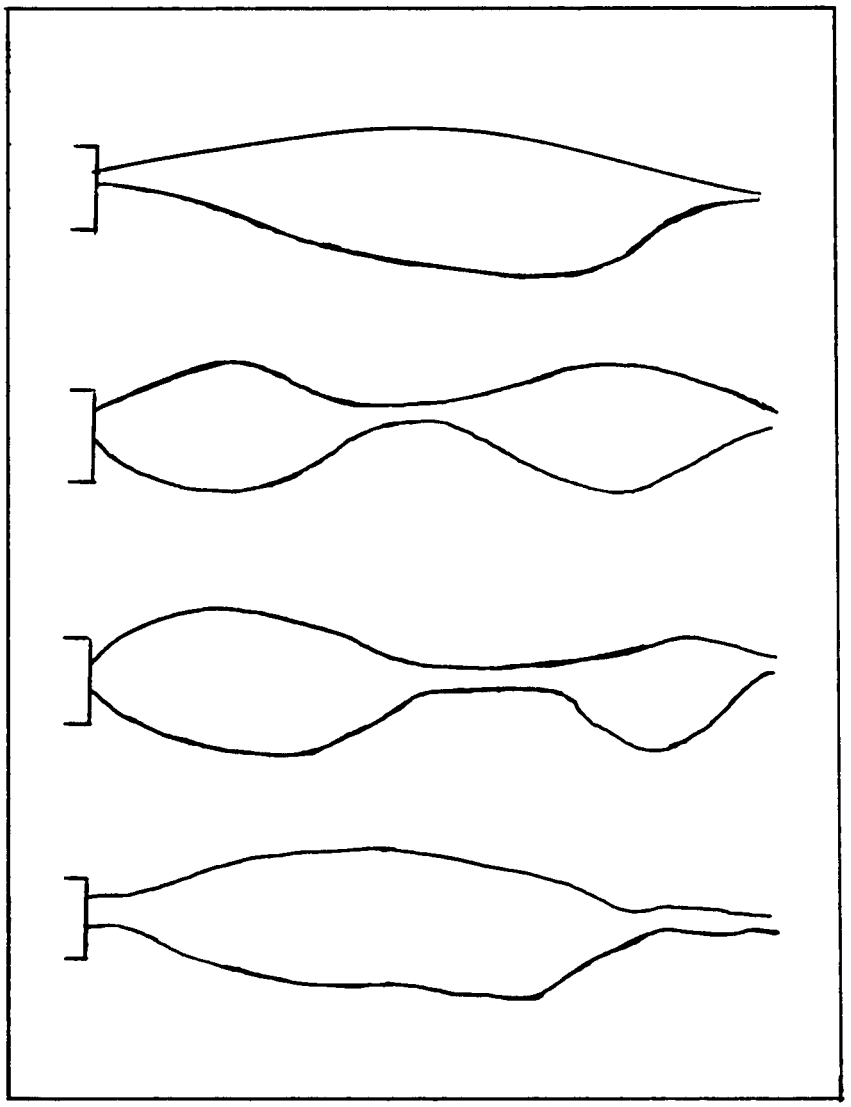

Figure 51. Typical Bubble Instability Behaviour

Table XXIV. Total Transmission Factor of Films
Films - BUR 1.0, DDR 4.0

Film Sample	MI of resin	Tb (%)	Ts (%)	T (%)
PPN-11	1.5	85.98	56.64	48.70
PPN-41	3.9	86.18	55.18	47.55
PPN-101	10.29	87.17	53.53	46.66
PPB-21	2.3	86.35	51.73	44.67
PPB-41	3.9	86.91	50.63	44.00
PPB-141	14.4	87.50	47.00	41.13
PPB-271	27.4	88.18	42.45	37.44
PPN-41NA	4.5	85.32	62.31	53.16
PPB-21NA	2.6	84.84	60.77	51.56
PPB-41NA	3.8	85.20	59.73	50.89
PPB-251NA	24.5	85.72	56.61	48.53

Table XXV. Total Transmission Factor of Films
Films - BUR 1.0, DDR 10.0

Film Sample	MI of resin	Tb (%)	Ts (%)	T (%)
PPN-12	1.5	89.64	57.90	51.90
PPN-42	3.9	88.39	56.30	49.76
PPN-102	10.29	90.06	51.61	46.48
PPB-22	2.3	89.74	56.67	50.86
PPB-42	3.9	90.36	55.09	49.78
PPB-142	14.4	90.68	50.20	45.52
PPB-272	27.4	91.04	42.67	38.84
PPN-42NA	4.5	88.13	65.71	57.91
PPB-22NA	2.6	87.97	65.29	57.43
PPB-42NA	3.8	88.03	63.97	56.31
PPB-252NA	24.5	88.94	59.19	52.65

Table XXVI. Total Transmission Factor of Films
Films - BUR 3.0, DDR 7.0, FLH 2.5 - 5 cm.

Film Sample	MI of resin	Tb (%)	Ts (%)	T (%)
PPN-13	1.5	94.88	60.36	57.27
PPN-43	3.9	95.93	58.32	55.95
PPN-103	10.29	96.18	53.35	51.31
PPB-23	2.3	96.50	58.03	56.00
PPB-43	3.9	96.60	55.52	53.63
PPB-143	14.4	98.30	52.97	52.07
PPB-273	27.4	97.50	47.34	46.15
PPN-43NA	4.5	94.63	67.85	64.20
PPB-23NA	2.6	92.32	67.28	62.11
PPB-43NA	3.8	93.25	65.75	61.31
PPB-253NA	24.5	93.83	61.32	57.54

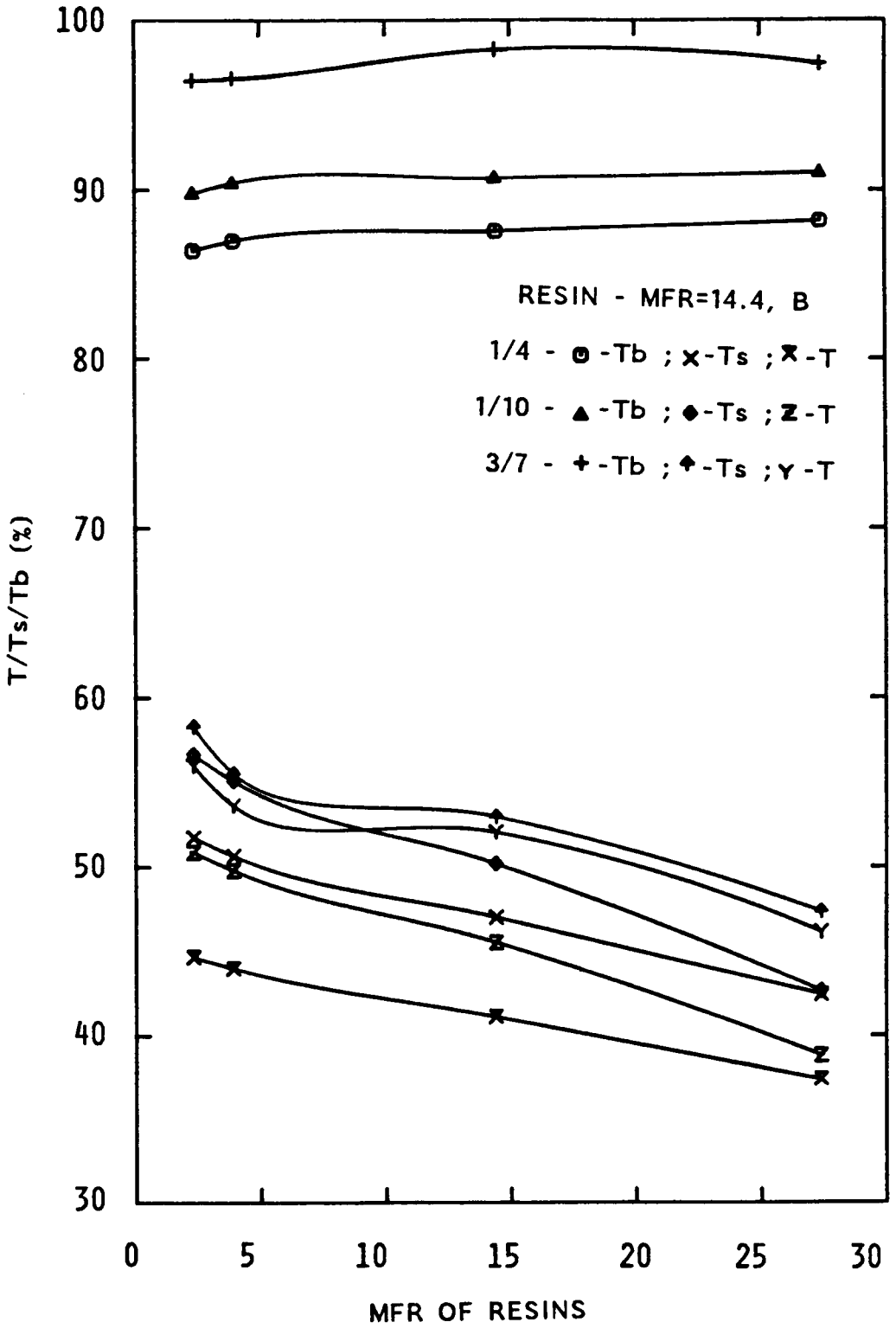

Figure 52. Comparison of Overall, Surface and Bulk Phase Transmission Factors (T, Ts, Tb) as a function of Melt Flow Rate (MFR) of Resin

T follows that for Ts suggesting that T is controlled by Ts rather than Tb. Thus it appears that even though internal spherulite structure of film has size in the range of 2 to 7 μm in radius, the light scattered by the film is dominated by the contribution due to surface roughness of the film which is of the order of 0.05 to 0.5 μm.

For the broad MWD resin with MFR=14.4 Tb, Ts and T are given in Tables XXVII, XXVIII and XXIX for the films with varying DDR , BUR and FLH respectively and respective plots are shown in Figures 53, 54 and 55. Again it is seen that T is controlled by Ts rather than Tb These plots suggest that T decreases initially with increasing DDR up to 6.0 and then increases with DDR. The higher value of T at low DDR seems to suggest Howell and Benbow's explanation (41) that decrease of extrusion haze at low DDR is due to greater relaxation of surface defects occurring between the die and frost line. For the variation of BUR Huck and Clegg (42) pointed out that an increase in BUR and consequent drawing of the melt reduces the size of extrusion defects frozen in to the film. But we find that initially with increasing BUR, T decreases up to 2.5 and then increases with BUR. We also found that in the region of BUR = 1.5 to 2.5 the bubble becomes increasingly unstable. It seems from higher values of Ts in case of films from nucleated resins that surface irregularities are governed more importantly by crystallization mechanism than the flow defects. Flow

Table XXVII. Bulk, Surface and Total Transmission Factors of Film as a function of DDR
Resin - MFR 14.4, Broad MWD
Films - BUR 3.0, FLH 2.5 - 5.0 cm.

Film Sample	DDR	Tb (%)	Tsi (%)	Tso (%)	Ts (%)	T (%)
PPB-1411	4.0	86.23	77.52	66.03	51.19	44.14
PPB-1412	5.0	88.79	76.00	63.23	48.05	42.67
PPB-1413	6.0	91.35	75.03	61.11	45.85	41.88
PPB-1414	7.0	98.30	78.34	67.54	52.91	52.01
PPB-1415	8.0	98.06	81.20	68.42	55.56	54.48
PPB-1416	9.0	98.46	83.54	70.42	58.83	57.92
PPB-1417	10.0	99.00	83.67	71.53	59.85	59.25

Table XXVIII. Bulk, Surface and Total Transmission Factors of Films as a function of BUR
Resin - MFR 14.4, Broad MWD
Films - DDR 7.0

Film Sample	BUR	Tb (%)	Tsi (%)	Tso (%)	Ts (%)	T (%)
PPB-1410	1.0	92.11	74.83	62.29	46.61	42.93
PPB-1415	1.5	92.89	72.86	61.41	44.74	41.56
PPB-1420	2.0	93.93	72.36	59.23	42.86	40.26
PPB-1425	2.5	89.48	70.52	60.06	42.35	37.90
PPB-1430	3.0	98.30	78.34	67.54	52.91	52.01
PPB-1435	3.5	98.53	79.46	68.31	54.28	53.48

Table XXIX. Bulk, Surface and Total Transmission Factors of Films as a function of FLH
Resin - MFR 14.4, Broad MWD
Films - BUR 3.0, DDR 7.0

Film Sample	FLH (cm)	Tb (%)	Tsi (%)	Tso (%)	Ts (%)	T (%)
PPB-143	2.5	98.30	78.34	67.54	52.91	52.01
PPB-144	5.0	94.48	77.87	67.49	52.55	49.65
PPB-145	8.0	91.16	73.42	59.05	43.36	39.53
PPB-146	10.0	89.24	69.35	54.90	38.07	33.97
PPB-147	13.0	89.12	65.66	50.42	33.11	29.51
PPB-148	15.0	88.52	59.91	44.82	26.85	23.77

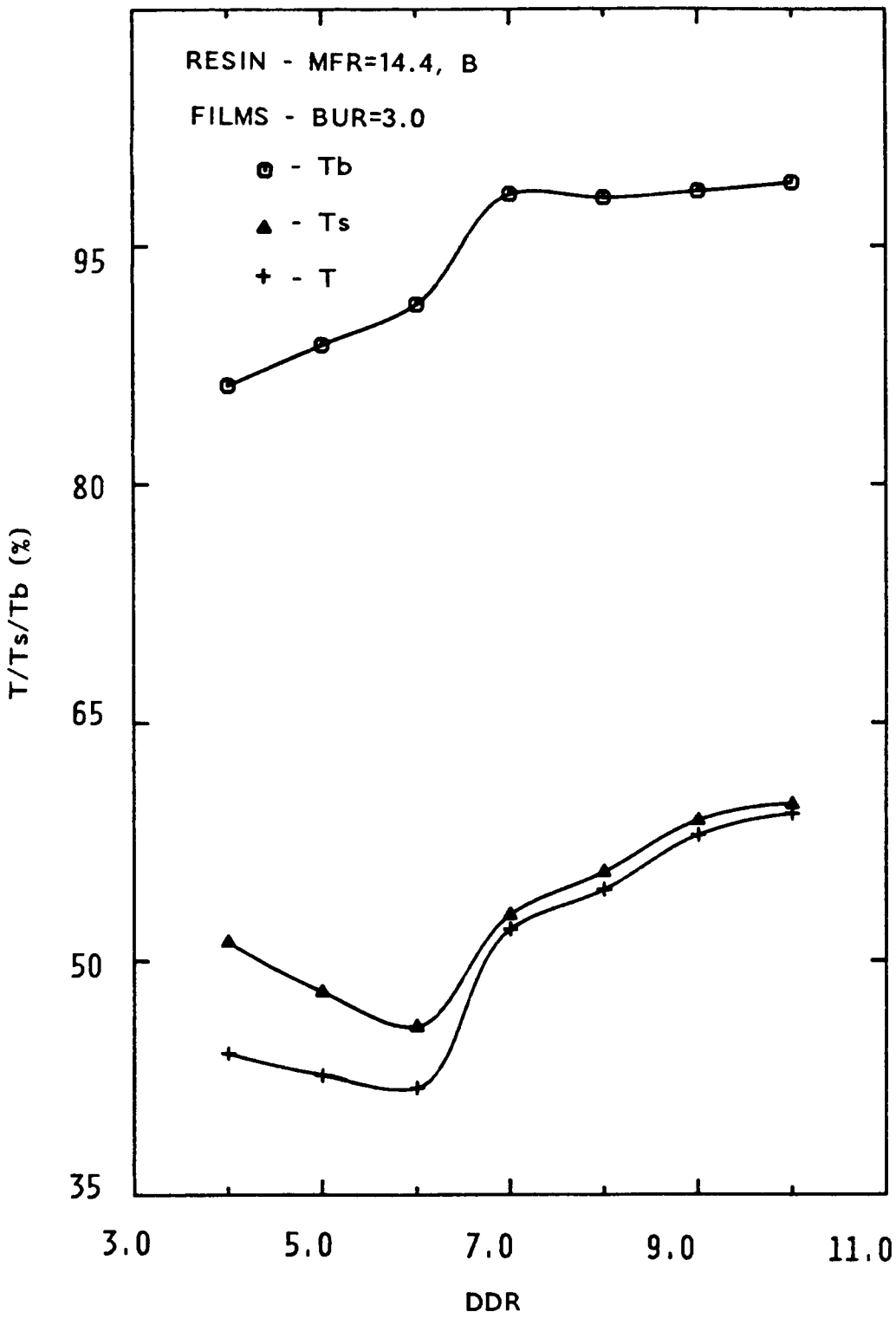

Figure 53. Comparison of Overall, Surface and Bulk Phase Transmission Factors (T, Ts, Tb) as a function of Draw Down Ratio (DDR)

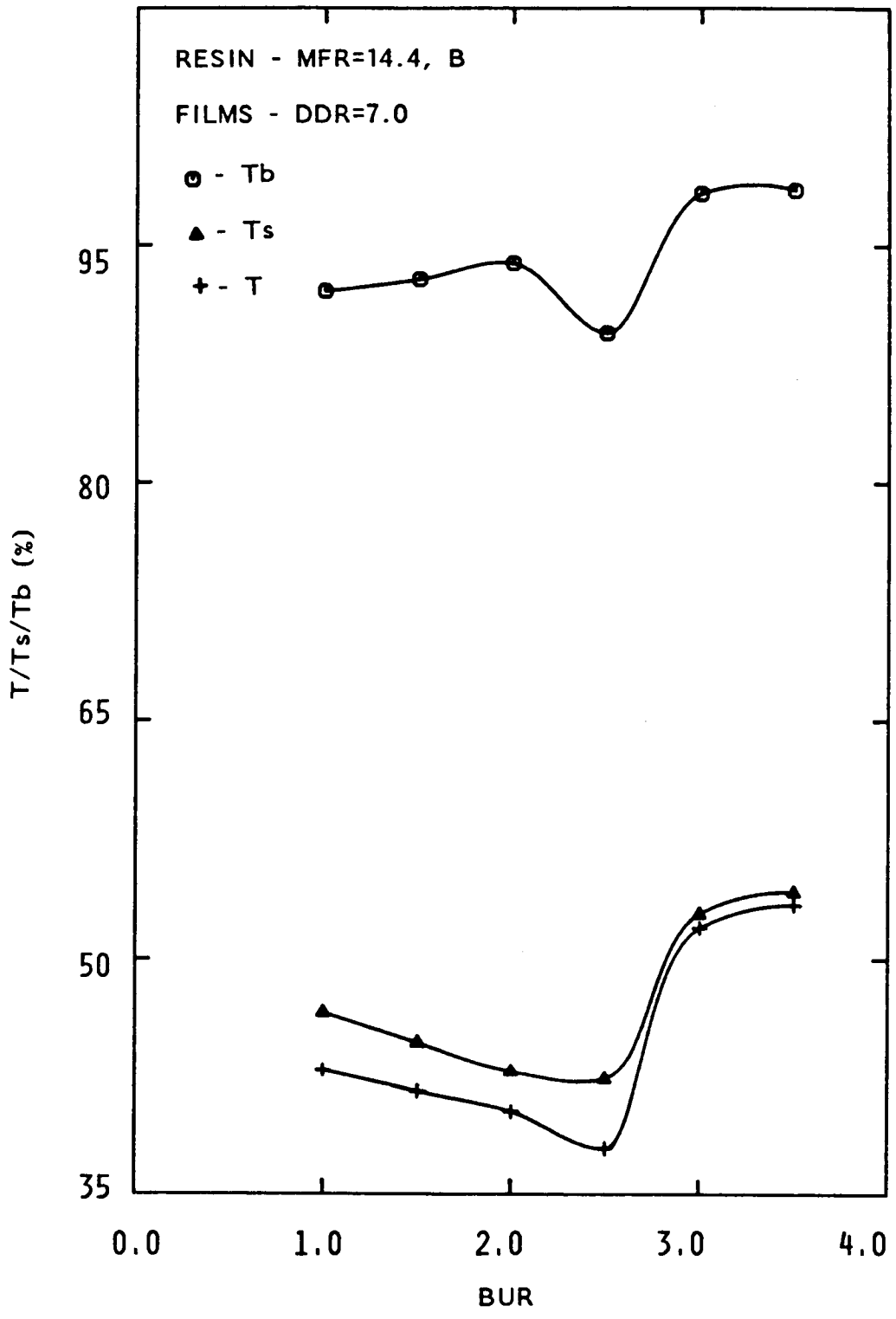

Figure 54. Comparison of Overall, Surface and Bulk Phase Transmission Factors (T, Ts, Tb) as a function of Blow-Up Ratio (BUR)

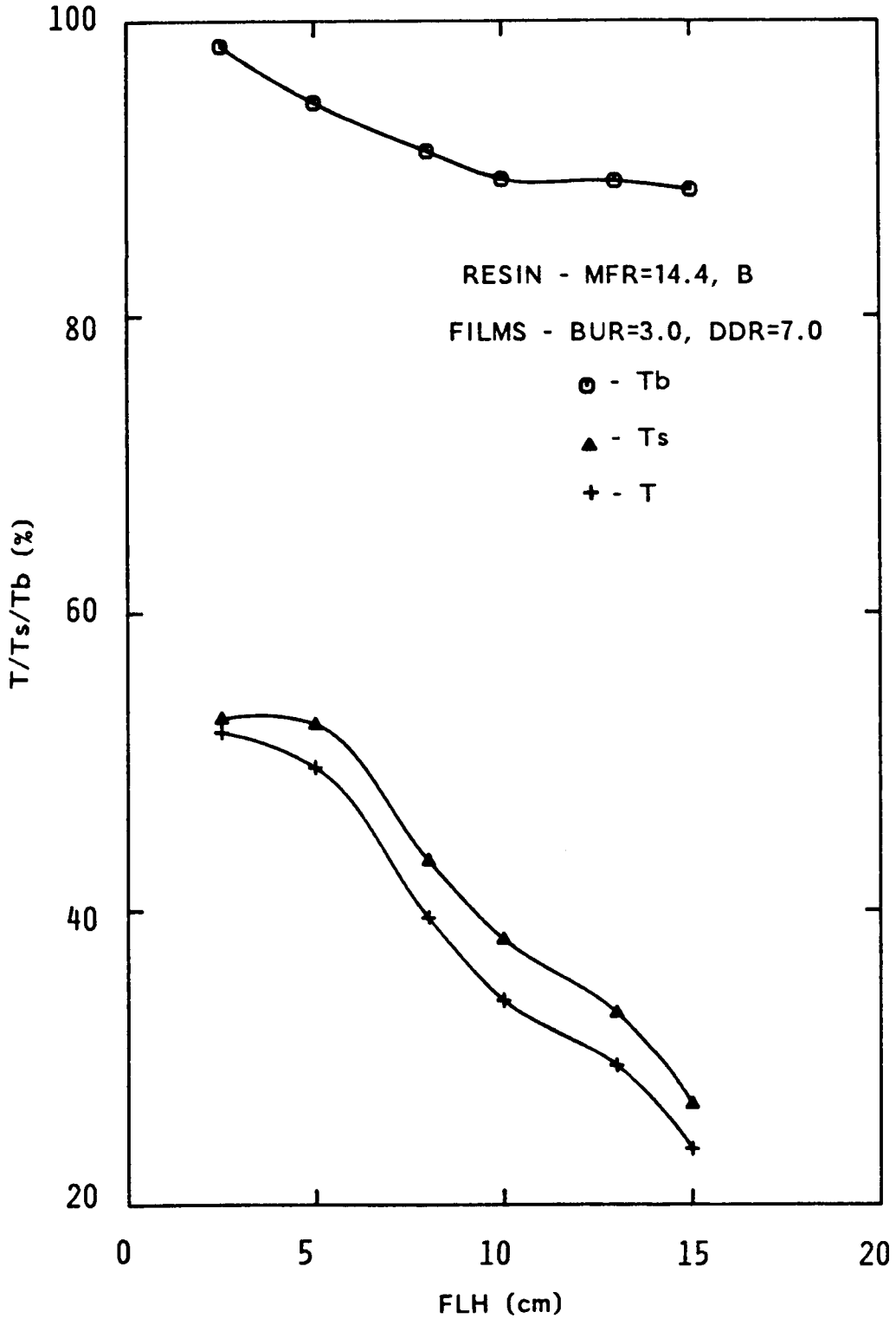

Figure 55. Comparison of Overall, Surface and Bulk Phase Transmission Factors (T, Ts, Tb) as a function of Frost Line Height (FLH)

defects seem important, however, in explaining the difference between the inside and outside surface transmission factors of the films. Also,in the unstable region of PP blown films it appears that the flow defects become more important but we do not have any data to support this view. T decreases substantially with increasing FLH thus suggesting that cooling rates of bubble have considerable effect on light transmission of films.

CHAPTER 5

CONCLUSIONS AND RECOMMENDATIONS

From the results and discussions in Chapter 4 we arrive at following important conclusions :

I. PP blown films have essentially spherulitic morphology. At low BUR and DDR spherulites are relatively large (up to radius of 5 to 7 μm) but with increasing BUR and DDR their size is much reduced (radii of 1.9 to 3.0 μm). Films from higher MFR and broad MWD resins have higher spherulite size than those from lower MFR and narrow MWD resins respectively. Films from nucleated resins have very small spherulite sizes (radii of 1.4 to 1.9 μm).

II. Bulk phase transmission factors Tb of various films lie in the range of 85 to 97%. Tb varies directly with spherulite size at specific conditions of BUR and DDR. But with increasing BUR and DDR, Tb increases eventhough spherulite size decreases suggesting that apart from spherulite size orientation of film also controls Tb.

III. Surface phase transmission factors Ts of various films lie in the range of 55 to 75%. Ts increases with increasing BUR, DDR and decreasing FLH. Films from low MFR and narrow MWD resins have higher Ts values than those from high MFR and broad MWD resins, respectively. Films from nucleated resins have the highest Ts values.

IV. The standard deviation of surface height of the films correlates well with Ts thus indicating that the rougher the film surfaces are, the lower will be the value of Ts. Typically the magnitude of standard deviation varies from 0.06 μm to 0.5 μm. Correlation distance Dc ranges from 4.0 to 7.0 μm indicating that hills or valleys on surface of film are 4 to 7 μm apart. However, the light transmission did not seem to have any particular trend with changes in Dc.

V. Total transmission factors T of all the films were controlled largely by Ts rather than Tb values indicating that even though internal spherulite structure of film has size in the range of 2 to 7 μm, essentially light scattering is dominated by roughness of surface which is of the order of 0.05 to 0.5 μm. The latter size also happens to be near the wavelength of the light.

VI. T decreases initially up to DDR of 6.0 and then increases with increasing DDR. BUR dependance of T has complex trend up to values of 2.5 but T increases onwards with increasing BUR. Increase in FLH decreases both Ts and Tb thus decreasing T.

VII. Narrow MWD and high MFR resins show greater bubble instabilities with film preparation conditions.

Summarizing all the conclusions we conclude that clarity of blown PP films is controlled by surface roughness of films rather than the bulk phase of the film. For clearer

PP blown films one should select low MFR, narrow MWD resin with nucleating agent and films should be blown at high BUR, DDR and as low a FLH as possible.

Since we did not study quantitative orientation achievement and mechanical properties of PP blown films, attempt should be made to study these for the films having high optical clarity for the sake of completeness. Even though it appeared that for the surface roughness of PP blown films the crystallization mechanism is more important than extrusion (flow) mechanism, this was not found to be satisfactory to explain the trend for variation of transmission factors with BUR. We felt that in the unstable region of film blowing of PP, extrusion mechanism becomes important without supporting by any data, an attempt should be made in that direction for the selected PP resin. Extrusion mechanism can be followed by rheological measurements and knowledge of surface roughness of die particularly near the die exit. Statistical parameters obtained to characterize surface roughness of film in our study were limited to small regions (0.4 mm long scan) and digitizing profile data involved error due to manual retracing of the profile. These limitations could be overcome by interfacing analog digitizer with surface profiler.

LIST OF REFERENCES

LIST OF REFERENCES

1. Albright, L. F., Chem. Eng., 73, 113(1966).

2. Alexander, R. L., Polym. Eng. Sci., 6, 1(1966).

3. Anderson, P. G. and S. H. Carr, Polym. Eng. Sci., 16, 217(1976).

4. Ashizawa, H., M.S. Thesis in Polym. Eng., University of Tennessee, 1982.

5. ASTM D1003 - 61 (1977).

6. ASTM D2457 - 70 (1977).

7. Beckmann, P. and A. Spizzichino, The Scattering of Electromagnetic Waves from Rough Surfaces, McMillan, New York, 1963.

8. Bendat, J. S. and A. G. Piesol, Measurement and Analysis of Random Data, John Wiley and Sons, New York, 1966.

9. Bennett, J. M., Appl. Opt., 15, 2705(1976).

10. Bennett, J. M. and J. H. Dancy, Appl. Opt., 20, 1785(1981).

11. Billmeyer, F. W., J. Opt. Soc. Am., 49, 368(1959).

12. Choi, K. J., J. L. White and J. E. Spruiell, J. Appl. Polym. Sci., 25, 2777(1980).

13. Choi, K. J., J. L. White and J. E. Spruiell, J. Polym. Sci., Phys. Ed., 20, 27(1982).

14. Clampitt, B. H. and D. E. German, Analytical Chemistry, 41,1306(1969).

15. Clark, E. S. in "Structure and Properties of Polymer Films", R. W. Lenz and R. S. Stein, eds., Plenum Press, New York, 1973.

16. Clegg, P. L., Trans. J. Plast. Inst., 26,151(1958).

17. Cogswell, F. N., J. Non-Newt. Fluid Mech., 2, 37(1977).

18. Dancy, J. H. and J. M. Bennett, Semiannu. Rep. 7 and 8, 166 NWC.

19. Debye, D. and A. M. Bueche, J. Appl. Phys., 20, 518(1949).

20. Dees, J. R. and J. E. Spruiell, J. Polym. Sci., 18, 1053(1974).

21. Desper, C. R., J. Appl. Polym. Sci., 14, 4284(1970).

22. Desper, C. R. and R. S. Stein, J. Appl. Phys., 37, 3990(1966).

23. Elias, H. G., Macromolecules, Vol. 1, Plenum Press, New York, 1977.

24. Elson, J. M. and J. M. Bennett, J. Opt. Soc. Am., 69, 31(1979).

25. Elson, J. M., H. E. Bennett and J. M. Bennett, Appl. Opt. and Opt. Eng., 7, 191(1979).

26. Falkai, B. V., Makromol. Chem., 41, 86(1960).

27. Foster, G. N., Polym. Prepr., Am. Chem. Soc., Div. Polym. Chem., 20, 463(1979).

28. Fujiki, T., J. Appl. Polym. Sci., 15, 47(1971).

29. Gailey, J. A. and R. H. Rabton, SPE Trans., 29, 103(1964).

30. Gogos, C. G. and V. Tan, Polym. Eng. Sci., 16, 512(1976).

31. Goldstein, M. and E. R. Michalik, J. Appl. Phys., 26, 1450(1955).

32. Grange, P. W., Editor, Polym. Age, 1, 265(1970).

33. Guillet, J. E., R. L. Coms, D. F. Slonaker, D. A. Weemes and H. W. Coover Jr., J. Appl. Polym. Sci., 9,757(1965).

34. Haas, T. W. and B. Maxwell, Polym. Eng. Sci., 9, 225(1969).

35. Han, C. D. and J. Y. Park, J. Appl. Polym. Sci., 19, 3257(1975).

36. Han, C. D. and J. Y. Park, J. Appl. Polym. Sci., 19, 3277(1975).

37. Han, C. D. and J. Y. Park, J. Appl. Polym. Sci., 19, 3291(1975).

38. Han, C. D., R. R. Lamonte and Y. T. Shah, J. Appl. Polym. Sci., 16, 3307(1972).

39. Hawkins, S. W. and R. B. Richards, J. Polym. Sci., 4, 515(1949).

40. Holmes, D. R. and R. P. Palmer, J. Polym. Sci., 31, 345(1958).

41. Howells, E. R. and J. J. Benbow, Trans. J. Plast. Inst., 30, 240(1962).

42. Huck, N. D. and P. L. Clegg, SPE Trans., 1, 121(1961).

43. Jones, A. T., J. M. Aizlewood and D. R. Beckett, Makromol. Chem., 75, 134(1964).

44. Kanai, T. and J. L. White, Polymer science and Engineering Report, No. 203, University of Tennessee, 1983.

45. Kargin, V. A., T. I. Sogolova, N. Ya. Rapoport and I. I. Kurbanova, J. Polym. Sci., Polym. Symp., Part C, 16, 1609(1967).

46. Kase, S. and T. Matsuo, J. Appl. Polym. Sci., 11, 251(1967).

47. Keane, J. J. and R. S. Stein, J. Polym. Sci., 20, 327(1956).

48. Keith, H. D., F. J. Padden Jr., N. M. Walter and H. W. Wyckoff, J. Appl. Phys., 30, 1485(1959).

49. Keller, A., J. Polym. Sci., 15, 31(1955).

50. Keller, A., Makromol. Chem., 34, 1(1959).

51. Keller, A., Nature, 174, 826(1954).

52. Keller, A. and M. J. Machin, J. Macromol. Sci., Phys. Ed., Part B, 1, 41(1967).

53. Kishi, N. and H. Iizuku, J. Polym. Sci., Part B, 2, 399(1964).

54. Kuhre, C. J., M. Wales and M. E. Doyle, SPE J., 20, 1113(1964).

55. Liebhafsky, H. A. and H. G. Pfiffer, J. Chem. Educ., 30, 450(1953).

56. Lindenmeyer, P. H. and S. Lustig, J. Appl. Polym. Sci., 9, 227(1965).

57. Lodge, A. S., Trans. Faraday Soc., 52, 120(1956).

58. Lodge, A. S., Elastic Liquids, Academic Press, New York, 1964.

59. Maddams, W. F. and J. E. Preedy, J. Appl. Polym. Sci., 22, 2721(1978).

60. Maddams, W. F. and J. E. Preedy, J. Appl. Polym. Sci., 22, 2739(1978).

61. Maddams, W. F. and J. E. Preedy, J. Appl. Polym. Sci., 22, 2751(1978).

62. Maron, S. H. and C. F. Prutton, Principles of Physical Chemistry, Mc Millan, New York, 1958.

63. Matonis, V. A. in "Contemporary Thermoplastic Materials", Polymer Handbook, 1974.

64. Matsumoto, T. and D. C. Bogue, Polym. Eng. Sci., 18, 564(1978).

65. McCallum, W. H., SPE J., 28, 39(1972).

66. McRae, M. A. and W. F. Maddams, Makromol. Chem., 177, 473(1976).

67. McRae, M. A., W. F. Maddams and J. E. Preedy, J. Mater. Sci., 11, 2036(1976).

68. Mejer, J., Kunstst., 54, 578(1964).

69. Mendelson, R. A., J. Polym. Sci., Part A, 1, 2361(1963).

70. Mie, G., Ann. Phisik, 25, 377(1968).

71. Minoshima, W., J. L. White and J. E. Spruiell, J. Appl. Polym. Sci., 25, 287(1980).

72. Minoshima, W., J. L. White and J. E. Spruiell, Polym. Eng. Sci., 20, 1166(1980).

73. Minoshima, W., Ph.D. Dissertation in Polym. Eng., University of Tennessee, 1983.

74. Morrow, D. R., J. A. Sauer and A. E. Woodward, J. Polym. Sci., Part B, 3, 463(1965).

75. Nadella, H. P., H. M. Henson, J. E. spruiell and J. L. White, J. Appl. Polym. Sci., 21, 3003(1977).

76. Natta, G. and P. Corradini, Nuovo Cimento, Suppl., 15, 40(1960).

77. Pearson, J. R. A. and C. J. S. Petrie, J. Fluid Mech., 40, 1(1970).

78. Pearson, J. R. A. and C. J. S. Petrie, J. Fluid Mech., 40, 609(1970).

79. Pearson, J. R. A. and C. J. S. Petrie, Plastics and Polymers, 38, 85(1970).

80. Perron, P. J. and P. D. Lederman, Polym. Eng. Sci., 12, 340(1972).

81. Pilaro, J. F. and R. J. Kremer, Mod. Plast., 38, 115(1960).

82. Pilaro, J. F., R. J. Kremer and L. A. Kuhlman, Mod. Plast., 39, 123(1961).

83. Rank Precision Ind. Ltd., Technical Manual, Luchester, England.

84. Rasigni, M., G. Rasigni and J. P. Palmari, J. Opt. Soc. Am., 71, 1124(1981).

85. Rasigni, M., G. Rasigni and J. P. Palmari, J. Opt. Soc. Am., 71, 1130(1981).

86. Rayleigh, L., The Theory of Sound, Vol. 2, Dover, New York, 1945.

87. Rokudai, M., J. Appl. Polym. Sci., 23, 463(1969).

88. Ross, G. and A. W. Birley, J. Phys., Part D, 6, 795(1973).

89. Samuels, R. J., J. Polym. Sci., Part A-2, 9, 2165(1971).

90. Shida, M., R. N. Shroff and L. V. Cancio, Polym. Eng. Sci., 17, 769(1977).

91. Shimomura, Y., J. E. Spruiell and J. L. White, Polymer Science and Engineering Report, No. 175, University of Tennessee, 1981.

92. Southern, J. H. and R. S. Porter, J. Macromol. Sci., Phys. Ed., Part B, 4, 541(1970).

93. Southern, J. H. and R. S. Porter, J. Appl. Polym. Sci., 14, 2305(1970).

94. Stehling, F. C., C. S. Speed and L. Westerman, Macromolecules, 14, 698(1981).

95. Stein, R. S. and A. Plaza, J. Polym. Sci., 40, 267(1959).

96. Stein, R. S. and F. H. Norris, J. Polym. Sci., 27, 87(1959).

97. Stein, R. S. and J. J. Keane, J. Polym. Sci., 17, 21(1955).

98. Stein, R. S. and M. B. Rhodes, J. Appl. Phys., 31, 1873(1960).

99. Stein, R. S. and M. B. Rhodes, J. Appl. Phys., 32, 2344(1961).

100. Stein, R. S. and R. Prud'home, J. Polym. Sci., Part B, 9, 595(1971).

101. Stein, R. S., F. H. Norris and A. Plaza, J. Polym. Sci., 24, 455(1957).

102. Stein, R. S., J. J. Keane and F. H. Norris, J. Polym. Sci., 20, 209(1956).

103. Tang, M., Ph.D. Dissertation in Polym. Eng., University of Tennessee, 1984.

104. Tordella, J. P., J. Appl. Phys., 27, 454(1956).

105. Tordella, J. P., Trans. Soc. Rheol., 1, 203(1957).

106. Wang, T. T., H. S. Chen and T. K. Kwei, J. Polym. Sci., Part B, 8, 505(1970).

107. Weber, A. C., J. Opt. Soc. Am., 47, 785(1957).

108. White, J. L., Appl. Polym. Symp., 20, 155(1973).

109. White, J. L. and J. E. Spruiell, Polym. Eng. Sci., 21, 859(1981).

110. Wibbens, R. L., Plast. Technol., 7, 35(1960).

111. Wilchinsky, Z. W., J. Appl. Phys., 30, 792(1959).

112. Wilchinsky, Z. W., J. Appl. Polym. Sci., 15, 48(1961).

113. Williamson, D. A., Plastics and Polymers, 38, 169(1970).

114. Zukor, L. J., Plast. Technol., 7, 44(1961).

APPENDIXES

APPENDIX A

GRAPHICS TABLET PROGRAM

```
C    THIS PROGRAM IS TO DIGITIZE THE SURFACE PROFILE USING
C    GRAPHICS TABLET -TEKTRONIX 4953 GRID AND DIGITIZER
C    CURSOR. EACH POINT ON PROFILE IS DIGITIZED IN TERMS OF
C    (X,Y) CO-ORDINATES OF TABLET GRID.UPON READING THE FIRST
C    POINT THE TERMINAL RINGS TO SAY IT IS READY TO READ
C    OTHER POINTS. SUCCESIVE POINTS ARE READ AT INCREMENT OF
C    FOUR ON X-COORDINATE. THE TERMINAL RINGS EVERY TIME A
C    POINT IS READ. THE POINTS READ ARE IN THE RANGE OF 0-900
C    FOR X CO-ORDINATE AT THE END THE TERMINAL REDRAWS THE
C    PROFILE IN ORDER TO SHOW THAT POINTS READ LIE ON THE
C    PROFILE.


     DIMENSION IH(3000),IXR(3000),IYR(3000),
      1  IXD(1000),IYD(1000)
     CALL INITT
     CALL TABINT (0,1,1)
     CALL ONEPNT (IXR(1),IYR(1))
     IXD(1)=IXR(1)
     IYD(1)=IYR(1)
     WRITE (21,60) IXD(1),IYD(1)
     CALL BELL
     IC=IXD(1)+4
     J=2
     DO 10 I=2,3000
     CALL ONEPNT (IXR(I),IYR(I))
     IF (IXR(I).GT.900) GO TO 30
     IF (IXR(I).LT.IC) GO TO 10
     IF (IXR(I).EQ.IC) GO TO 20
     JJ = J - 1
     TEMPX = IXR(I) - IXD(JJ)
     TEMPY = IYR(I) - IYD(JJ)
     PROP  = (4 * TEMPY) / TEMPX + 0.5
     IXR(I) = IC
     IYR(I) = PROP + IYD(JJ)
20   IXD(J)=IXR(I)
     IYD(J)=IYR(I)
     WRITE (21,60) IXD(J),IYD(J)
60   FORMAT (2I5)
     J=J+1
     IC=IC+4
     CALL BELL
10   CONTINUE
30   CONTINUE
```

```
      CALL ANMODE
      CALL MOVABS (IXD(J),IYD(J))
      NUM=J-1
      DO 40 J=2,NUM
      CALL DRWABS (IXD(J),IYD(J))
40    CONTINUE
50    CONTINUE
      CALL FINITT (0,0)
      END
```

APPENDIX B

PROFILE STATISTICS PROGRAM

```
C    THIS PROGRAM IS TO PERFORM STATISTICS ON THE DIGITIZED
C    PROFILE DATA. FIRST A BASELINE THROUGH THE PROFILE IS
C    OBTAINED USING A LEAST SQUARE LINEAR REGRESSION
C    SUBROUTINE (IMSL:RLONE). THIS IS DONE BY TAKING A GROUP
C    OF 20 DATA POINTS TO TAKE CARE OF CHANGE IN SLOPE OF
C    PROFILE. AT EACH DATA POINT DEVIATION FROM BASELINE
C    AND ULTIMATELY MEAN DEVIATION AND STANDARD DEVIATION IS
C    CALCULATED. FINALLY AUTOCORRELATION COEFFICIENT IS
C    CALCULATED FROM MEAN DEVIATION AND DEVIATION AT EACH
C    DATA POINT.


     DOUBLE PRECISION FILE
     DIMENSION W(1000),IXD(1000),IYD(1000),V(1000)
     DIMENSION Z(1000)
     DIMENSION XY(1000,2),ALBAP(3),DES(5),ANOVA(14)
         DIMENSION  STAT(9),PRED(1,7)
     IX=1000
     WRITE(5,50)
50   FORMAT( ' INPUT FILE NAME ',1H$)
     READ(5,100) FILE
100  FORMAT(A6)
     OPEN(UNIT=21,FILE=FILE)
     DO 200 I=1,11
     IA=I*20
     IB=IA-19
     IC=0
     DO 160 J=IB,IA
     READ (21,150) IXD(J),IYD(J)
     WRITE(1,150) IXD(J),IYD(J)
     WRITE(22,150) IXD(J),IYD(J)
     WRITE(5,150) IXD(J),IYD(J)
150  FORMAT (2I5)
     IC=IC+1
     XY(IC,1)=IXD(J)
     XY(IC,2)=IYD(J)
160  CONTINUE
     N=IC
     IMOD=0
     IPRED=0
     ALBAP(1)=0.05
     ALBAP(2)=0.05
     IP=1
     NN=7
```

```
      CALL RLONE(XY,IX,N,IMOD,IPRED,ALBAP,DES,ANOVA,
     1  STAT,PRED,IP,NN,IER)
      IF(IER.EQ.0) GO TO 16
      WRITE(5,116) IER
  116 FORMAT( 'ERROR NUMBER ',I4)
   16 CONTINUE
      WRITE(5,250)DES(2),DES(4),DES(5),STAT(1),STAT(5)
      WRITE(22,250)DES(2),DES(4),DES(5),STAT(1),STAT(5)
  250 FORMAT( ' MEAN= ',G15.6,/,' SIGM= ',G15.6,/,' RE.COEFF= '
     1  ,G15.6,/,' SLOPE= ',G15.6,/,' INTERCEPT= ',G15.6)
      A=STAT(1)
      B=STAT(5)
      DO 201 K=IB,IA
  201 Z(K)=IYD(K)-IXD(K)*A-B
  200 CONTINUE
      IC=IA
      FIC=FLOAT(IC)
      DO 500 I=1,IC
  500 AL=AL+Z(I)
      AMEAN=AL/FIC
      DO 600 I=1,IC
  600 D=D+(Z(I)-AMEAN)**2
      VARI=D/FIC
      SIGM=VARI**0.5
      WRITE(5,800) AMEAN,SIGM
      M=50
      DO 700 I=1,M
      G=0
      NM=IC-I-1
      DO 700 J=1,NM
      K=J+I-1
      G=G+(Z(J)-AMEAN)*(Z(K)-AMEAN)
      V(I)=G/NM
  700 W(I)=V(I)/VARI
      WRITE(22,800) AMEAN,SIGM
  800 FORMAT(' MEAN= ',G15.6,/,' SIGM= ',G15.6)
      WRITE(22,900) (W(I),V(I),I=1,M)
      WRITE(23,901) (W(I),I=1,M)
      WRITE(25,901) (Z(K),K=1,IC)
  901 FORMAT(F15.6)
  900 FORMAT(G15.6,G15.6)
      WRITE(22,1000)IC
 1000         FORMAT(' DATA PTS= ',G15.6)
      CLOSE (UNIT=21,FILE=FILE)
      STOP
      END
```

APPENDIX C

TYPICAL DATA FROM PROGRAMS

Digitized Data of Surface Profile in Tablet Grid Units

14	345	186	326	358	302
18	340	190	326	362	303
22	341	194	325	366	302
26	339	198	324	370	302
30	338	202	324	374	300
34	338	206	322	378	294
38	336	210	321	382	293
42	337	214	318	386	292
46	338	218	314	390	291
50	337	222	310	394	292
54	337	226	309	398	293
58	336	230	309	402	293
62	337	234	310	406	292
66	338	238	310	410	293
70	338	242	312	414	293
74	337	246	311	418	292
78	336	250	309	422	293
82	335	254	308	426	295
86	335	258	309	430	297
90	335	262	310	434	296
94	333	266	310	438	295
98	331	270	308	442	296
102	330	274	304	446	296
106	331	278	298	450	295
110	330	282	296	454	296
114	328	286	295	458	296
118	324	290	295	462	294
122	323	294	298	466	292
126	324	298	301	470	291
130	325	302	301	474	291
134	324	306	299	478	293
138	321	310	298	482	293
142	320	314	297	486	293
146	320	318	296	490	291
150	320	322	298	494	292
154	320	326	301	498	292
158	322	330	302	502	291
162	325	334	302	506	290
166	326	338	305	510	289
170	326	342	304	514	297
174	326	346	303	518	298
178	327	350	303	522	295
182	327	354	302	526	295

530	290
534	286
538	284
542	283
546	282
550	284
554	285
558	285
562	287
566	288
570	287
574	287
578	283
582	283
586	282
590	281
594	283
598	285
602	283
606	284
610	283
614	285
618	285
622	287
626	286
630	284
634	281
638	280
642	281
646	283
650	284
654	287
658	287
662	286
666	287
670	289
674	293
678	291
682	293
686	294
690	296
694	295
698	295
702	292
706	293
710	294
714	294
718	292
722	287
726	284
730	286
734	289
738	288
742	288
746	290
750	297
754	304
758	307
762	308
766	304
770	303
774	302
778	301
782	299
786	300
790	301
794	302
798	301
802	301
806	303
810	303
814	303
818	306
822	305
826	304
830	305
834	304
838	301
842	300
846	302
850	304
854	306
858	307
862	306
866	303
870	301
874	302
878	301
882	300
886	300
890	309

Data from Profile Statistics Program

```
   14   345
   18   340
   22   341
   26   339
   30   338
   34   338
   38   336
   42   337
   46   338
   50   337
   54   337
   58   336
   62   337
   66   338
   70   338
   74   337
   78   336
   82   335
   86   335
   90   335
 MEAN=      337.650
 SIGM=      2.34577
 RE.COEFF=    -0.771777
 SLOPE=    -0.765038E-01
 INTERCEPT=      341.628
   94   333
   98   331
  102   330
  106   331
  110   330
  114   328
  118   324
  122   323
  126   324
  130   325
  134   324
  138   321
  142   320
  146   320
  150   320
  154   320
  158   322
  162   325
  166   326
  170   326
 MEAN=      325.150
 SIGM=      4.15838
 RE.COEFF=    -0.689951
 SLOPE=    -0.121241
 INTERCEPT=      341.154
  174   326
  178   327
  182   327
  186   326
  190   326
  194   325
  198   324
  202   324
  206   322
  210   321
  214   318
  218   314
  222   310
  226   309
  230   309
  234   310
  238   310
  242   312
  246   311
  250   309
 MEAN=      318.000
 SIGM=      7.38419
 RE.COEFF=    -0.933708
 SLOPE=    -0.291353
 INTERCEPT=      379.767
  254   308
  258   309
  262   310
  266   310
  270   308
  274   304
  278   298
  282   296
  286   295
  290   295
  294   298
  298   301
  302   301
  306   299
  310   298
  314   297
  318   296
  322   298
  326   301
  330   302
 MEAN=      301.200
 SIGM=      5.18703
 RE.COEFF=    -0.629448
 SLOPE=    -0.137970
 INTERCEPT=      341.487
```

334	302
338	305
342	304
346	303
350	303
354	302
358	302
362	303
366	302
370	302
374	300
378	294
382	293
386	292
390	291
394	292
398	293
402	293
406	292
410	293

MEAN= 298.050
SIGM= 5.21612
RE.COEFF= -0.897973
SLOPE= -0.197932
INTERCEPT= 371.681

414	293
418	292
422	293
426	295
430	297
434	296
438	295
442	296
446	296
450	295
454	296
458	296
462	294
466	292
470	291
474	291
478	293
482	293
486	293
490	291

MEAN= 293.900
SIGM= 1.94395
RE.COEFF= -0.430185
SLOPE= -0.353383E-01
INTERCEPT= 309.873

494	292
498	292
502	291
506	290
510	289
514	297
518	298
522	295
526	295
530	290
534	286
538	284
542	283
546	282
550	284
554	285
558	285
562	287
566	288
570	287

MEAN= 289.000
SIGM= 4.73509
RE.COEFF= -0.618131
SLOPE= -0.123684
INTERCEPT= 354.800

574	287
578	283
582	283
586	282
590	281
594	283
598	285
602	283
606	284
610	283
614	285
618	285
622	287
626	286
630	284
634	281
638	280
642	281
646	283
650	284

MEAN= 283.500
SIGM= 1.96013
RE.COEFF= -0.163392
SLOPE= -0.135338E-01
INTERCEPT= 291.783

654	287
658	287
662	286
666	287
670	289
674	293
678	291
682	293
686	294
690	296
694	295
698	295
702	292
706	293
710	294
714	294
718	292
722	287
726	284
730	286

MEAN= 290.750
SIGM= 3.72580
RE.COEFF= 0.101480
SLOPE= 0.159774E-01
INTERCEPT= 279.694

734	289
738	288
742	288
746	290
750	297
754	304
758	307
762	308
766	304
770	303
774	302
778	301
782	299
786	300
790	301
794	302
798	301
802	301
806	303
810	303

MEAN= 299.550
SIGM= 6.06522
RE.COEFF= 0.574246
SLOPE= 0.147180
INTERCEPT= 185.927

814	303
818	306
822	305
826	304
830	305
834	304
838	301
842	300
846	302
850	304
854	306
858	307
862	306
866	303
870	301
874	302
878	301
882	300
886	300
890	309

MEAN= 303.450
SIGM= 2.58488
RE.COEFF= -0.173806
SLOPE= -0.189850E-01
INTERCEPT= 319.625
MEAN= -0.312112E-06
SIGM= 3.01617

0.985376	8.96426
0.725080	6.59627
0.378583	3.44408
0.510473E-01	0.464392
-0.190242	-1.73069
-0.313455	-2.85159
-0.356798	-3.24589
-0.370161	-3.36746
-0.337229	-3.06787
-0.293762	-2.67244
-0.232898	-2.11874
-0.174825	-1.59043
-0.127668	-1.16144
-0.509652E-01	-0.463645
0.705193E-01	0.641535
0.138372	1.25881
0.157626	1.43397
0.166826	1.51766
0.148344	1.34952
0.108347	0.985666
0.106478	0.968663
0.876598E-01	0.797467
0.532190E-01	0.484149

Data for Height Deviation at Digitized Point of Surface Profile.

1	4.442856	50	2.417294	99	0.679699
2	-0.251129	51	0.582706	100	2.471428
3	1.054886	52	-2.251881		
4	-0.639099	53	-5.086468		
5	-1.333084	54	-4.921055		
6	-1.027069	55	-3.755638		
7	-2.721054	56	-1.590225		
8	-1.415039	57	-0.424812		
9	-0.109024	58	2.740601		
10	-0.803009	59	2.906013		
11	-0.496994	60	2.071426		
12	-1.190979	61	1.557144		
13	0.115036	62	3.109024		
14	1.421051	63	4.660904		
15	1.727066	64	5.212784		
16	1.033081	65	3.764664		
17	0.339096	66	0.316544		
18	-0.354889	67	-5.131577		
19	-0.048874	68	-6.579697		
20	0.257141	69	-7.027817		
21	3.242855	70	-6.475937		
22	1.727818	71	-2.924061		
23	1.212780	72	0.627819		
24	2.697742	73	1.179699		
25	2.182705	74	-0.268421		
26	0.667667	75	-0.716541		
27	-2.847370	76	-1.164661		
28	-3.362408	77	-1.612782		
29	-1.877445	78	0.939098		
30	-0.392483	79	4.490978		
31	-0.907520	80	6.042858		
32	-3.422558	81	-3.571430		
33	-3.937595	82	0.220299		
34	-3.452637	83	0.012028		
35	-2.967674	84	-0.196239		
36	-2.482712	85	0.595490		
37	0.002251	86	0.387218		
38	3.487213	87	1.178947		
39	4.972176	88	2.970676		
40	5.457138	89	2.762405		
41	-3.071430	90	3.554134		
42	-0.906017	91	2.345863		
43	0.259399	92	-2.862408		
44	0.424812	93	-3.070679		
45	1.590225	94	-3.278950		
46	1.755638	95	-3.487217		
47	1.921051	96	-1.695488		
48	3.086464	97	0.096241		
49	2.251881	98	0.887970		

VITA

Jayendra Hiralal Bheda was born in India on August 8, 1952. He grew up in a small city, Akola, where he earned his first bachelor's degree in 1967. In 1971 he graduated from Bombay University Department of Chemical Technology, Bombay in Plastics Technology. He worked for about seven years in various areas of polymer processing including two years in Houston, Texas.

He entered The University of Tennessee, Knoxville, in March 1982 and received a M.S. in Polymer Engineering in March 1984. He is a member of Society of Plastics Engineers.

He is married to former Hansa Punshi Hariya and they have a daughter Poonam.